

Chapter one

Introduction

Medical imaging departments are complex and offer a variety of customer services that are constantly changing to meet the need of the patients and physicians they serve. In a typical medical imaging department, the services offered include diagnostic imaging, CT, MRI, ultrasound, and nuclear medicine. Since 1958, Anger gamma camera system has been introduced to the field of nuclear medicine studies (Anger H.O. 1958) and followed by continuous development, and by the early 1970s the modality known as positron emission tomography (PET) was invented followed by the end of the 1970s single photon emission computerized tomography (SPECT) by which 3D images could be acquired in a way similar to computerized tomography CT systems (Youngho Seo. et.al. 2008). Such technique actually measures the coincidence of the two annihilated photons that follow positron decay in the organ of interest to diagnose pathologic evidence e.g. (studies of dementia and/or epileptic foci) and in the determination of myocardial viability. The technique is also indicated in the study of various malignancies, including staging, therapy response and follow-up (Youngho Seo. et.al. 2008). The development of gamma camera SPECT, has been accompanied with regular developing in the field of computers programs and quality Assurance technologies to optimize the SPECT performance and eliminating the errors, as SPECT has well-recognized limitations in spatial resolution and statistical quality (Cherry SR. et.al. 2003, Jaszczak RJ 1980). The performance parameter most commonly evaluated as a part of a routine gamma camera quality control program (QCP) include uniformity, spatial resolution, spatial linearity, and energy resolution and peaking (Zanzonico,2008). Nuclear medicine is critically dependent on the accurate, reproducible performance of clinical radionuclide counting and imaging instrumentation. Quality control which may be defined as an established set of ongoing measurements and analysis designed to ensure that the performance of a procedure or instrument is within a predefined acceptable range, thus a critical component of routine nuclear medicine practice (Lin.et.al. 1993, Graham LS et.al. 1995). , and routine quality assurance program should be developed and followed where test are performed on regular interval (Staden JA. et.al. 2007). In general phantom used for quality assurance can be expensive and not always easily accessible.

In addition, due to the fact that there are different cameras configurations and detector size, such phantoms should, in some cases, be camera specific. It will therefore be of great benefit to nuclear medicine departments to have an alternative and cheaper way to manufacture phantoms according to their own need (Staden JA. et.al. 2007). Also in some QA procedures such as spatial linearity (intrinsic or extrinsic and refers to the maximum deviation between the measured coordinates X, Y with respect to the real position coordinate), in which the phantom placed directly over the detector (without or with collimator) to obtain an image which in turn should show in visually inspection that: all bars are straight (Zanzonico,2008), with consideration to the risk of crystal breaking attained with collimator removal (intrinsic test) or moiré patterns appearance due to interplay of the bar or hole pattern and the lead septa of the collimator (extrinsic test) (Bone FJ,1971). System linearity is more sensitive to change in PMT performance; fortunately, such change is also manifested as a change in system uniformity. The 4-quadrant bar phantom is commonly used to measure system resolution, while it is not ideally suiting to measure system linearity as orthogonal holes pattern or the parallel line equal spacing phantom did, which they also allow assessment of both linearity and resolution (Michael et.al, 2008). The flood field uniformity (intrinsically without collimator or extrinsically with collimator) of a scintillation camera is the ability of the camera to produce a uniform image when exposed to a homogeneous spatial distribution of gamma rays (Doed SB,1994, Smith EM.1998), such parameters have validity range, for differential and integral uniformity are (1.0-2.5%) and (1.5 - 3.5% or 2 - 4%) respectively (Cherry SR. ea.al. 2003, John E. 2011), hence when the differential uniformity exceeds 3%, the maintenance service should be carried out on the gamma camera (Cherry SR. ea.al. 2003, Young KC.et.al 1990). For the potential limitation of the QA phantom highlighted above, the designing of specific phantom became evitable. Within Nuclear Medicine, image abnormalities and artifacts Within Nuclear Medicine, image abnormalities and artifacts affecting the quality of images are well known phenomena (Steven et.al,2006) Therefore, it is of great importance to have Quality Assurance for gamma and SPECT cameras to minimize the occurrence of these abnormalities and artifacts. National Electrical Manufacturers Association NEMA has made recommendations of routine quality control for nuclear medicine instrumentation (Ellinor et.al, 2010). After installation and before the camera is put into clinical use, it should undergo National Electrical Manufacturers Association (NEMA) Performance standard measurements to verify that the camera performs according to specification supplied by

the manufacturer and to establish baseline conditions for all future measurements. The NEMA (NU 1-2007) Standards Publication (NEMA, 2007) describes how to perform process and report of QC tests for gamma and SPECT cameras (Ellinor et.al, 2010). Often, with support from the manufacturers, all necessary phantoms can be supplied and acquisitions can be done according to NEMA standards, but Quality Assurance also requires a careful handling of the measured QC data. For optimal diagnostic use of nuclear medicine instruments it is essential that routine performance evaluation must be carried out as part of an ongoing quality assurance program. The NEMA publication (NU 1-2001) (NEMA, 2001) is the basic recommended standard for performance evaluation and acceptance tests of scintillation cameras, however, the methodology and guidelines described is more complex than necessary for many nuclear medicine departments to use on a routine basis. The intrinsic flood uniformity test of a gamma camera is a measure of the response of the gamma camera to a uniform flux of radiation from a point source when the collimator is removed or extrinsic flood uniformity test which assess the response of camera and collimator to uniform flux of radiation from ^{99m}Tc liquid flood phantom, which is one of the primary tests performed on the gamma cameras. Also there are two different uniformity parameters, usually measured during this test are: integral uniformity and differential uniformity. These are calculated for both the central field of view (CFOV) and useful field of view (UFOV) of the gamma camera. The integral uniformity has typical values of 2% to 4% (Ellinor et.al, 2010). For differential uniformity in most cases, a value of less than 3% is obtained after uniformity correction (O'Connor et.al, 1991). When the value for differential uniformity exceeds 3%, maintenance service should be carried out on the gamma camera (Young KC. Et.al, 1990). Values of differential uniformity in the range 1.0% to 2.5% and values of integral uniformity in the range of 1.5% to 3.5% when the uniformity correction is applied are an indication that the system is working optimum. Generally, between 10 and 30 million count flood images are adequate for verification of non uniformity of the system, for all clinical studies. Spatial linearity is one of the parameters that influence flood field uniformity. In the ideal system, a straight line source of gamma rays should yield a straight line in the image. The NEMA protocol for measuring linearity involves the acquisition along the X and Y directions of an image from a multi-slit phantom, the same one used for the spatial resolution measurement, followed by an analysis of the line spread peak positions (John et al, 2011). A deviation of the peak position from the true location of the center of the slits is a measure of the deviation from

linearity. Typically, most departments do not measure linearity separate from either spatial resolution or flood field uniformity (Abdalhamid et.al, 2000). The development of gamma camera SPECT, has been accompanied In order to obtain optimum image quality and accurate diagnosis regular inspection of the gamma camera should be done. It is now widely recognized the attainment of high standards of efficiency and reliability in the practice of nuclear medicine; as in other specialties' based on advanced technology, requires an appropriated quality assurance program. The concept of quality in term quality assurance expresses the closeness with which the outcome of a given procedure approaches some ideal, free from all errors and artifacts. The term quality control is used in reference to the specific measures taken to ensure that one particular aspect of the procedure is satisfactory (Busemann, 1993). The purpose of quality control (QC) is to detect changes in the performance of a gamma camera system that may adversely affect the interpretation of clinical studies. Clearly, there are a large number of factors that contribute to the final image quality, including uniformity, resolution (both intrinsic and energy), collimation and the hard copy device. In addition, for certain types of studies, other factors such as count rate capability come into play. With the addition of Tomographic imaging, comes an additional suite of parameters that can influence the clinical images - these include system center of rotation, gantry and collimator hole alignment, rotational stability of the detector head and the integrity of the reconstruction algorithms. On a day-to-day basis, there is a limited amount of time that can be reasonably devoted to system QC. QC schedule for NM instrumentation prepared by a 1979 IAEA advisory group. The acceptance tests recommended from the American association of physicists in medicine (AAPM), the International Electrotechnical commission (IEC),and NEMA. The QC Tests should done before the equipment is commissioned which called (acceptance testing) when there is cause to suspect a malfunction or a change in operation of an item of equipment and at specified intervals according to device-specific instructions (periodic testing) . Also Q.C can be done following significant repairs or servicing. The main goal of QC tests to monitor those parameters that are most sensitive to changes in system performance most likely to impact clinical studies. (name,2005).

It is now widely recognized that the attainment of high standards of efficiency and reliability in the practice of nuclear medicine, as in other specialties based on advanced technology, requires an appropriate quality assurance programme. The concept of quality in the term "quality assurance" expresses the closeness with which the outcome of a given procedure approaches

some ideal, free from all errors and artifacts. Quality assurance embraces all efforts made to this end. The term "quality control" is used in reference to the specific measures taken to ensure that one particular aspect of the procedure is satisfactory. A clear distinction between these terms should be made. Hence, quality assurance in nuclear medicine should cover all aspects of clinical practice. Specifically, quality control is necessary in the submission of requests for procedures; the preparation and dispensing of radiopharmaceuticals; the protection of patients, staff and the general public against radiation hazards and accidents caused by faulty equipment; the scheduling of patients; the setting-up, use and maintenance of electronic instruments; the methodology of the actual procedures; the analysis and interpretation of data; the reporting of results and, finally, the keeping of records. The present document deals with a single, albeit highly important, component of such a comprehensive programme, namely quality control of instruments. (IAEA,1991). The measurement of several performance parameters of a scintillation camera at the time of Installation and there after at regular intervals is necessary to ensure that the camera is Operating within specifications and to detect changes overtime that can initiate a request for service. There are varied opinions on what constitutes a satisfactory acceptance test and quality control program. Few individuals would disagree that either an acceptance test or routine quality control measurements are necessary, yet agreement on the contents and frequencies of these tests is lacking.

1-2 Problem of the study:

Significantly in Sudan, imaging equipment may be installed with little or no funding for maintenance, quality control and adequate scientific support .In such circumstances, commercially produced phantoms can be prohibitively expensive and consequence quality control procedures are not implemented. This situation dictates the needs for an indigenous phantom development and hence an algorithm to score the phantom image. If phantoms are available Generally Many of the quality control procedures previously published are complicated, time consuming, or require a special testing environment and also require manufacture specific software. It is noticeable that the time consuming for daily quality control (e.g MB and NM center U of G) are too long to be done daily. On the other hand uniformity, linearity and resolution should be done every morning. Due to disadvantages of techniques used to measure gamma camera system Q.C (removal of the collimator which may implies crystal break or deformity of lead septa of the collimator), the complexity of technique, and due to

shortness\little funding for maintenance and the lack of a manufacturer independent QC-software supporting a NEMA performance standard which is considered as a major problem to perform NEMA QC tests; the researchers feel curious to develop a full suite of data handling software based upon the NEMA Standard Publication of NEMA NU-1 2007 (NEMA, 2007) using interactive data language (IDL) program together with a developed phantom which is friendly applicable for routine gamma camera (SPECT) tests and low cost in Sudan

1-3 Purpose of the study:

1-3-1 General objective:

The general objective of this study is to generate a multi use quality control phantom with computer program to assess the uniformity, linearity and resolution in the same time for planer and SPECT gamma camera.

1-3-2 Specific objectives:

- To generate a multi use quality control phantom which can measure the uniformity, linearity, and resolution at the same time for planer and SPECT gamma camera
- To design a computer program to assess the result of the multi use phantom for planer and SPECT gamma camera.
- To evaluate the efficacy of the locally manufactured phantom in detection of gamma camera malfunctions with comparison to standard one.

1-4 Significances of the study:

This study will provide low cost, fast and accurate analysis for daily gamma camera quality control; by generate a multi use phantom with computerized program for assessment of the result therefore it will:

- Decrease the time for daily quality control form 1 hr 40min to half an hour.
- Decrease the cost of the phantom from cost of three different phantoms to cost of indigenus and very cheap phantom.
- The analysis using computer program provide accurate result than the visually assessment when an independent software is not available.

1-5 thesis layouts:

The thesis contains five chapters, chapter one includes the introduction, problem of the study and research objectives. Chapter two lists the theoretical backgrounds and previous study. Chapter

three discuss the materials and methods used while chapter four contains the results, chapter five includes the discussion, recommendations and conclusion of the study.

Chapter two

Theoretical background and literature review

2-1 Theory and Structure:

The daily workload in a nuclear medicine department consists of “functional” imaging of organs including thyroid, brain, heart, liver, and kidney. This is accomplished using a large scintillation device. In the 1950s, Dr. Harold Anger developed the basic design of the modern nuclear medicine camera. The Anger camera was a significant improvement over its predecessor, the rectilinear scanner. The components of the Anger camera are depicted in Figure 2-1.

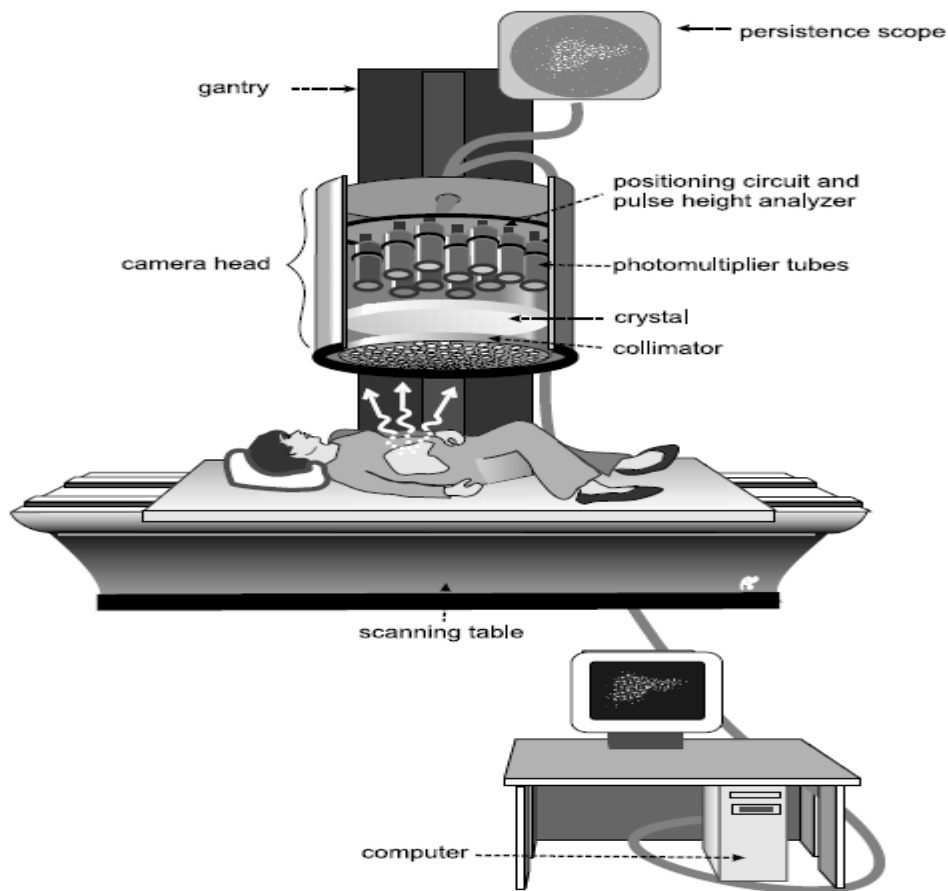


Figure 2-1: Components of a standard nuclear medicine imaging system.

A gamma camera, in particular a scintillation camera, occupies a central place in every nuclear medicine department. In a gamma camera, as opposed to a rectilinear scanner where an organ is scanned point by point, the whole organ or a large part of the body is imaged simultaneously. In this respect, a gamma camera behaves similarly to a photographic camera, although the two types of cameras are entirely different in construction and operation. Unlike light rays, x- or gamma-rays cannot be reflected or refracted by using mirrors, lenses, or prisms. Therefore, the general principles of light photography cannot be applied to imaging of objects emitting x- or gamma-rays. Instead, the selective attenuation and transmission of x- and gamma-rays by different materials, such as lead and air, forms the basis of imaging with a gamma camera. The simultaneous visualization of an entire organ or organs by a gamma camera is its single most important quality that made rectilinear scanners obsolete. This feature makes the study of rapid dynamic processes possible. Dynamic studies with 10-20 images/sec are now routinely obtained to determine cardiac output and ejection fraction. Of a variety of approaches attempted in research laboratories for the development of gamma cameras, the scintillation camera developed by Anger has emerged as a superior choice in clinical nuclear medicine. Since its commercial introduction in 1966, the modern scintillation camera has gone through several waves of technologic innovations, from improved photomultiplier (PM) tubes and collimators, non uniformity correction modules, to all digital cameras of the present. It is now almost a new instrument. The only constant element is the scintillator material, which is still a NaI (Tl) crystal.

2-1-1 Scintillation Camera:

In a scintillation camera, a large disc- or rectangular-shaped NaI (Tl) crystal is viewed from one side by an array of PM tubes. Such an array of PM tubes not only determines the total amount of light produced by a gamma-ray interaction, as is common in a scintillator detector, but also the location of light production in the crystal. The other side of the crystal is attached to a collimator that acts like a lens of a photo camera. Physically, a scintillation camera is divided in two parts. The detector head contains the collimator and the NaI (Tl) crystal with PM tubes and associated electronics and is mounted on a stand where it can be easily moved up or down or rotated in any desired position with hand-held controls or automatically under the direction of a computer (Fig. 2-1). Recently, two or even three detector heads have become popular, particularly with single-photon emission computed tomography (SPECT).

Increased geometric efficiency is the obvious advantage of multiple detector heads. The second part is the console, which houses the power supplies and operational controls of the scintillation camera, including the display module and quite often an integrated digital computer. In portable scintillation cameras, the detector head and console are joined together in one unit so that it can be moved from one location to another without too much difficulty. Operationally, a scintillation camera consists of four basic parts: collimator, detector, multiple PM tubes and position (x, y coordinates) determining circuit, and display (Chandra, 2004).

2-1-2 Collimators:

The purpose of a collimator in a scintillation camera is to allow gamma-rays originating from a selected area of an organ to reach a selected area of the detector. Thus, a collimator establishes a one-to-one correspondence between different locations on the detector and those within the organ. Another feature of a scintillation camera collimator is that its field of view is large enough to encompass completely the total organ or the desired part of the body to be imaged, there are several types of collimators designed to channel photons of different energies. By appropriate choice of collimator it is possible to magnify or minify images and to select between imaging quality and imaging speed.

2-1-2-1 Parallel Hole:

A parallel-hole collimator is made of a large number (many thousands) of small holes in a lead disc. The diameter of the lead disc is the same as that of the scintillation crystal used. Thickness of the lead disc and the diameter of the holes depend on the desired spatial resolution and sensitivity of these collimators. Lead walls between the holes, called septa, for a well-designed collimator, absorb most, if not all, radiation incident on them. Holes are axial, parallel to each other and circular or hexagonal in shape.

2-1-2-1-1 Low-energy all-purpose collimators (LEAP):

These collimators have relatively large holes which allow the passage of many of the photons emanating from the patient. As such they have relatively high sensitivity at the expense of resolution. Because the holes are larger, photons arising from a larger region of the source are accepted. As a result, image resolution is decreased. The sensitivity of one such collimator has been calculated at approximately 500,000 cpm for a 1- μ Ci source, and the resolution is 1.0 cm at 10 cm from the surface of the collimator (Nuclear Fields Precision Micro cast Collimators, Nuclear Fields B.V., The Netherlands; 140-keV ^{99m}Tc source). These collimators are useful for

imaging low-energy photons such as those from ^{201}Tl for which thick septa are not necessary. In addition, because of their moderately high sensitivity (resulting from thinner septa and bigger holes) they are advantageous for images of short duration such as the sequential one-per-second images for a renal flow study.

2-1-2-1-2 High-resolution collimators:

These collimators have higher resolution images than the LEAP collimators. They have more holes that are both smaller in diameter and longer in length. The calculated sensitivity of a representative high-resolution collimator is approximately 185,000 cpm for a 0.037 MBq (1- μCi) source, and its nominal resolution is 0.65 cm at 10 cm from the face of the collimator (Nuclear Fields B.V.). To compare the performance of a LEAP with a high-resolution collimator, let us look at the photons from two radioactive points in a liver. The photons from each of the points are emitted in all directions, but the detector can “see” only those photons that pass through the holes of the collimator. The relatively large hole in the LEAP collimator will also admit photons scattered at relatively large angles from the direct line between the liver and the crystal. This lowers the resolution because the angled photons have the effect of merging the images of two closely adjacent points (Fig. 2-2). At the same time, the larger holes and correspondingly thinner septa give the LEAP a higher sensitivity by admitting a higher percentage of the photons. The high resolution collimator, on the other hand, admits photons from a smaller fraction of the organ, because more of its face is blocked by septa. In a reciprocal way, the narrower (see Fig 2-2) and/or longer (Fig. 2-3) bore of its holes better collimate those photons that do enter the collimator. As a result, relatively closely spaced details in the source are more likely to appear clearly separated in the image.

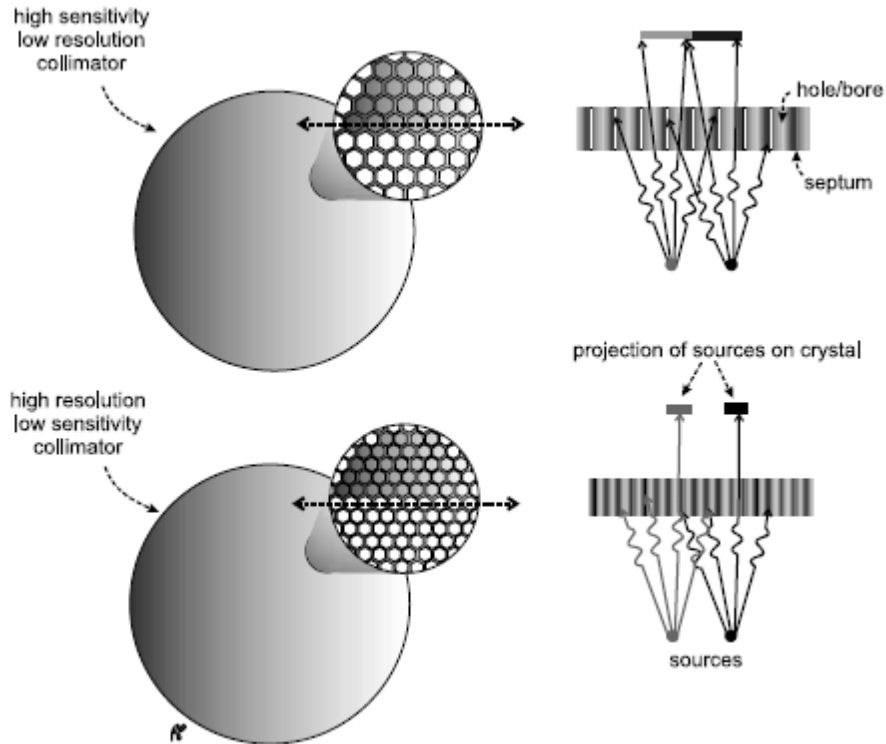


Figure 2-2 for the same bore length, the smaller the diameter the higher the resolution

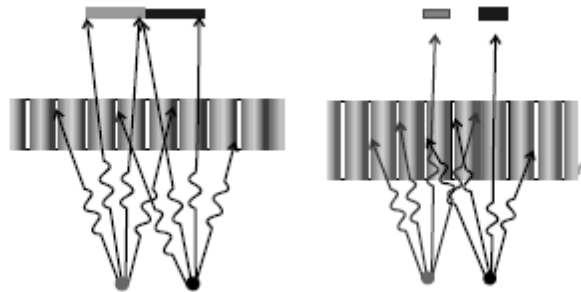


Figure 2-3: for the same hole diameter, the longer the bore the higher the resolution.

2-1-2-1-3 High- and medium-energy collimators:

Low-energy collimators are not adequate for the higher energy photons of nuclides such as ⁶⁷Gallium (it emits 394-keV, 300-keV, and 185-keV photons, in addition to its low-energy 93-keV photon), ¹³¹Iodine (376 keV), ¹¹¹Indium (245 KeV and 173 keV), nor for positron emitters such as ¹⁸Fluorine (511-keV annihilation). The photons of these nuclides can penetrate the thinner septa of both the LEAP and the high-resolution collimators, resulting in poorer resolution. High-energy collimators with thicker septa (Fig. 2-5) to reduce septal penetration are used, but thicker septa also mean smaller holes and, consequently, lower sensitivity.

High-energy collimators are useful for ^{131}I Iodine. Medium-energy collimators have characteristics between those of low and high energy collimators. They can be used to image photons emitted by ^{67}Ga Gallium and ^{111}In Indium. The terms high, medium, and low-energy are not rigidly defined, and usage may vary from institution to institution.

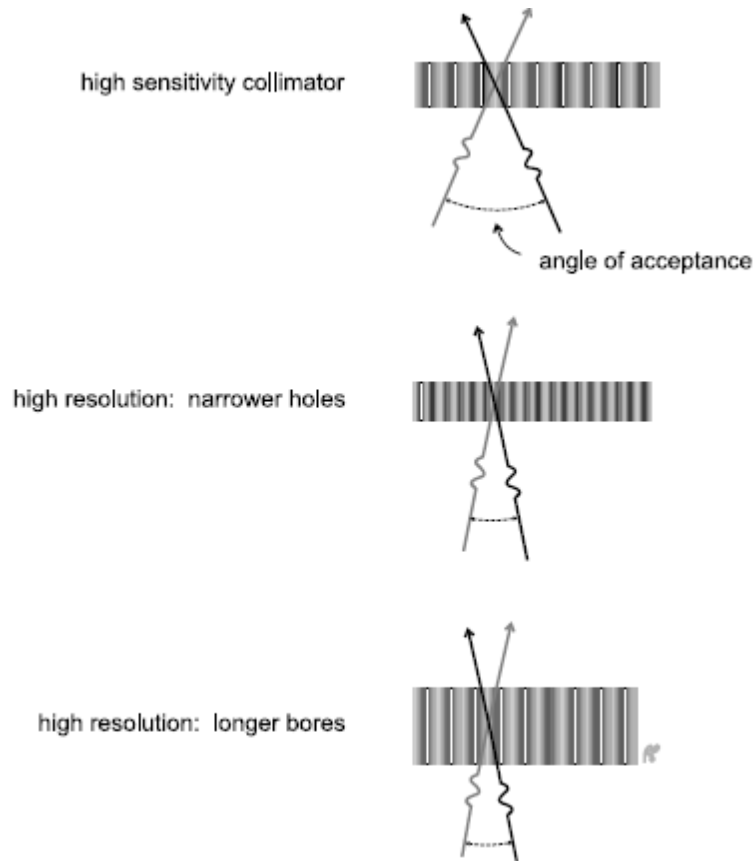


Figure 2-4 Angle of acceptance.

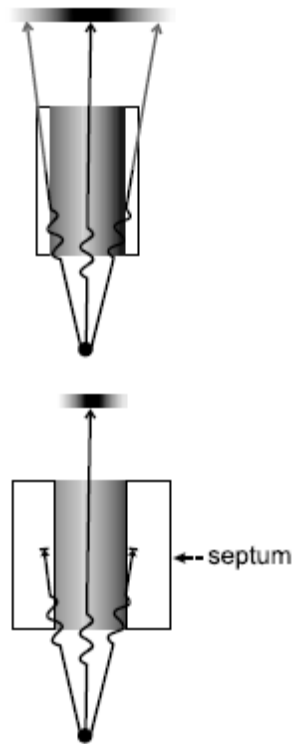


Figure 2-5 thicker septa are used to block high and medium energy photons.

2-1-2-1-4 Slant-hole collimators:

These are parallel-hole collimators with holes directed at an angle to the surface of the collimator. The slant-hole collimator provides an oblique view for better visualization of an organ that would otherwise be obscured by an overlying structure while permitting the face of the collimator to remain close to the body surface (Fig. 2-6).

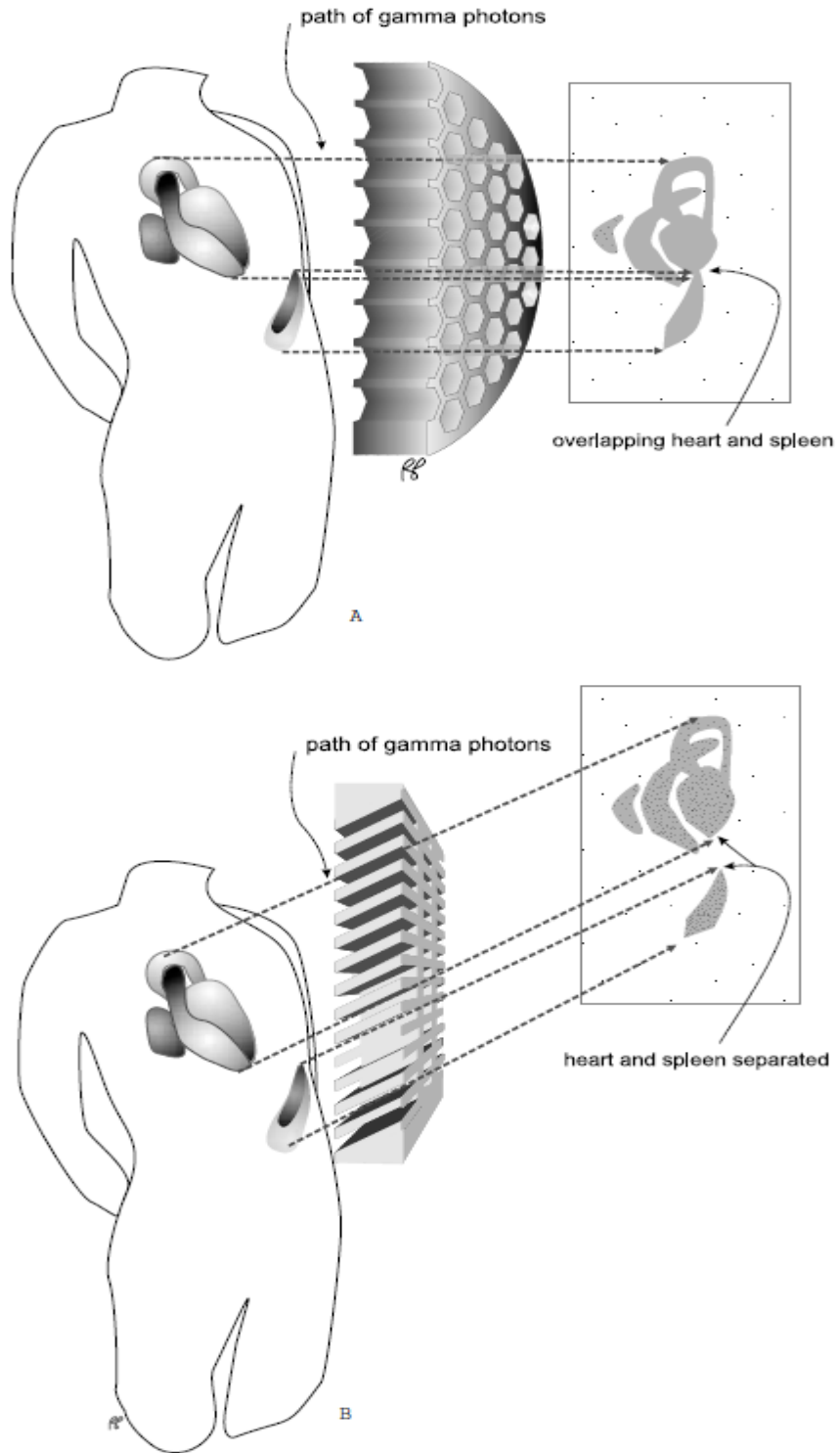


Figure 2-6 Parallel-hole (A) and slant-hole (B) collimators

2-1-2-2 Nonparallel-Hole Collimators:

Nonparallel-hole collimators provide a wider or a narrower field of view. The cone-like pattern of holes allows these collimators to enlarge or reduce the size of the image.

2-1-2-2 -1 Pinhole:

A pinhole collimator consists of a single hole, about 5 mm in diameter, at the top of a hollow lead cone. The diameter at the base of the lead cone is the size of the NaI (Tl) crystal. The top of the cone faces the patient. The height of the cone can range from 12 to 20 inches.

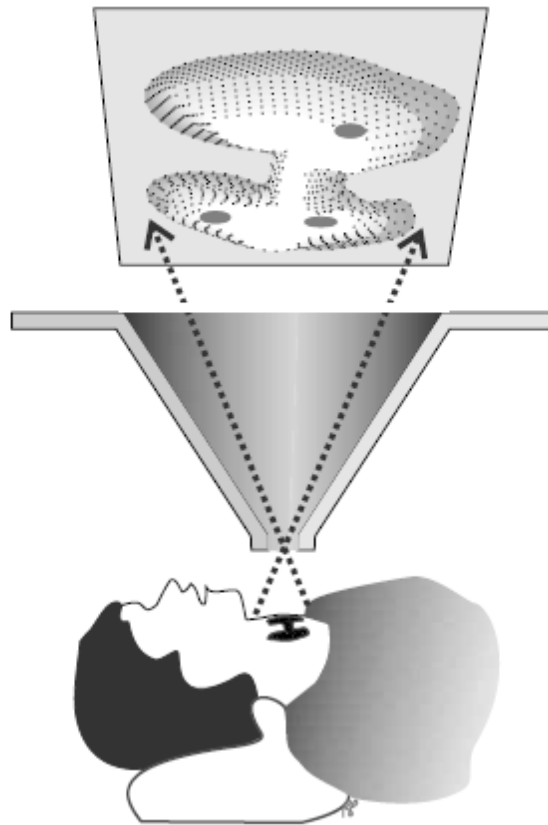


Figure 2-7: Pinhole collimator

2-1-2-2 -2 Converging:

A converging collimator is similar to a parallel-hole collimator except that the holes, as one move from the center of the collimator toward the edge of the collimator, start tilting toward the center, (as shown in Figures 2-7 and 2-8). Outermost holes have the most tilt. All holes focus at

an axial point, outside the collimator (typically 10-20 inches) and toward the radioactive source or the patient.

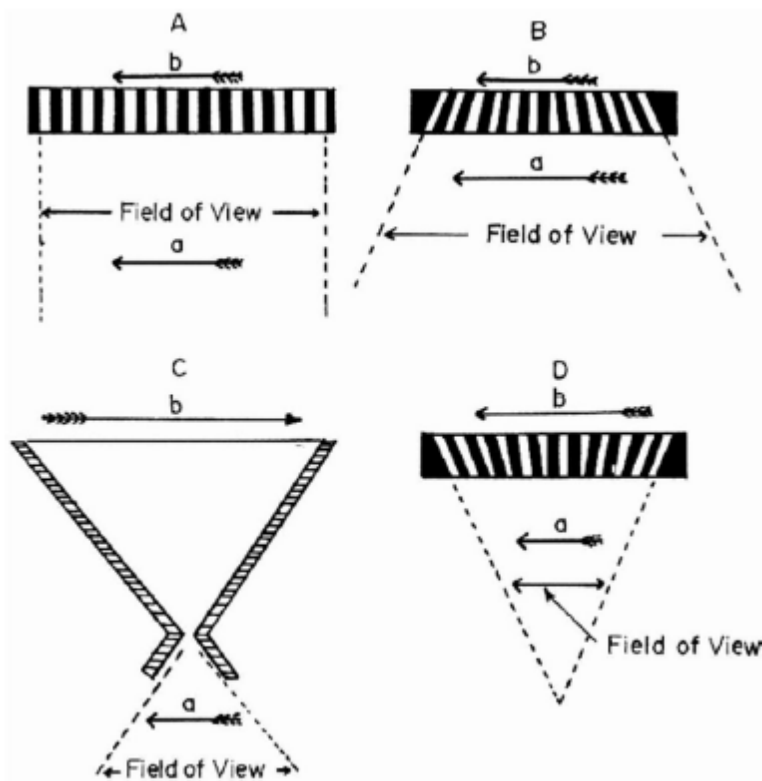


Fig 2-8: Collimators used in a scintillation camera. A Parallel-hole collimator: The object a projects the same size image b on the crystal face. The field of view of such a collimator does not vary significantly with distance from the collimator. B Diverging collimator: The size of the image b is smaller than the size of the object a and the field of view increases as one moves away from the collimator. C Pinhole collimator: A magnified or minified image b of an object a is produced, depending on its distance from the pinhole. The field of view of a pinhole increases rapidly as one moves away from the pinhole. D Converging collimator: This collimator produces a magnified image b of an object a. The field of view decreases as one moves away from the detector. A converging collimator provides the optimum sensitivity and spatial resolution for an object that is smaller than the crystal size used in the scintillation camera.

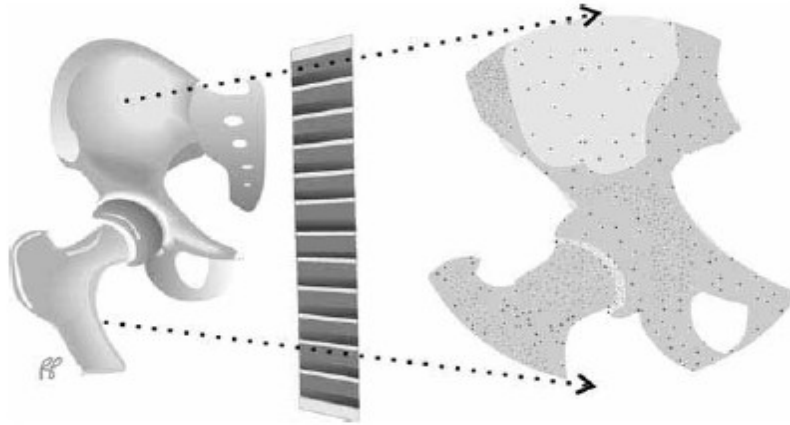


Figure 2-9: Converging collimators.

2-1-2-2 -3 Diverging:

In a diverging collimator, the tilt of the holes is away from the center. As a result, these holes converge toward the detector. In fact, if one flips over a converging collimator, it becomes a diverging collimator and vice versa. As can be seen, in all these collimators, gamma-rays originating from one area of the arrow reach only a selected area on the crystal. Thus, gamma-rays originating from the front of the arrow reach a different location on the crystal than gamma-rays originating from the middle or back of the arrow. The size of the image formed on the crystal depends on the type of collimator and distance of the object from the collimator. In the case of a pinhole collimator, the image is also inverted. The choice of a particular type of collimator is basically dictated by the size of the organ to be imaged. For imaging organs that are similar in size to the size of the detector [NaI (Tl)] crystal, parallel-hole collimators provide the best sensitivity and spatial resolution. For organs larger than the size of the crystal, diverging collimators are preferred. For organs smaller than the size of the crystal, converging collimators have shown great merit. When the size of the organ is small, such as the thyroid, a pinhole collimator is the collimator of choice. One problem that makes the use of pinhole, converging, or diverging collimators less satisfactory than parallel hole collimators is the fact that for three-dimensional objects (which all organs are), the different planes of the object (front, back, or middle of the organ) are magnified or minified to different degrees by these collimators. This produces distortions in the image that under most clinical circumstances are unacceptable. Commercially, the collimators, besides being characterized by the above four types, are also classified according to their spatial resolution or sensitivity as high-sensitivity (for dynamic studies), all purpose (for most clinical applications), or high-spatial-resolution (for fine details)

collimators and according to the energies of gamma-rays for which they have been optimized as low-energy (0-200 keV), medium-energy (200-400 keV), and high-energy (400-600 keV) collimators. High-energy collimators are used sometimes with positron-emitting radionuclides. The main difference between collimators designed for different energies is the thickness of septum that increases with energy.

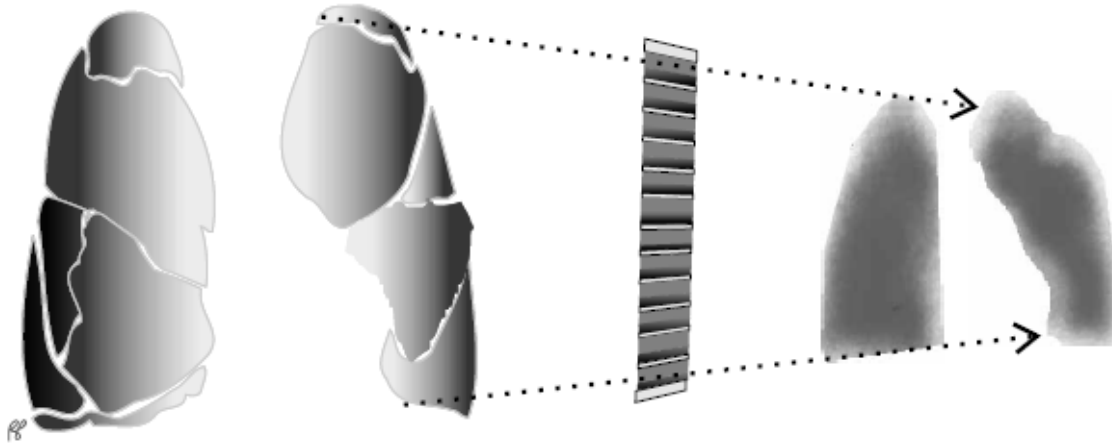


Figure 2-10: Diverging collimator

2-1-2-2-4 Fan-beam collimators:

These are a cross between a converging and a parallel-hole collimator. They are designed for use on cameras with rectangular heads when imaging smaller organs such as the brain and heart. When viewed from one direction (along the short dimension of the rectangle), the holes are parallel. When viewed from the other direction (along the long dimension of the rectangle), the holes converge (Fig2-9). This arrangement allows the data from the patient to be spread to better fill the surface of the crystal. (Chandra,2004).

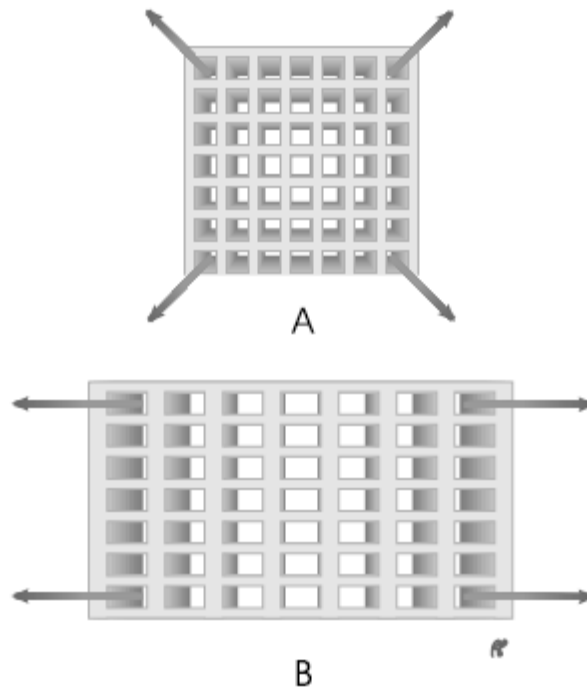


Figure 2-11: (A) in a converging collimator, holes converge toward the patient in both planes and uniformly enlarge an image. (B) In a fan-beam collimator, holes converge in one plane but are parallel in the other. Arrows demonstrate the paths of photons coming from the patient.

2-1-3 Detector, NaI (Tl) Crystal:

2-1-3-1 Size and Thickness:

As has already been pointed out, the basic detector element in a scintillation camera is a large disc shaped [NaI (Tl)] crystal that is viewed from one side by a large number of PM tubes. The diameter of the crystal varies from 11 to 20 inches. Eleven-inch-diameter crystals are used in the standard scintillation camera, whereas 16- to 20-inch-diameter crystals are used in so-called large field of view (LFOV) scintillation cameras. The main advantage of a large crystal is the increased sensitivity for large organs such as lungs or the whole body. For a more effective use of the crystal area, rectangular crystals are also available in some scintillation cameras. The thickness of the crystal is generally $\frac{1}{2}$ inch, but scintillation cameras with $\frac{3}{8}$ - or $\frac{1}{4}$ -inch-thick crystals are also in vogue, particularly for nuclear cardiology work. Reduced thickness of the crystal improves the intrinsic spatial resolution. The trade-off for improved intrinsic spatial resolution is the reduction in intrinsic sensitivity, particularly for higher energy (>150 keV) gamma-rays (Chandra, 2004).

2-1-3-2 Energy Selection:

The detection and measurement of energy of the gamma-rays passing through the collimator is performed as in any NaI (Tl) detector system, except that in scintillation cameras a large number of PM tubes are used instead of a single PM tube. To determine the energy of a gamma-ray, one has to determine the total amount of light produced in the crystal. In a scintillation camera, the total light produced is distributed among many or all PM tubes. Therefore, to determine the total amount of light produced, the outputs of all PM tubes have to be summed to produce a pulse equivalent to that produced in a simple NaI (Tl) detector (with only one PM tube). The summated pulse is known as the Z pulse (a misnomer as this should be called E pulse). Pulse-height analysis on Z pulses allows us to select the pulses of the desired energy. Two important attributes of the Z pulse are linearity with gamma-ray energy and its spatial independence (Z pulse-height should not depend on the location of the point of light production in the crystal). On both scores, newer scintillation cameras have improved significantly. The remainder of the nonlinearity and spatial dependence is reduced further by using online correction methods. Summation of pulses from many PM tubes to obtain a Z pulse in a scintillation camera makes its energy resolution slightly worse than a simple NaI (Tl) detector. Like any other NaI (Tl) detector, in a scintillation camera there are four controls related to the detection of gamma-rays and their energies: high voltage, gain of the amplifier, peak energy E, and window width gamma E or % gamma E. Energy selection is usually automated; to choose a gamma -ray of a particular energy, one presses a designated button and appropriate pulses are automatically selected. Another useful feature is a provision for simultaneous selection of two or even three gamma -rays of different energies. This feature requires two or three pulse-height analyzers (PHAs) and is useful for imaging the distribution of radionuclides that emit more than one gamma-ray (e.g., ^{67}Ga , ^{111}In , or even ^{201}Tl) or for rejecting the scattered radiation (Chandra, 2004).

2-1-3-3 Automatic Peak Tracking:

Scintillation detectors are prone to slow drifts in their outputs, mainly due to the changes in the gain of a PM tube. Changes in the PM gain are caused by small ambient temperature and high-voltage fluctuations. In newer cameras, electronic circuits have been provided that monitor these drifts and readjust the high voltage or amplifier gain to its original value. The automatic peak tracking circuits track the PM gains either on demand or continuously, depending on the

manufacturer of a scintillation camera. In either case, the output of PM tubes and therefore the stability of the scintillation camera itself have improved tremendously.

2-1-3-4 Counting:

Pulses selected by the PHA, besides being sent to a logic circuit for generation of X and Y pulses, are fed into scalar timer module. The scintillation camera can either count for a fixed-time interval (preselected time) or for an assigned number of counts (preselected counts). There is also a provision for imaging to stop at preselected time intervals or a preselected number of counts, depending on which happens first. A manual control allows one to start or stop counting at any time. Another feature found only in some scintillation cameras is pre selection of the information density in a given area of the image. The scintillation camera will stop when a preselected number of counts have been acquired in the desired area of the image. Scintillation cameras interfaced or integrated with digital computers have these functions start, stop, time, or number of count under computer control (Chandra, 2004).

2-1-4 Position Determining Circuit (X, Y Coordinates):

2-1-4-1 Pulse-height Distribution among PM Tubes:

A collimator in a scintillation camera allows gamma- or X-rays originating from one small part of an organ to reach a small part of the crystal in a one-to-one correspondence. To keep this correspondence intact electronically, we should know where the gamma-rays are interacting in the crystal. This is accomplished with the help of a large number (commonly 37 or 67) of PM tubes, but in Fig below, it is illustrated by considering a simple array of seven PM tubes. In this case, when light is produced at point a in the crystal, it is distributed among all seven PM tubes. However, by knowing which PM tube received the maximum amount of light, it is possible to know the rough location (near the PM tube receiving the maximum amount of light) of the point of light production. To locate the point of light production more accurately, the amount of light received by each PM tube, rather than the one receiving the most light, has to be taken into account (i.e., the distribution of light among different PM tubes and therefore the pulse-height distribution produced by the PM tubes is considered). The distribution of light or the pulse heights produced among different PM tubes are directly proportional to the solid angle subtended by each PM tube at the point of light production. This fact is used in the determination of the exact location of the point of light production. The PM tubes can be either a circular or hexagonal cross-section. A hexagonal cross-section has the advantage of close packing and

therefore less dead space between the PM tubes. The output of a PM tube is analog, and it was as such used by Anger to produce two position determining analog pulses, X and Y. However, in present-day scintillation cameras, the output of each PM tube is digitized and all subsequent processing is done with a microcomputer to produce, in digital form, the two position-localizing pulses, X and Y, and the energy pulse Z. To determine the position-localizing pulses, in analog or digital version, the outputs of various PM tubes are summed with appropriate “weighting factors” (these depend on the distance of the PM tube from the center of the crystal and are not relevant here) to yield four analog signals, known as X+, X-, Y+, and Y-. In commercial scintillation cameras, the number of PM tubes varies from 19 to 96, and the summation circuits are complex and differ from one manufacturer to another. The position-defining voltages X and Y and the energy-defining Z pulse are generated from the four voltages X+, X-, Y+, and Y- as follows: $Z = X+ + X- + Y+ + Y-$ $X = K(X+ - X-) \div Z$ $Y = K(Y+ - Y-) \div Z$ where K is a constant. The most desirable property of the X and Y pulses is their linearity with distance of the point of light production along the x or y axis from the center of the crystal. The farther the distance (X, Y coordinate) of the source of light from the center of the crystal, the higher the pulse heights, X and Y. However, because of the geometry of light collection, these pulses are not as linear with distance as one would like them to be. Use of light pipe, or nonlinear pulse shaping are two common methods to improve the linearity of X and Y pulses. These methods do not remove the nonlinearity completely. The residual nonlinearity has to be measured and corrected online. To display the gamma-ray interaction, X and Y pulses (if digital, these have to be converted back into analog form) are used to deflect a light spot on a cathode-ray tube (CRT) or oscilloscope in direct proportion to the amplitude (magnitude) of X and Y. The final image of the distribution is formed from the oscilloscope. If a digital computer is used, this information (X- and Y-pulse amplitudes) is stored in memory for further processing or later display.

2-1-5 Intrinsic Spatial Resolution:

Even after considering the amount of light received by all PM tubes and making all the corrections, there is always a small error involved in the exact localization of the point of light production. This error is a measure of the intrinsic spatial resolution of the scintillation camera. Intrinsic spatial resolution is a complex function of the thickness of the crystal, the number of PM tubes used for position determination, the type and shape of PM tubes, and the thickness of light pipe, if used, to couple the PM tubes with the crystal. The most important of these is the

thickness of the crystal. Reducing the thickness of the crystal improves the intrinsic spatial resolution, but it also decreases sensitivity of a scintillation camera as a lesser number of gamma-rays interact in the crystal. Therefore, a compromise has to be made between the intrinsic spatial resolution and sensitivity of the scintillation camera. The optimum range of thickness for scintillation cameras is 3/8 to 1/2 inches for 140-keV gamma-rays. Another factor that also affects intrinsic spatial resolution of the scintillation camera is the energy of gamma-rays. This is due to the fact that a higher energy gamma-ray produces more light in the crystal (for photoelectric events that are always selected) than a lower energy gamma-ray. More light enables better localization of the point of gamma-ray interaction, and better localization means better intrinsic spatial resolution (Chandra, 2004).

2-1-6 Display:

Gamma-rays originating in the field of view of a collimator interact in the crystal at different locations. These interactions in general occur in a random fashion. A display device should be able to portray such a randomly generated position information (X, Y) quickly (at least 106 events per minute) and accurately a CRT or an oscilloscope, of which a CRT is an integral part, is effectively used for this purpose.

2-1-6-1 Cathode-ray Tube:

A CRT is an evacuated glass tube consisting of five basic components: an electron gun, a focusing electrode, and horizontal deflection plates (x direction), vertical deflection plates (y direction), and a phosphor screen. The electron gun produces a stream of fast electrons. The number of electrons or the intensity of the electron stream can be varied, if desired, by intensity control I. The focusing electrode allows focusing the electron stream to a narrow circular beam (about 0.1 mm in diameter). When voltage pulses are applied to the horizontal and vertical plates, the electron beam moves in the x and y directions in direct proportion to the magnitude of the voltage pulses applied at the horizontal and vertical plates, respectively. The duration for which the electron beam stays at its new location depends on the duration of the voltage pulses applied to the horizontal and vertical plates. It is generally less than a microsecond. When there is no voltage pulse applied to the horizontal and vertical plates, the electron beam remains at the center of the phosphor screen. The location of the electron beam on the screen is made visible by the phosphor that emits light at the point where the electron beam strikes it. In this way, when voltage pulses of different magnitudes are applied in succession to the horizontal and vertical

plates, the light spot on the CRT screen moves from one place to another but always at a distance that is directly proportional to the magnitude of the applied voltage pulses. The intensity of the light spot is controlled by the intensity control I.

2-1-6-2 Display of Individual Interactions:

For displaying position information from the scintillation detector, the X and Y voltage pulses are applied to the horizontal and vertical plates of a CRT. The Z signal that carries the energy information exercises a veto on the X and Y signals in such a manner that these are applied to the CRT horizontal and vertical plates only if the Z signal is within the energy range selected by the PHA. If the Z pulses are outside the range selected by PHA, then X and Y are not applied to the CRT horizontal and vertical plates. Thus, only those gamma-ray interactions that deposit energy in the crystal in the range selected by PHA are displayed on the CRT screen. In summary, the display functions as follows. A gamma -ray interacts in the detector and the detector produces three signals, giving the location (X and Y pulses) of the gamma -ray interaction and the energy transfer (Z pulse) by the gamma -ray interaction. The Z pulse is analyzed, and if it is within the selected range, the position signals (X and Y pulses) are applied to the CRT plates, which deflect the light spot from the center of the screen to a distance proportional to the X and Y voltages. When a new gamma -ray interacts in the crystal, a new set of X, Y, and Z signals is produced that then deflects the light spot to a new location given by these signals. In this way, as more and more gamma -rays interact in the crystal, the light spot on the CRT screen keeps moving from one place to another in correspondence with the location of gamma -ray interaction in the crystal up to 500,000 times or more in a typical image. Because the usual size of CRTs range from 3 to 5 inches in diameter, the image on the CRT screen is displayed in a smaller size than the actual size of the organ or part of the body imaged.

2-1-6-3 Integration on a Film:

A flying light spot on the screen of a CRT does not constitute an image. This image is formed by point by- point integration of this information on a photographic film.

2-1-6-3-1 Film Characteristics:

On a film, darker areas represent more radioactivities, whereas lighter areas represent less activity. Film darkening is quantitatively measured by a parameter known as optical density or, simply, density. It is defined as the logarithm (base 10) of the ratio of the intensity of incident light on the film to the intensity of the light transmitted by the film. According to this definition,

an area of the film with a density of 2 will transmit only 1% light and will therefore appear almost black to the naked eye. A density of 0 represents 100% transmission; therefore, an area with 0 densities will appear white. Densities between 0 and 2 will appear as shades of gray. A high-contrast film displays smaller exposure variations than a low-contrast film, but a high-contrast film has smaller latitude. Therefore, the range of exposures that can be displayed on a high-contrast film is smaller.

2-1-6-3-2 Film Exposure:

Normally, count rates in an organ may vary from zero to a maximum R_{\max} . For effective display, R_{\max} (also known as the “hot spot”) should correspond to point B and zero count rate to point A on the H-D curve. The R_{\max} for individual patients differs because of variations in the administered radiopharmaceutical dose, localization and distribution in the organ, and the size and shape of the organ. Some variations are taken care of when one uses fixed number of counts rather than fixed amount of time for exposure. The proper exposure of the film, which is controlled by the intensity I of the CRT, is inversely related to the number of counts. The more counts in an image, the lower setting of I needed and vice versa. Generally, a table is made for the number of counts in an image and I setting needed for proper exposure for those counts. In fast dynamic studies where the exposure is for a fixed time, the I settings are only a guess. This quite often produces bad results. The only solution to this problem is to interface the scintillation camera with a computer, store images, and make exposures after the number of counts in each image has been determined.

2-1-6-3-3 Multi format Recording:

A multi format recording system is commonly used in nuclear medicine. In this system, multiple images are recorded on a single sheet of x-ray film, usually 8×10 or 11×14 inches in size. The number of images and therefore the size of the image that can be recorded on a single sheet can be varied easily with the help of controls provided for such purposes. Thus, a single sheet may contain from one to as many as 64 images. The main advantage of this device is that all views from one patient, including dynamic studies, can be recorded on a single sheet of film, thus consolidating most of the information in one place (Chandra, 2004).

2-1-7 Imaging with a Scintillation Camera:

Generally, the following steps are taken to obtain an image with a scintillation camera: Selection of the study to be performed (e.g., brain, liver, etc.); Selection of the radiopharmaceutical and

the dose of radiopharmaceutical. A radiopharmaceutical is generally administered to patients away from the scintillation camera, but sometimes, particularly when fast dynamic studies are to be performed, it may have to be administered with the patient in the appropriate position under the camera. Selection of the PHA parameters (peak energy and % window corresponding to the gamma -ray emitted by the radionuclide to be used); Selection of an appropriate collimator (with respect to energy and spatial resolution); Selection of the mode: accumulation of a certain number of counts or exposure for fixed amount of time. Selection of the appropriate intensity of the CRT for the number of counts expected or to be acquired in the image; Positioning of the patient under the camera and, if the radiopharmaceutical has not been administered, administration of the radiopharmaceutical; Start and finish of the exposure; Development of the film. If more than one view is to be displayed on the same film, then the development of the film takes place at the end of the study.

2-1-8 Interfacing with a Computer or All-digital Camera:

Digital computers have acquired an important role in nuclear medicine. The main advantage of a Computer is the speed and ease with which it can acquire, analyze, store, and display large amounts of complex data. Presently, scintillation cameras either completely integrated with a digital computer (all digital cameras) or interfaced with a dedicated digital computer are commercially available. Besides SPECT and heart studies, which cannot be performed without a digital computer, many other applications of computers are now an integral part of standard nuclear medicine procedures (e.g., renogram).

2-1-9 Digitization in General:

A digital computer handles numbers or digits only and these too in binary (or powers of 2) form only (base 2 instead of base 10). Therefore, any instrument from which data are to be acquired and analyzed by a digital computer in an automatic fashion has to present the data to the computer in binary (or similar) digital form. Unfortunately, most instruments produce signals or data in an analog form. Analog signals are continuously varying and do not produce data in numbers. Such a device, which automatically changes analog signals into digital (binary) signals, is known as an analog-to-digital converter, or simply an ADC. Two important parameters of an ADC, accuracy and speed, are relevant for our purpose. Accuracy of ADC tells how close the numeric data is to the analog signal. The second parameter of an ADC is the speed. The faster an ADC is, the higher the rate of data it can digitize without any loss of information. Thus, speed

and accuracy are inversely related. More accuracy means less speed and more speed means less accuracy.

2-1-9-1 Digitization in the Scintillation Camera:

In a scintillation camera, unless it is an all-digital scintillation camera, in which case the digitization has already been done at the PM tube, the X, Y, and Z pulses are analog and have to be digitized before being recorded by a digital computer. The ADCs used for digitizing X and Y signals of a scintillation camera are 7-9 bits, which means that the X and Y ranges are equally divided into $2^7 = 128$, $2^8 = 256$, or $2^9 = 512$ equal divisions, respectively. In a scintillation camera, the maximum range of X or Y signals will equal the diameter d of the crystal. Therefore, each division of an ADC will correspond to either $d/128$ or $d/256$ cm of distance, depending whether the ADC is 7 or 8 bit. For an 11-inch (28 cm) diameter crystal and 7-bit ADC or for an LFOV (20-inch-diameter) crystal and 8-bit ADC, this value equals 0.2 cm. Because the intrinsic spatial resolution of a scintillation camera presently is in this range, greater accuracy is not needed. In terms of the speed of the ADC, it should be able to handle about 100,000 signals per second, because higher count rates are seldom encountered in nuclear medicine. The digitization of X and Y signals into 64, 128, or 256 divisions yields a 64×64 , 128×128 , or 256×256 matrix. Thus, the analog image (which is two dimensional or areal distributions) is divided into $64 \times 64 = 4096$, $128 \times 128 = 16,384$, or $256 \times 256 = 65,536$ equal small areas known as pixels. A specific area on the crystal corresponds to a specific pixel, and each pixel is assigned a specific location in the computer memory. Therefore, when a gamma-ray interacts in the crystal, its pixel location is determined by the ADCs and a count is stored in the corresponding location in the computer. As more and more gamma-rays interact, they are stored in the appropriate locations, and finally a digitized image is formed.

2-2 Primary quality control Tests of Gamma Cameras:

2-2-1 Intrinsic Spatial Resolution:

The radionuclide employed for this test shall be ^{99m}Tc . A source holder, which shields the source from walls, ceilings and personnel without restricting the gamma flux from the source to the camera, shall be employed. One or more copper plates may be used to adjust the count rate. The energy window for ^{99m}Tc shall be 15 percent centered on the photopeak. The count rate shall not exceed 20,000 cps through the energy window. If other radionuclides are used, the energy

window should be set according to the manufacturer's recommendations. The test pattern shall consist of a lead mask in closest possible proximity to the crystal, covering the entire UFOV with 1 millimeter wide parallel slits. Adjacent slit centers shall be 30 millimeters from each other and the thickness of the mask shall be 3 millimeters for ^{99m}Tc . Then the lead mask with the parallel slits shall be positioned on the camera detector with one of the slits centered perpendicular to the axis of measurement. The radionuclide shall be a point source centered at least five times the largest linear dimension of the UFOV above the lead mask with the parallel slits. The digital resolution perpendicular to the slits is recommended to be less than or equal to 0.1 FWHM. The digital resolution parallel to the slits shall correspond to a channel width less than or equal to 30 millimeters i.e. a profile up to 30 mm wide is used. At least 1,000 counts shall be collected in the peak channel of each line spread function measurement. Full Width at Half Maximum (FWHM) and Full Width at Tenth Maximum (FWTM) of the line-spread function shall be measured. If the digital resolution perpendicular to the slits is less than or equal to 0.1 FWHM, then the maximum value pixel is taken to be the peak value. If the digital resolution perpendicular to the slits is more than 0.1 FWHM, a three point parabolic fit, using the peak point in each line spread function and its two nearest neighboring points respectively, shall be employed. The peak value shall be then determined from the largest value of this parabolic fit. The half maximum and tenth maximum locations shall be determined by linear interpolations from the nearest two neighboring points of the half peak value and the tenth peak value respectively, using the peak value in each line spread function curve as the maximum. The distance between adjoining peaks shall be averaged over the entire UFOV for determining the millimeters per channel calibration factor. The calculated average distance shall correspond to the 30 mm distance between the slits. This calibration factor shall be used to convert the calculated values of FWHM and FWTM from units of channels to millimeters per channel. The value of FWHM and FWTM shall be calculated as the average of all such values for both axes, lying within the UFOV and CFOV respectively. The calculated values shall not be corrected for background or slit width.

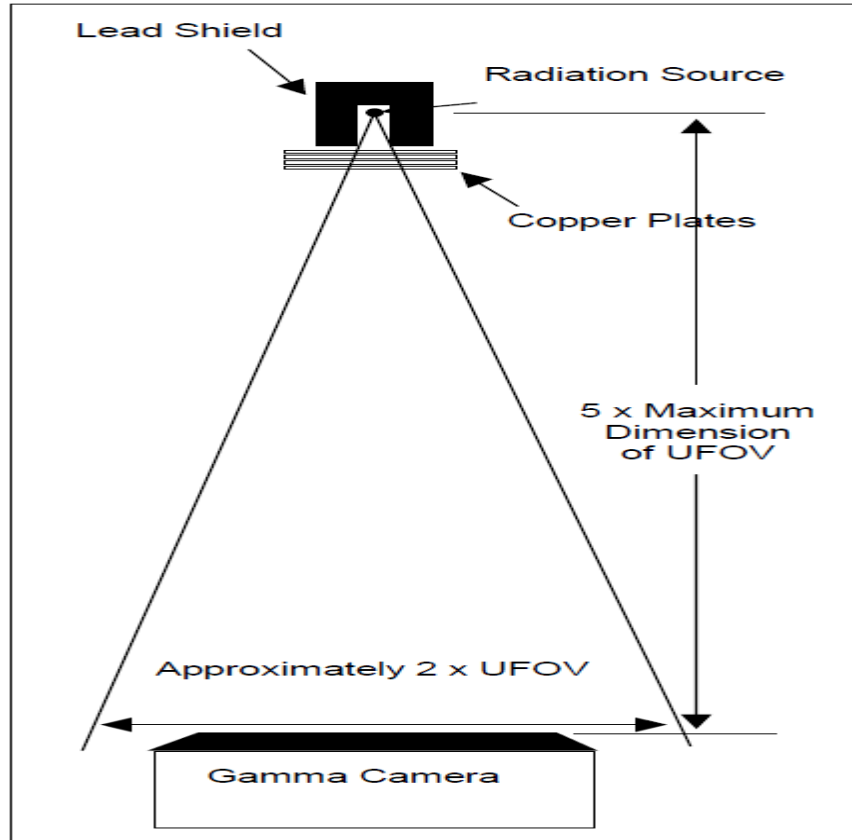


Figure 2-12: Collimated Source Geometry

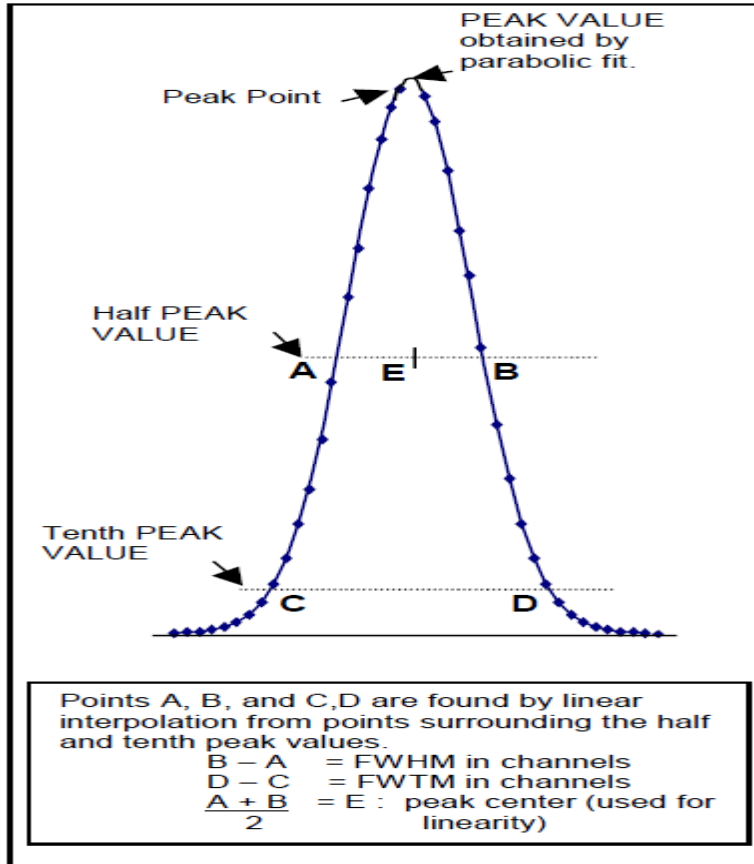


Figure 2-13: Determination of FWHM and FWTM

2.2.2 Intrinsic Energy Resolution:

Intrinsic energy resolution shall meet or exceed the Specification, and shall be expressed as the ratio of the photopeak FWHM to the photopeak center Energy, stated as a percentage. The radionuclide employed for this test shall be ^{99m}Tc . A source holder which shields the source from Walls, ceilings and personnel without restricting the gamma flux from the source to the camera shall be employed. At least 2 mm of copper shall be used. The detector shall be masked with a 3 mm thick lead aperture to establish UFOV. The integral count rate shall not exceed 20,000 cps. The test equipment shall include means to digitize the energy spectrum with a channel depth of at least 10,000 counts, and a digital resolution of less than or equal to 0.05 FWHM of ^{99m}Tc photopeak. The radionuclide shall be a ^{99m}Tc point source centered at least five times the largest linear dimension Of the UFOV above the detector. A second radionuclide, ^{57}Co , shall be employed as a reference in order to determine the KeV per channel calibration factor. The spectra for ^{99m}Tc and ^{57}Co shall be separately stored. At least 10,000 counts shall be

stored in the peak channel of each spectra measurement. For each of the stored spectra, the photopeak location shall be determined as the average of the linearly Interpolated half height channel values, calculated for each side of the photopeak. The difference between the two photopeak locations in channel numbers should correspond to 18.4 KeV, which is the difference between 140.5 KeV of the ^{99m}Tc photopeak center energy and the 122.1 keV of The ^{57}Co photopeak center energy. The intrinsic energy resolution shall be calculated from the ^{99m}Tc Stored spectrum. The FWHM in channel numbers shall be determined from the linearly interpolated half Height channel values and calculated for each side of the ^{99m}Tc photopeak. This value shall be multiplied by the calibration factor (KeV per channel), divided by 140.5 KeV corresponding to the ^{99m}Tc Photopeak center energy, and multiplied by 100 in order to obtain the value as a percentage. If other radionuclides are used, the reference nuclide for calibration (KeV/channel) shall be ^{57}Co (National Electrical Manufacturers Association recommendation 2001).

2.2.3 Intrinsic Flood Field Uniformity:

The intrinsic uniformity of the system shall be measured for the CFOV and UFOV. The measured values shall meet or exceed the specification. The intrinsic uniformity is the response of the system without a collimator to a uniform flux of radiation from a point source. Two different uniformity parameters shall be determined: integral uniformity and Differential uniformity. Integral uniformity is a measure of the maximum pixel count deviation in the CFOV or UFOV. Differential uniformity is a measure of the maximum deviation over a limited range designed to approximate the size of a photomultiplier tube. The radionuclide used to measure intrinsic uniformity is to be ^{99m}Tc . Any other radionuclide used shall be reported separately. The count rate shall not exceed 20,000 counts per second through a symmetric 15 Percent photopeak window. The status of uniformity corrections used shall be stated with the results. If other radionuclides are tested, the energy window settings recommended by the manufacturer shall be used. The test equipment required for this measurement consists of a source holder, a lead mask for the detector, and a computer or multi-channel analyzer. The source holder shall consist of a lead shield to prevent back and side scatter but be open at the front so that it does not restrict the gamma flux from the source to the detector. The lead mask for the detector is a lead Aperture of at least the dimensions of UFOV. The detector shall be masked using a lead mask. The source in the source holder shall be placed on the central axis of the detector. The distance from the

detector to the source shall be at least Five times the largest dimension of the UFOV. The flood field image shall be stored in a matrix size which Produces pixel sizes with a linear dimension of 6.4 mm ± 30%. The pixels shall be square. A minimum of 10,000 counts shall be collected in the center pixel of the image. Prior to performing the uniformity calculations, the pixels for inclusion shall be determined as First, any pixels at the edge of UFOV containing less than 75% of the mean counts per pixel in the CFOV Shall be set to zero. Second, those pixels which now have at least one of their four directly abutted neighbors containing zero counts will be also set to zero; the remaining non-zero pixels are the pixels to be included in the analysis for the UFOV. This step shall be performed only once. Any pixel that has at least 50% of its area inside the CFOV shall be included within the CFOV analysis.

2.2.3.1 Integral Uniformity:

For pixels within each area (CFOV and UFOV), the maximum and the minimum values are to be found from the smoothed data. The difference between the maximum and the minimum is divided by the sum of these two values and multiplied by 100.

$$\text{Integral Uniformity} = \pm 100 * ((\text{Max} - \text{Min}) / (\text{Max} + \text{Min})) \quad \text{Equation 2-1}$$

2.2.3.2 Differential Uniformity:

For pixels within each area (FOV and UFOV) the largest difference between any two pixels within a set of 5 contiguous pixels in a row or column shall be calculated. The calculation shall be done for the X and the Y directions independently and the maximum change expressed as a percentage using the following:

$$\text{Differential Uniformity} = 100\% ((\text{Max} - \text{Min}) / (\text{Max} + \text{Min})) \quad \text{Equation 2-2}$$

The filtered data are treated as a number of rows (X slices) and columns (Y slices). Each slice is processed by starting at the beginning pixel for the respective field of view. A set of five contiguous pixels is examined to find the maximum and minimum pixels. The differential uniformity is calculated using these values. The next set of five pixels is analyzed by stepping forward one pixel and again determining the Percent uniformity. This is repeated until the outermost pixel is reached. The maximum differential Uniformity is found in the slice. This process is then repeated for all of the slices. (National Electrical Manufacturers Association recommendation 2001).

2.2.4 System Spatial Resolution without Scatter:

The system spatial resolution without scatter shall be measured and expressed as FWHM and FWTM of The line spread function the Measurement depends on the collimator, as well as the detector and must be repeated for each collimator type. The radionuclides employed for these measurements shall be those for which the collimators were designed. The count rate shall not exceed 20,000 cps for ^{99m}Tc a symmetric 15 percent energy window shall be used for other radionuclides the energy settings recommended by the manufacturer Shall be used. The test equipment required for these measurements shall consist of two capillary tubes with an inside diameter of less than or equal to 1.0 mm and a length greater than 30 mm. The capillary tubes shall be filled with the desired radionuclide. One of these tubes shall be positioned 100 Mm from the face of the system collimator and along the diameter corresponding to the axis of Measurement, X or Y. The digital sampling perpendicular to the tube shall be ≤ 0.1 FWHM and the digital sampling parallel to the tube shall be no greater than 30 millimeters. At least 10,000 counts shall be collected in the peak point of each line-spread function. measure the FWHM and FWTM in pixels of all the line spread functions that fall within the CFOV, first in The X direction and then in the Y direction. A second measurement for each axis shall be performed with the second capillary tube also positioned 100 mm from the face of the collimator and 50 mm away from, and parallel to, the first tube. This Measurement shall be used for calibration of the millimeters per pixel only. Convert the FWHM and FWTM measurements from pixels to millimeters, using the measured millimeter per pixel calibration factor. Average the measurements in both the X and Y directions.

2.2.5 Whole body System Spatial Resolution without Scatter:

System spatial resolution without scatter shall be measured parallel and perpendicular to the direction of Motion, and expressed as full width at half maximum (FWHM) and full width at tenth maximum (FWTM) of The line spread function. The measured values shall meet or exceed the specification. The radionuclide to be employed for this measurement shall be ^{99m}Tc . Any other radionuclide(s) Employed shall be separately reported. The activity of the source shall be adjusted to yield a count rate between 10,000 and 20,000 cps, through a 15 percent energy window, with two capillary tubes in the detector field of view. The camera shall be equipped with a collimator. The sources shall consist of two capillary tubes, each having an inside

diameter less than or equal to 1.0 Mm and a length of at least 200 mm. Sources shall be placed on the whole body scanning table, parallel to the plane of the detector.

2.2.5.1 Resolution Parallel to the Direction of Motion:

One capillary tube shall be placed at the center of the scanned field of view, perpendicular to the direction of motion to within 1 mm. The second source shall be placed parallel to the first one, at a distance of 100 Mm, (Figure 2-14a).

2.2.5.2 Resolution Perpendicular to the Direction of Motion:

One capillary tube shall be placed at the center of the scanned field of view, parallel to the direction of motion to within 1 mm. The second source shall be placed parallel to the first one, at a distance of 100 mm.

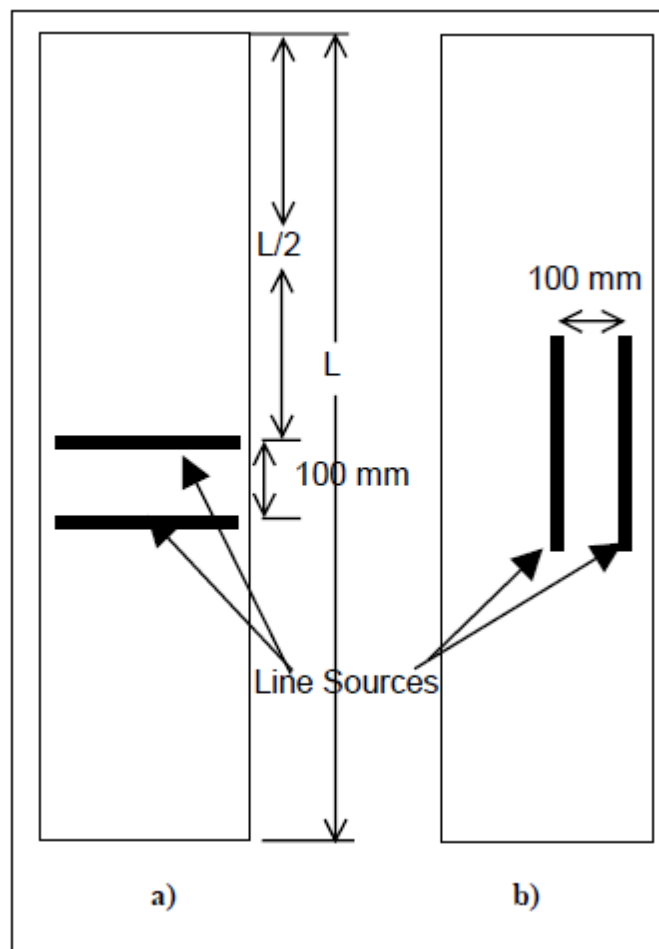


Fig 2-14: source position for whole body resolution measurements

A. Scan speed: The scan speed shall be in the range recommended for clinical use.

B. Camera position: Scans shall be performed with the detector both above and below the table for the two source orientations. The camera shall be positioned at a distance of 100 millimeters from the Sources to the face of the collimator.

C. Digital sampling: The digital sampling perpendicular to the tubes shall be no less than 0.25 of the FWHM of the system resolution of the collimator being used. The digital resolution parallel to the tubes shall be no less than 25 mm and no More than 30 mm. The average millimeters/pixel shall be calculated from the known line spacing. This calculation shall be done separately, parallel and perpendicular to the direction of the motion. The FWHM and FWTM shall be calculated in each segment of the central capillary tube. The values of the FWHM and FWTM shall be averaged separately for the tubes parallel and perpendicular to the Direction of motion (National Electrical Manufacturers Association recommendation 2001).

2.3 Secondary quality control tests of Gamma Camera Systems:

2.3.1 Intrinsic spatial linearity:

Intrinsic spatial differential and absolute linearity shall meet or exceed the specifications. Differential Linearity shall be expressed in millimeters as the standard deviation of the measured peak locations from a best fit line. Absolute linearity shall be expressed as the maximum displacement of any peak from the best Fit of a two dimensional grid. The radionuclide employed for this test shall be ^{99m}Tc . A source holder, which shields the source from walls, ceilings, and personnel without restricting the photon flux from the source to the camera, shall be employed. One or more copper plates may be used to adjust the count rate. The energy window for ^{99m}Tc shall be 15 percent centered on the photopeak. The count rate shall not exceed 20,000 cps through the energy window. If other radionuclides are used, the energy window should be set according to the manufacturer's recommendations. The test pattern shall consist of a lead mask in closest possible proximity to the crystal covering the entire UFOV with 1 millimeter wide parallel slits. Adjacent slit centers shall be 30 mm one from the other. The thickness of the mask shall be 3 millimeters for ^{99m}Tc or ^{57}Co . The lead mask with the parallel slits shall be positioned on the detector with the center slit centered on the detector. The center slit shall be perpendicular to the axis of measurement and aligned to within ± 1 Millimeter at the edge of the UFOV. The radionuclide shall be a point source centered at least five times the largest linear dimension of the UFOV above the lead mask with the parallel slits. The digital resolution perpendicular to the slits shall be less than or equal to 0.1 FWHM. The data shall be integrated parallel to the direction of

the slits to form line-spread functions. The digital resolution parallel to the direction of the slits shall be less than or equal to 30 mm. At least 1,000 counts shall be collected in the peak channel of each line spread function measurement after integration parallel to the direction of the slits. Two sets of data shall be acquired one with the slits in the X direction and one in the Y direction. If the data are acquired in a two dimensional matrix, the data shall be summed parallel to the direction of the slits to form line spread functions of width 30 mm or less. The distances between the peaks in each of the line spread functions shall be determined as the average of the interpolated half maximum locations on both sides of each peak. The half maximum locations shall be determined by linear interpolations from the nearest two neighboring points of the half peak value. The locations of the peaks shall be calculated for each subsequent line spread function. This will generate a two dimensional array of peak locations. One dimension will be along the slits and one will be perpendicular to the slits. Note that there will be two dimensional arrays, one from data acquired with slits in the X direction and the other with slits in the Y direction. The value of intrinsic spatial differential linearity (in pixels) shall be calculated as the standard deviation of the locations of the peaks in each slit. The standard deviations for the slits in the X and Y directions shall be averaged together. Separate values shall be calculated for the UFOV and for the CFOV. Intrinsic spatial absolute linearity shall be determined by fitting a two dimensional orthogonal grid of equally spaced points to the data using a least squares minimization technique. Different grids shall be fitted to the UFOV and to the CFOV data. There shall also be separate grids fitted for data acquired with the slits in the X and in the Y directions. The maximum displacement for each set shall be the largest difference between the data and the grid fit (in pixels) in the X or the Y direction. The millimeters per channel calibration factor shall be calculated as. This factor shall be used to convert the differential linearity and absolute linearity to millimeters.

2.3.2 Multiple window spatial registration:

Multiple window spatial registration is a measure of the camera's ability to accurately position photons of different energies when imaged through different photopeak energy windows. Measurements shall be made at nine specified points on the entrance plane of the scintillation camera. The measured values of multiple window spatial registration shall meet or exceed the specification. The radionuclide used to measure multiple window spatial registration shall be ^{67}Ga . The energy window settings for each of the three Gallium peaks shall be set as

recommended by the manufacturer. The count rate shall not exceed 10,000 counts per second through each photopeak energy window. A lead-lined source holder shall collimate the ^{67}Ga source through a cylindrical tunnel in the lead. This tunnel shall be 5 mm in diameter and 25 mm in length. Images shall be acquired using collimated ^{67}Ga source located at nine specific points on the entrance surface of the uncollimated camera. These nine points shall be the central point, four points on the X-axis and four points on the Y-axis. The off central points shall be located 0.4 times and 0.8 times the distance from the central point to the edge of the UFOV of the camera along the respective axes. Separate images of the collimated ^{67}Ga source shall be acquired through separate energy windows of the ^{67}Ga photopeaks at each of these image locations. These images shall be acquired with a pixel size of not more than 2.5 mm. For cameras with two energy windows, two images shall be acquired at each point; one is using the 93 KeV photopeak and the second using the 300 KeV Photopeak. For cameras with three or more energy windows, the 184 KeV photopeak shall also be Imaged. At least 1,000 counts shall be acquired in the peak pixel of each photopeak image. The displacement of the count centroid from each other in the X and Y directions shall be determined for each measurement point's photopeak images. A square region of interest (ROI) centered on the maximum count pixel associated with each photopeak image shall be used to analyze the individual photopeak images. The pixel dimensions of the square ROI shall be approximately four times the FWHM of the image count profile to be analyzed. Each image shall be integrated in the Y direction to determine the X count profile and integrated in the X direction to determine the Y count profile. The centroid of counts in the X and Y directions shall be determined for each image from that direction's count profile. The maximum difference in position of the centroid of counts acquired from each photopeak shall be determined. The largest pixel displacement shall then be converted to millimeters using an accurate millimeter per pixel calibration. The center of counts in the X and Y directions for each of the photopeak count profiles shall be determined as follows. Find the maximum count pixels in the integrated X or Y profile and calculate the centroid of counts using the following formula:

$$L_j = \sum_{i=1}^n (X_i \times C_i) / \sum_{i=1}^n C_i$$

Equation 2-3

Where:

JL = calculated centroid location for energy window j where j can equal 1,2 or 3.

IX = X or Y count profile pixel at the i th location

IC = counts at the X_i or Y_i location.

$$\sum_{i=1}^n$$

= is the sum over an odd number of count profile pixels centered on the maximum count profile pixel. The exact odd number of pixels will depend on the FWHM of the count Profile and the pixel size. The minimum number of pixels in this sum shall include both the Left and right half maximum counts.

The displacement D_{ij} between energy windows i and j is then:

$$D_{ij} = |L_i - L_j| \quad \text{Equation 2-4}$$

Where $i = 1, 2$ or 3 ; $j = 1, 2$ or 3 . The maximum displacement is simply the largest D_{ij} .

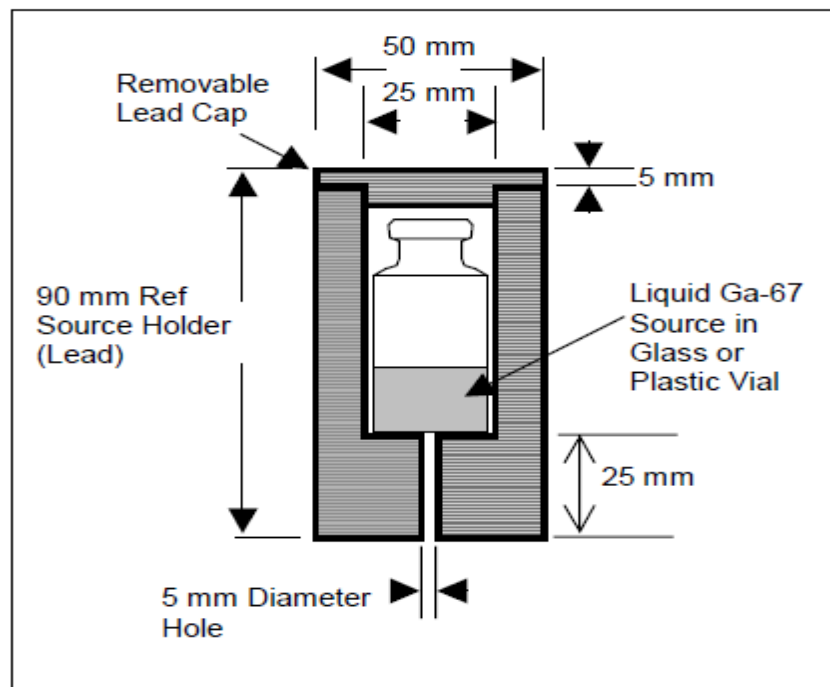


Figure 2-15 :Cylindrical source holder for multiple window spatial registration measurement showing liquid ga-67 source inside

2.3.3 Intrinsic count rate performance in air:

The decaying source method shall be used to determine count rate performance. Two parameters shall be measured and reported: observed count rate for a 20% count loss and a maximum count

rate. Both Parameters shall be measured without induced scatter. The curve of observed versus input count rates shall be provided. The radionuclide employed for the test shall be ^{99m}Tc . Any other radionuclide(s) employed shall be separately reported. The energy window for ^{99m}Tc shall be 15% Centered on the photopeak. For other radionuclides the energy settings recommended the manufacturer shall be used. Peaking shall be performed at a low count rate and shall not be manually readjusted during the test. A camera under test shall have the camera crystal masked to the UFOV. The open side (facing the camera crystal) shall be covered by 6 mm of copper plates. The source intensity shall be such that it produces an input count rate which is larger than the count rate required to cause fold over in the observed count rate. Determine the background count, N_{bkg} and the background count rate $rbkg = N_{bkg}/\Delta t_{bkg}$ **Equation 2-5**. The suggested time for this determination is 10 minutes. The lead holder with the source shall be placed in a suitable position in front of the detector. The source holder shall be positioned so that the collimated cone of radiation is centered within the UFOV and that the Irradiated area of the crystal extends fully across the smaller dimension of the UFOV. Care must be taken to minimize scatter. The start (t_i) and elapsed time (Δt_i) of the measurement shall be recorded for each data point, C_{ti} , where (i) is the number of the data point and C_{ti} is the number of counts recorded the time shall be measured relative to the start of acquisition time of the measurement of the first data Point. For each data point (C_{ti}), at least 100,000 counts shall be collected. Data should be acquired for 10 Sec. or 100,000 counts, which ever time is longer. The measurement should be performed so that the points are taken as soon as the observed count rate drops by 10,000 cps below the previous measured point. The last (n-th) point taken should be measured when the observed count rate drops below 4,000 cps. Each data point is first corrected for background:

$$C_i = C_{ti} - R_{bkg} \cdot \Delta t_i \text{ Equation 2-6}$$

The observed count rate (ocr_i) shall be determined for each data point according to the following Formula:

$$OCR_i = \frac{C_i \ln(2)}{T_{half} \cdot \{1 - \exp[(-\Delta t_i) \cdot \ln(2) / T_{half}]\}}$$

Equation 2-6

Where T-half is the half-life of ^{99m}Tc in the same units as t_i and Δt_i (21672 seconds). For decay of the source during the i' the measurement. The input count rate ($icri$) for each data point shall be calculated according to the following formula:

$$ICR_i = OCR_n \cdot \exp\left\{\frac{(t_n - t_i) \cdot \ln(2)}{T_{half}}\right\}$$

Equation 2-7

The observed count rate at 20% loss shall be determined by linear interpolation between the two closest Points to the equation: $Li = 0.8 \times icri$ **Equation 2-8**

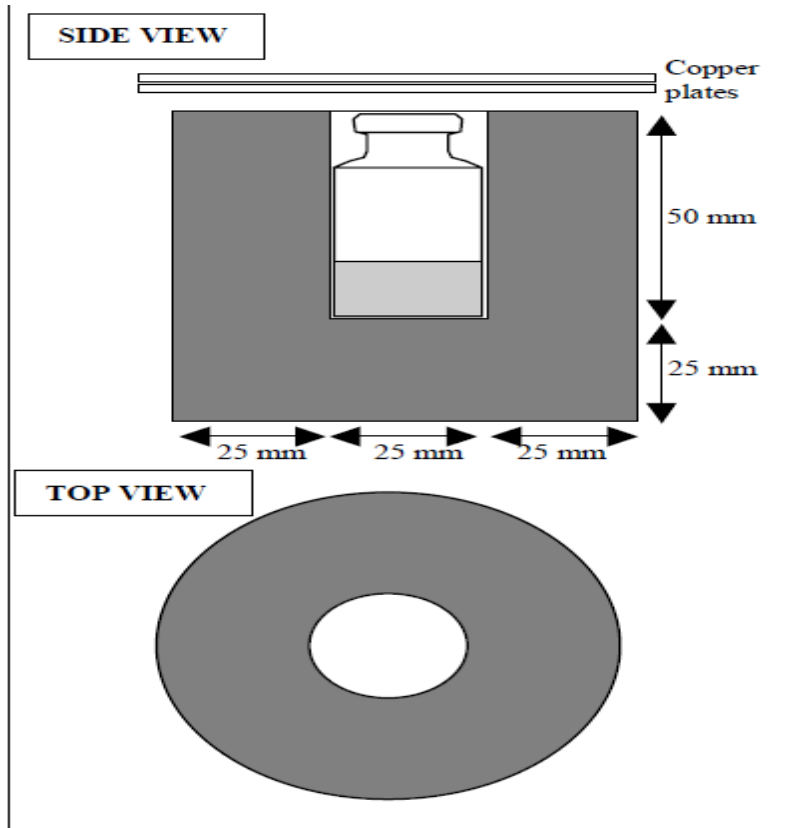


Figure 2-16: Source holder for count rate measurements

2.3.4 System Count Rate Performance with Scatter:

The decaying source method shall be used to determine count rate performance with scatter. Two Parameters shall be measured and reported: observed count rate for a 20% count loss and a maximum count rate. Both parameters shall be measured with induced scatter. The curve of observed versus input count rates shall be provided. The radionuclide employed for the test shall be ^{99m}Tc . Any other radionuclide(s) employed shall be separately reported. The energy window for ^{99m}Tc shall be 15 percent centered on the photopeak. For other radionuclides the energy window used shall be that recommended by the manufacture. Peaking shall be performed at a

low count rate and shall not be manually readjusted during the test. A camera under test shall have a low energy collimator mounted. The source shall be in a water solution filling a disk container. The source intensity shall be such that it produces an input count rate which is larger than the count rate required causing fold over in the observed count rate. The source shall be placed within a plastic cylindrical phantom. (The Phantom may be all acrylic, or may be water filled. The well above the source holder is also filled with Acrylic or water.) The detector shall be positioned to view the 50 mm thick plastic base of the phantom. The distance between the phantom and the face of the collimator shall not be greater than 20 mm. The phantom shall be centered within the UFOV. Prior to the beginning of the measurement, the background count rate, N_{bkg} shall be determined. The start (t_i) and elapsed time (Δt_i) of the measurement shall be recorded for each data point, where (i) is the number of the data point. The time shall be measured relative to the start of acquisition time of the measurement of the first data point. For each data point (C_i), at least 100,000 counts shall be collected. Data should be acquired for 10 Sec. Or 100,000 counts, whichever time is longer. The measurement should be performed so that the points are taken as soon as the observed count rate drops by 10,000 cps below the previous measured point. The last (n-th) point taken should be measured when an observed count rate drops below 4,000 cps (National Electrical Manufacturers Association recommendation 2001).

2.3.5 Intrinsic Spatial Resolution at 75,000 Counts per Second:

Intrinsic spatial resolution shall be measured at 75,000 counts per second measured values of average FWHM and average FWTM shall be reported. The measured values shall meet or exceed the specification.

2.3.6 Intrinsic Flood Field Uniformity at 75,000 Counts per Second:

Intrinsic flood field uniformity shall be measured at 75,000 counts per second. Integral and Differential Uniformity for both CFOV and UFOV shall be calculated

2.3.7 System Spatial Resolution with Scatter:

The system spatial resolution with scatter shall be measured and expressed as FWHM and FWTM of the Line spread function the measurement depends on the collimator, as well as the detector, the measurement must be made with each collimator type. The radionuclides employed for these measurements shall be those for which the collimators were designed. The count rate shall not exceed 20,000 cps through a symmetric 15 percent energy window or windows. For

other radionuclides the energy settings recommended by the manufacturer shall be used. The test equipment required for these measurements shall consist of two capillary tubes with an inside diameter of less than or equal to 1.0 mm and a length greater than 30 mm. Also required are acrylic scattering blocks, the size of the UFOV of the system to be measured and 100 and 50 mm thick. The required acrylic scattering thickness may be assembled from thinner pieces but still must cover the entire UFOV. The capillary tubes shall be filled with the desired radionuclide. 100 mm of acrylic scattering block shall be positioned immediately in front of the collimator and one of the capillary tubes shall be positioned as close as possible to the block. The other 50 mm of scattering shall be positioned on the other side of the capillary tube. The digital sampling resolution perpendicular to the tube shall be ≤ 0.1 FWHM and the digital sampling parallel to the tube shall be no greater than 30 millimeters. At least 10,000 counts shall be collected in the Peak point of each line-spread function. Measure the FWHM and FWTM in pixels of all the line spread functions that fall within the CFOV, first in the X direction and then in the Y direction. A second measurement for each axis shall be performed with the second capillary tube also positioned 100 mm from the face of the collimator and 50 mm away from, and parallel to, the first tube. This measurement shall be used for calibration of the millimeters per pixel only. Convert the FWHM and FWTM measurements from pixels to millimeters, using the measured millimeter Per pixel calibration factor. Average the measurements in both the X and Y directions together.

2.3.8 System Planar Sensitivity and Penetration:

The system planar sensitivity is the ratio of collimated counts detected in one acquisition plane to the activity of a specific planar source placed parallel to that plane. However, detected counts may also arise from radiation which penetrates or scatters off the septa of the collimator. This penetrated or scattered radiation degrades the overall image quality and thus should be considered separately from the sensitivity due to properly collimated counts. Both system planar sensitivity and penetration depend on the collimator type, window width, gamma energy, source configuration and system factors. Therefore, the configuration of these system variables for the purpose of this measurement should match those employed in clinical settings unless explicitly noted otherwise. The planar sensitivity and penetration fraction of the system shall be measured for each collimator type with the appropriate isotopes and reported in (counts/sec)/mbq. This measurement relies on the accuracy of the calibration of the radionuclide activity, and therefore

the specification shall be for typical devices of this model. The radionuclides employed for these measurements shall be those for which the collimators are designed. The count rate shall be less than 30,000 counts per second through a symmetric 15% energy window (for ^{99m}Tc). If other radionuclides are used, the energy settings used should be those recommended by the manufacturer. The test equipment required for this measurement consists of a 1 to 5 cc plastic syringe, a 30 to 50 cc plastic syringe, a calibrated dose calibrator, and a 100 mm diameter flat plastic dish. The source activity inside the plastic syringe, ASR, shall be accurately measured using a dose calibrator. This source shall then be dispersed from the syringe into water in a 150 mm diameter flat plastic Phantom. The residual activity remaining in the syringe, ARES shall be promptly measured in the dose calibrator and the reading subtracted from the original reading to obtain the amount of activity in the phantom, $ACAL = ASR - ARES$, at the time of preparation. Calibration methods shall be those set forth in the NRC Regulatory Guide 10.8, or alternatively NIST Traceable calibration sources shall be used as references with appropriate half-life corrections. The measurements of syringe activity should be reproducible to better than 5%. All measurement times should be recorded to at least the nearest minute, or 1% the half-life of the radionuclide, whichever is more precise. A consistent clock should be used for all time measurements. The prepared phantom shall be placed near the center of the field of view and in a plane such that the bottom inside face of the phantom is 10 ± 1 mm from the face of the detector. It may be helpful to determine this distance using a 10 mm spacer and an empty phantom. No scatter material shall be present. It is critical that the base of the phantom is level such that the activity is distributed evenly. Acquire at least 4 million counts with the imaging system. Record the start time of the acquisition to the precision stated above. The duration of the acquisition should be measured with a precision of better than 1%. Repeat this measurement for the same number of counts with the bottom inside face of the phantom 20 ± 1 , 50 ± 1 , 100 ± 1 , 150 ± 1 , 200 ± 1 , 250 ± 1 , 300 ± 1 , 350 ± 1 and 400 ± 1 mm from the face of the collimator. The phantom should be near the center of the field-of-view and in the plane of the detector for all Measurements. For each acquisition sum the number of counts in a circular ROI which is 60% of the diameter of the Phantom and centered over the region of activity. Include pixels with their centers within the ROI. Determine the decay-corrected count rate for the acquisition (National Electrical Manufacturers Association recommendation 2001).

2. 3.9 Detector Shielding:

The detector shielding measurements assess the sensitivity of the gamma camera detector to:

A) Radioactivity in the patient being imaged which lies outside the field of view.

B) Stray sources of radiation that might be present in the vicinity of the camera (e.g. Patients in adjoining examination rooms or patients awaiting examination who have been injected with a radioactive tracer). To assess the effectiveness for case (a), measurements are made of the leakage from a test source Positioned outside the field of view in the plane of the patient table. To assess the effectiveness of Shielding for stray sources, case (b), measurements are made of the count rates obtained from sources Positioned at two meters from the detector at the side and in front of the system. The measured values of Detector shielding shall meet or exceed the specification. The radionuclides employed for these Measurements shall be those for which the system is designed. Measurements shall be made with Tc-99m and with the highest energy nuclide for Which the camera is specified to operate (or the Highest energy that is expected to be used). The Amount of radioactivity shall be sufficient to generate a count rate of at least 1,000 cps and not More than 30,000 cps through the collimator at the First imaging position (centered under the Collimator). For Tc-99m a 15% energy window shall be used. For other radionuclides, the manufacturer's recommended energy settings for the nuclide being tested should be used. The collimator used shall be that recommended for imaging the test isotope. The test equipment required for this measurement Consists of a 1 to 5 cc plastic vial containing the Radionuclide source. A) The unshielded source shall be placed on the Imaging table under the collimator. The detector shall be positioned 20 cm above the table and facing down. The count rate shall be measured at fixed positions starting with the source centered in the field of view, then at 10 cm, 20 cm, 30 cm outside the edge of the field of view, in each direction (seven measurements in all). At each source position, i , the number of counts, cai , collected in time, tai , shall be recorded. Cai shall be greater than 10,000. A) Background count rate, CB , shall be measured by Collecting counts for one minute or longer. B) To assess the effectiveness of the shielding in relation to stray sources two additional sets of measurements are required. A source similar to that used in part(a) is positioned two meters from the detector and directly in front of it and one meter above the floor. The source may be shielded with the open end of the shield pointing directly toward the detector. The count rate shall be measured with the detector positioned at each of 4 equally spaced positions in a 360 degree arc used for tomographic acquisitions (i.e. With the detector

facing up, down, left, and right). At each of these positions the number of counts, c_{fi} , in the time t_{fi} , is recorded. The source and source holder is then positioned 2 meters to the side of the gantry and one meter from the floor. The source holder opening should be pointed directly at the detector during the measurement. Measurements of count rate are then made with the detector at three positions: with the detector facing up, down, and away from the source. At each of these positions the number of counts, CS_i , in the time TS_i , is recorded. For each of the source positions compute the background-subtracted count rate:

$$B_{ci} = (c_{ai} - CB)/t_{ai}$$

$$B_{c_{fi}} = (c_{fi} - CB)/t_{fi} \text{ Equations 3-12}$$

$$B_{c_{si}} = (c_{si} - CB)/TS_i$$

The shield leakage is expressed as the count rate (minus background) at each position, as a percentage Of the count rate (minus background) when the source was in the central position (BC_0):

$$L_i = 100 * b_{ci}/BC_0$$

$$L_{f_i} = 100 * b_{f_i}/BC_0 \text{ Equation 3-13}$$

$$L_{s_i} = 100 * b_{s_i}/BC_0.$$

The largest of the count rate measurements for each position shall be identified; i.e. the largest of the L_i (excluding $i=0$), the largest of the L_{f_i} , and the largest of the L_{s_i} , (excluding the three values where the Detector points towards the source). (National Electrical Manufacturers Association recommendation 2001).

2.3.10 system volume sensitivity:

The system volume sensitivity shall be measured and the average volume sensitivity per axial centimeter determined from this measurement. The system volume sensitivity is the total system sensitivity to a uniform concentration of activity in a specific cylindrical phantom. System volume sensitivity measurements are dependent on detector configuration, collimator type, radionuclide type, energy window Setting, source configuration and other factors. The radionuclides employed for these measurements shall be those for which the collimators were designed. The measurement count rate for each projection image shall be $10,000 \pm 2000$ cps through a symmetric 15 percent photopeak energy window or windows. For other radionuclides, the manufacturer's recommended energy settings for the nuclide being tested should be used. The test equipment required for this measurement consists of a plastic syringe, an accurate dose

Calibrator and a specified 200 mm diameter cylindrical phantom (Figure 3-7). Accurately determine the activity concentration in K_{Bq}/cm³ within the specified cylindrical phantom at Initial time *T_i*. This is done by dividing the measured activity placed in the phantom at *T_i* by the measured volume of water in the phantom. This well mixed and uniform cylindrical source shall be positioned in the center of the system's image space with its symmetry Axis coincident within ± 5 mm of the axis of rotation of The SPECT system. perform a 360° circular orbit SPECT acquisition of Radius 150 ± 5 mm. At least 120 but not more than 128 Different projection angle images shall be acquired. Each projection image shall contain 100,000 ± 20,000 Counts through a 15 percent symmetric photopeak window. For multi-head systems, the images from all Heads may be summed to achieve the required number of projection images. Field uniformity correction Devices, or any other mechanisms which alter the Number of counts in these projection images, must be Disabled. Measure the total elapsed time to complete the required 360° SPECT acquisition. Also measure and sum the Counts from all the projection images to determine the Total counts detected in this total elapsed time. The system volume sensitivity (SVS) is then:

$$SVS = \frac{A(cts / sec)}{B_c(MBq / cm^3)}$$

The volume sensitivity per axial centimeter, VSAC, is then determined by dividing the SVS by the axial Length of the cylindrical source (i.e., 20 cm).

$$VSAC = \frac{SVS}{Length}$$

If the total length of the source cannot be used to obtain the volume sensitivity measurement, the actual Length used must be stated along with the results.

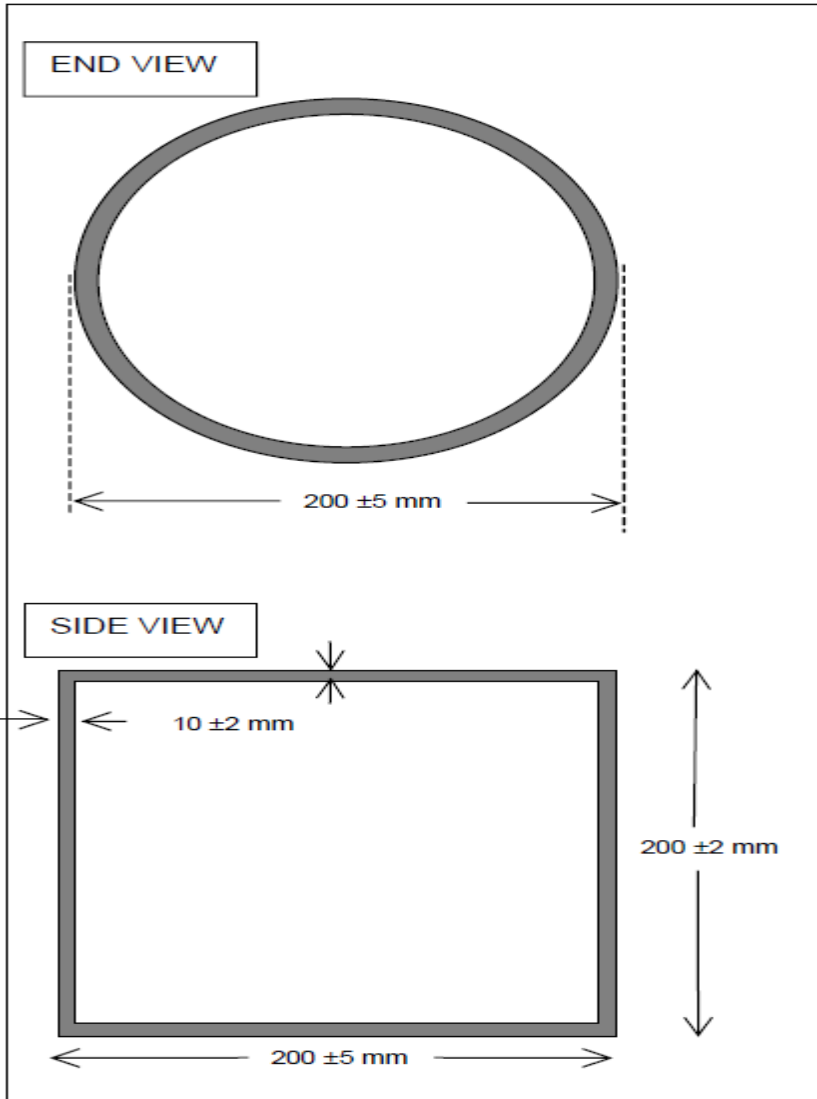


Figure 2-17: volume sensitivity cylindrical phantom (acrylic)

2-4 previous studies

A Vickery et.al (2011) developed software programme for gamma camera quality control based on NEMA NU-1 2007, Within Nuclear Medicine, image abnormalities and artifacts affecting the quality of images are well known phenomena. Therefore, it is of great importance to have a thorough Quality Assurance for gamma and SPECT cameras to minimize the occurrence of these abnormalities and artifacts. NEMA has made recommendations of routine quality control for nuclear medicine instrumentation. After installation and before the camera is put into clinical use, it should undergo National Electrical Manufacturers Association (NEMA) Performance standard measurements to verify that the camera performs according to specification supplied by the manufacturer and to establish baseline conditions for all future measurements. The NEMA Standards Publication NU 1-2007 describes how to perform process and report QC tests for gamma and SPECT cameras. Often, with support from the manufacturers, all necessary phantoms can be supplied and acquisitions can be done according to NEMA, but a thorough Quality Assurance also requires a careful handling of the measured QC data. The software is based on NEMA recommendations regarding processing and analysis of the data, and runs in MATLAB (Mathworks, Natick, Massachusetts, USA). It is capable of calculating Intrinsic Spatial Resolution and Linearity (ISR & ISL), Intrinsic Energy Resolution (IER), Intrinsic Flood Field Uniformity (IFFU), Multiple Window Spatial Resolution (MWSR), Intrinsic Count Rate Performance (ICRP), System Spatial/Scan Resolution (SSPR & SSCR), System Planar Sensitivity (SPS), System Alignment (SA), System Volume Sensitivity (SVS) and SPECT Reconstructed Spatial Resolution (SRSR). The data handling programs are aimed at making the processing of acquired QC-data a simple task, providing the users with instructive images of the processed data as well as text files containing the results of the QC. Results processed with different software and for different SPECT the researchers demonstrated that whom software is able to calculate several NEMA-specifications, and where possible, the results were compared to those obtained by the manufacturers. And there is an agreement between our software and the manufacturers' software. A novel quantitative analysis of orthogonal hole and quadrant phantoms was presented. The selection of the platform used to code the software was MATLAB, which, in principal, is independent of the operating system. Future development could be the compilation of our software, making it independent of the MATLAB environment and an

automatic report-generation using e.g. LaTeX. It is whom vision that the software will be open access.

A.H.Ng et.al. (2008) developed a simple sphere phantom for routine performance test of Single Photon Emission Computed Tomography (SPECT) gamma camera to be use in situation where the commercial expensive phantom is not available. The design of the low cost phantom was based on the common parameters measured using commercial phantom; these parameters are spatial resolution, contrast and sensitivity. The design of house phantom was based on the design of Perkins et.al. (2007). The phantom was consist of combination between the abdomen Computed Tomography (CT) phantom and acrylic support and based constructed in an (L) shape originally designed with circular array of blind hubs to hold laver lock syringes in a perpendicular array. The angle between each holder was 60° and the diameter across two opposite holder was 100mm. when filled with radioactivity the syringe would form standard source of radioactivity in a reproducible configuration, so that they seen as parallel rods during image reconstruction. All imaging of phantom was carried out at university of Malaya using a triple detector SPECT camera (Philips IRIX, USA). The scanning time and injected activity of the performance test evaluation recommended by NEMA-1 (2001). The sphere was filled with a range of concentration of ^{99m}Tc between 58 and 101MBqmL⁻¹. The phantom was placed on the couch and SPECT acquisition was performed using 120 continuous scanning modes with incremental views of 3° each time of acquisition with 90 min and the images were reconstructed on an Odyssey lx computer using filter back projection for 128X128 matrix size. In comparison, the cost of new phantom was 703 dollar while the commercial one was 2050 dollar. The first and obvious difference between the phantoms was that the sphere test was designed to measure hot spot detection, whereas the Jaszczak phantom demonstrated cold spot detection. The Jaszczak phantom required a nominal 750MBq or higher activity for use, while the sphere phantom could be used with less than 50% of that activity (of the order of 370 MBq). Increasing sphere volumes from 0.55 to 2.60 mL resulted in increase in contract. However a saturation effect was observed for higher volume. They lack from numerical result of the essential SPECT test, so the comparison of result to that of Jaszczak phantom was shorted. This phantom has advantage to do spatial resolution, linearity, uniformity, hot and cold contract, lesion detect ability and object size while the phantom cannot measure the Center of rotation (COR).

Alain Seret (2010) performed and assessed all primary and some secondary NEMA-NU1-2001 performance test on two Brightview Philips cameras and two hybrid cameras with computed tomography (CT) named Brightview XCT Philips system installed 2009 in institute of physics Belgium. The materials used was four Philips camera fitted with a 9.5mm thick NaI crystal, 9.28mm pixel size with 64X64 matrix size and the activity used was measured using Veenstra VDC-405 activity meter. The primary NEMA tests as well as intrinsic linearity and system sensitivity was performed using ^{99m}Tc with LEHR collimator fitted. Multiple window spatial registration was performed with ^{67}Ga on one SPECT-CT camera. The Philips jet stream reconstruction tools were used for SPECT reconstruction with filtered back projection reconstruction and a ramp filter without cutoff used. The data processed according to NEMA NU1-2001 using the NEMA package of the Philips Pegasus (Brightview) or EBW (Brightview XCT) software. The result showed that the Multiple window spatial registration was 0.55 ± 1.5 with ^{67}Ga , the measured sensitivity were 73.5 ± 1.5 cps/MBq for LEHR collimator and ^{99m}Tc , and 94.1 ± 2.6 cps/MBq for medium energy collimator and ^{67}Ga , and 47.0 ± 1.3 cps/MBq for high energy collimator and ^{131}I . The relationship between input and output count rate was found to be strictly linear up to a minimum of 30 Kcps for all heads. The maximum count rate was 239.8 ± 3.3 Kcps and the observed count rate at 20% loss was 238.8 ± 4.0 Kcps. The mean average distance between the SPECT and CT images was 1.34 ± 0.57 mm and the maximum differences distance was 1.93 ± 0.58 mm. Spatial resolution in UFOV is 3.17mm, resolution in CFOV FWHM 3.12mm, Spatial linearity in UFOV is 0.27, Spatial linearity in CFOV is 0.20mm Differential. The most important feature of this study was probably the opportunity to perform the NEMA tests on four SPECT cameras located in the same nuclear medicine department. Indeed, most of the NEMA data available in the literature were obtained on one single system. The measured parameters were almost identical for all the tested systems, and the vast majority of measurements were within manufacturer's specifications. The only exceptions were some of the uniformity indexes of two of the heads, but a new calibration solved the problem. The results obtained for the hybrid and stand-alone systems were very similar.

Andrew Rova et.al (2007) developed software programme for gamma camera quality control based on National Manufacture Electric Associations (NEMA). The programme language selected by the researchers was MATLAB because it offers programming simplicity and offer excellent image processing and plotting capacities and features built –in digital image and communication (DICOM support. Another attractive feature of MATLAB is the graphical users interface (GUI) design environment. This drag-and-drop user interface design tool allowed quick prototyping of the application user’s interface. Also the main advantage of MATLAB is the user can get MATLAB copy to execute or programme without complicating license requirement. By installing the free MATLAB common runtime (MCR) any one can run our software, even if they do not Owen a license for MATLAB or the image processing toolbox. MATLAB is used and accepted in both industry and academia to a degree which gives the researchers confidence that, despite being a private company offering. MATLAB is a safe choice in term of both longevity and cross-platform support. The nuclear medicine quality control software (NMQC) designed by researchers can read image and header information from DICOM files, which have become a generally recognized format for medical imaging file and also support interfile format which is still used in older nuclear medicine camera. The basic design principle of NMQC was to closely follow (NEMA) recommendation regarding processing and analysis of the data. The NMQC software has ability to measure uniformity, profile analysis, center of rotation evaluation, tomographic uniformity measurement, planer uniformity trend analysis and other wide range of gamma camera quality control tests. NMQC software runs on Microsoft Windows, Linux, Apple’s Mac Os X, and Sun Solaris. NMQC software has been tested on numerous gamma camera models, including GE Infinia and Infinia Hawkeys, Soph-GE DST; Philips Forte, Skylight and Vertex; and Siemens Ecam, MS2, MS3, DIACAM, orbiter and Symbia Cameras.

Connor et al. (2000) discussed the parameters used to evaluate the gamma camera quality control and the factor that affect the result of this parameter. There are a large number of factors that contribute to the final image quality including uniformity, resolution (intrinsic and energy), collimation and the hard copy device. The most sensitive parameter to change in system performance is system uniformity. The change in photopeak location, photo multiplayer tube performance, energy and linearity correction all affect the image uniformity. Uniformity measurement can be performed intrinsically using a small ($<100\mu\text{Ci}$) $^{99\text{m}}\text{Tc}$ point source placed at a distance of four time the detectors Field of View (FOV), or can be measured extrinsically

using either a solid disk of ^{57}Co or plastic phantom source containing $^{99\text{m}}\text{Tc}$ mixture in water. The disadvantage of intrinsic measurement is the remove of collimator which may result in crystal fracture, while the disadvantage of extrinsic measurement is the time taken in preparing the source and the consequential radiation exposure to the technologist. All of these problems can be avoided by careful preparation of the sheet source and by routine inspection of the source to check for warping, leakage or distortion of plastic. Measurement of system resolution and/or linearity was generally performed on a weekly basis and can be performed using either intrinsic or extrinsic technique. To evaluate the spatial resolution of the gamma camera, a wide variety of test patterns have been developed over the years. The most common test pattern is the four quadrants bar phantom, which account for over 80% of all resolution patterns used in nuclear medicine. The BRH and Hine Duley phantom can also be used to measure spatial resolution. Under most circumstances, intrinsic measurement is preferable to extrinsic measurement even though the intrinsic one has the disadvantage of attendant risk to the crystal. As to researcher experience the parameter of spatial resolution and linearity tend to be a very stable parameter and will often remain unchanged even in the presence of significant changes in image uniformity. The 4-quadrant bar phantom is the most commonly used phantom for measurement of system resolution, it is not ideally suited to the assessment of system linearity. Hence, test patterns such as the orthogonal hole pattern or the parallel line equal spacing phantom are preferable to the four-quadrant phantom as they allow assessment of both linearity and resolution. The international atomic (IAEA) and the national electrical manufacturing association (NEMA) presented details discussed to this parameter at year 2001 (NEMA-2001 and IAEA-TECDOC-602) while this work was presented at the year 2000, but there was no significant differences between the methods of uniformity, linearity and resolution before and after the year 2001.

D Minarik et al. (2008) designed phantom to implement simulation of bremsstrahlung imaging in the SIMIND code and to validate simulations against experimental measurements, to investigate the image quality of clinical bremsstrahlung Single Photon Emission Computed Tomography (SPECT) imaging and to evaluate the quantitative accuracy for liver and tumor-shaped sources, using phantom studies. Also to investigate the improvement obtained by applying model-based attenuation, scatter and collimator-detector response compensations in the reconstruction of SPECT image. ^{90}Y is rare-earth metal emit beta with mean energy of 0.935 MeV

and used in treatment of some malignant disease especially non-Hodgkin's lymphoma. Lack of gamma ray is a disadvantage in calculation of pre-therapy dose. ^{111}In is chemically similar to ^{90}Y but two problems associated with ^{111}In when used as pre-therapy dose calculation and post-therapy evaluation, the first problem is that free ^{111}In have different biokinetics of free ^{90}Y , the second problem is that the contribution to the image from bremsstrahlung generated by the β -particles emitted by ^{90}Y probably affects the measurement of ^{111}In . If the quantitative accuracy of the bremsstrahlung imaging is sufficiently accurate, it will also be possible to investigate the consistency of the Dosimetry estimates between ^{111}In -based pre-therapy and ^{90}Y -based therapy studies. To perform patient-specific Dosimetry, one needs to apply quantitative methods to correct for scatter, photon attenuation and the degradation in spatial resolution due to the design of the collimator. This can, to some extent, be made in planar scintillation camera imaging using the conjugate-view method, but generally SPECT is preferred. Several problems associated with use of ^{90}Y bremsstrahlung imaging for quantitative imaging especially when using SPECT camera which are, very complex energy spectrum and, photon scattered from patient. Bremsstrahlung spectra for water, soft tissue and bone were generated with the MCNPX Monte Carlo program by simulating a ^{90}Y point source located in the center of a sphere, the amount of created bremsstrahlung photons was determined as a function of energy as they passed the surface of the sphere. Also a measurement was performed with a high-purity germanium detector (HPGe). To evaluate the ability of the SIMIND program to simulate accurate bremsstrahlung images, a comparison between measurements and corresponding simulations was performed using a 1 mL plastic syringe as a small cylindrical source, the syringe had an inner diameter of 4 mm, an outer diameter of 6.5 mm and a length of 65 mm, and was filled with a solution of ^{90}Y up to a length of 60 mm, three measurements were performed with source-to-collimator distances of 10 cm, 20 cm and 30 cm, respectively. The camera system was a hybrid SPECT/CT Discovery VH system (General Electric Medical Systems, Milwaukee, USA) with a 25.4 mm thick NaI (Tl) crystal, the measurement was made with a high-energy general-purpose (HEGP) collimator and a 60% energy window centered at 150 keV. Also the researchers used the RSD thorax phantom (Radiological Support Services Inc., Long Beach, CA) with activity uniformly distributed in the liver insert, measurements were conducted without background activity, and with a liver-to-background activity ratio of 10:1, measurements were also performed using an elliptical water phantom (Data Spectrum Inc., Hillsborough, NC) with activity filled in a sphere with an inner

diameter of 60 mm without background activity, the same collimator and energy window settings that were used for the syringe measurement were applied. Also the camera sensitivity was measured using Petri dish containing a thin layer of ^{90}Y with an activity of 104 MBq. Also images of real patient were performed to the patient already treated with ^{90}Y using SPECT/CT camera. All images were reconstructed using program developed by Frey et al. The result of this study showed that the percentage number of emitted bremsstrahlung photon per decay was 2.20, 2.23 and 4.39% for energies from 50KeV to maximum electron energy. The Full width at Half Maximum (FWHM) was 13.8, 18.3 and 23.8mm for 10, 20 and 30 cm respectively, and the Full Width at Ten Maximum (FWTM) were 26.6, 33.7 and 42.5mm for 10, 20 and 30 cm respectively.

E.Porras et.al. (2002) developed and clinically tested a small, portable, and low cost gamma camera for medical application. The mini gamma camera has an overall size of 95mm in diameter and 240mm length, and total weight of 3 Kg. both, small dimension and light weight ensure the mobility of the system, which was one of the key points of researcher design. The camera was optimizing for $^{99\text{m}}\text{Tc}$ emitting at 140KeV. The camera composed of a collimator, a circular scintillator crystal coupled to a position sensitive photomultiplier tube (PSPMTs). The collimator has hexagonal parallel holes lead (1.2mm diameter holes, 0.2mm of septal thickness and 35mm long) providing about 120 cpm/ μCi of nominal geometric efficiency. The scintillation crystal used has dimension of 51mm made from CsI (Na) with white painted entrance face and black edge. Geant-3 and Detect 2000 package was used. The photomultiplier tube used was Hamamatsu R2486 PSPMT that enables the acquisition of 2-dimensional information providing 4 signals (2X + 2Y) and has an effective area of 50 mm diameter. Physical measurements according to the National Electrical Manufacture Association (NEMA) have been performed in order to evaluate the camera performance. The researchers adapt the NEMA protocol to be useful for the mini gamma camera because NEMA protocol developed to be using in large system. The sources used include a 2mm diameter point source, 2mm capillary tube source and a 6cm diameter plastic Petri dish for a uniform flood source. The intrinsic spatial resolution was measured as Full Width at Half Maximum (FWHM) for Useful Field Of View (UFOV) (2.2mm) and Central Field Of View (CFOV) (1.6mm) while the extrinsic spatial resolution measured with scatter (4.2mm) and without scatter (3.2mm). The differential linearity is 0.2 and 0.1mm,

absolute linearity is 1.3 and 1.1, intrinsic absolute uniformity 93.6% and 41.3% and the extrinsic absolute activity are 73.1% and 49.9% for both UFOV and CFOV respectively. The system energy resolution is 12.8% at 140KeV. The system planer sensitivity is 104.7cpm/ μ Ci. System dead time is 26.6 μ s. the result showed that there was no variations depending on the slit orientation but, as researcher expected, best values are obtained at the CFOV. The researcher used MLPE as reconstruction methods because it work well when using parallel hole collimator and, furthermore, allows reconstruction on real-time. A clinical test was performed on a thyroid phantom using ^{99m}Tc with a total activity of 200 μ Ci, showed that the system produced high quality images of a real thyroid with the usual dose (2mCi) in an about 10min.

Elshemey et.al (2013) evaluated the effect of scatter radiation on the performance of the gamma camera specially the extrinsic sensitivity and counting efficiency using a specially designed home-made phantom. An acrylic cylindrical phantom was constructed, providing a cylindrical distribution of ^{99m}Tc , made from Perspex and glass with diameter of 0.32mm, a height of 0.25mm and thickness of 25mm. the gamma camera used was Symbia SPECT/CT, Siemens, Germany with low energy parallel hole general purpose collimator and 59 photo multi player tubes, the thickness of the crystal was 9.9mm. The phantom was filled with water up to 12mm, and then ^{99m}Tc was injected with activity of 0.2 \pm 0.01GBq. the energy spectrum was then acquired at different source level 50, 100, 150 and 200 mm. only one head (facing the ceiling) of the dual head camera was used in the acquisition of the energy spectrum. The scattered fraction was calculated from the energy spectrum. The shape of the photopeak at 140KeV does not noticeably change with source thickness, but there was a gradual increase in the scattered photon energy (133-153 Kev) due to the increase in probability of multiple scattering of photon inside thicker source. The scatter fraction increased with increasing source thickness, from 0.29 up to 22.96. a decrease in the calculated extrinsic sensitivity, from 121.36 to 49.58 counts/s GBq at SDD $\frac{1}{4}$ 0.7 m with uncertainty ranging from 0.23 to 0.09 counts/s GBq ,respectively, with flood source thickness (from 12to200mm) at different source-to-detector distance (from SDD $\frac{1}{4}$ 0.7 to1.1m). With the increase in source -to- detector distance, the extrinsic sensitivity decreases (e.g. from 121.36 to 118.77 counts/s GBq at source thickness $\frac{1}{4}$ 12 mm). The reduction in the extrinsic sensitivity with increasing SDD is significant, beyond uncertainties. For example, at a flood source thickness of 12mm, the extrinsic sensitivity values were 121.29, 119.99 and 118.73 counts/s GBq, while the uncertainties were 0.23, 0.1and 0.15 counts/s GBq for SDD $\frac{1}{4}$ 0.7, 0.9

and 1.1m, respectively. Above results indicate that an increase in SDD is associated with an increase in extrinsic efficiency ; and a decrease in extrinsic sensitivity of both the extrinsic efficiency and the extrinsic sensitivity Vs SDD for H¹⁴ 12 and 200 mm, respectively. The results of this work indicate that instead of performing gamma camera QA using the common thin flood source, a thicker source would probably be more realistic. Such a source incorporate into account the effect of scattered radiation practically encountered when a patient is imaged using a gamma camera. It also shows that a source-to-detector distance equal to $0.967 \pm 9 \times 10^{-3}$ m represents a possible compromise for calculating the extrinsic sensitivity at areas on able counting efficiency in gamma camera QA tests.

Fernanda Carla et.al. (2010) designed and developed liver phantom has artifacts that simulate nodules and take different quantities, location and size and may also be mounted without the introduction of nodules. The objective of this study was to developed a liver phantom for quality control and training in nuclear medicine, and also may used specifically in spatial resolution test of the gamma camera, also it permit simulation of experiments to evaluate changes in the image caused by source distance variation and to assist in the choice of image matrix size and the selection of the optimum energy window system in image acquisition. The design of this liver phantom simulator was based on models already in use in nuclear medicine, include, the design of this liver phantom simulator was based on models already in use in nuclear medicine, include, the multi Contrast / Resolution phantom and the Jaszczak phantom. The phantom consists of three 28cm -30 cm -2 cm a crylic plates and an a crylic plate of 28cm-30 cm-5 cm, hollowed out in the centre and with the geometry of an adult liver. The final thickness of the liver phantom is 9.0cm. For the tests, the researcher used two gamma cameras, the Elscint SP4 and Milleniums MG. Simulations were performed using ^{99m}Tc diluted in water. Images for the analysis of simulated liver scintigraphy were obtained using a detector device located 5cm from the anterior surface of the phantom. Using a 32 _32 matrix size it was not possible to obtain diagnostic images. The higher the energy window, the greater was the loss of spatial resolution due to the detection of a larger amount of diffuse radiation, precluding observation of the nodules include din the phantom. Images obtained with a 64-64 matrix and an energy window of 5% enabled visualization of seven of the 32 nodules. Images obtained with an energy window larger than 5% showed greater loss of resolution with a consequent reduction in imaged nodules. Using an image matrix of 128 -128 pixels with any acquisition window, it was possible to view nodules

from 12.7mm in diameter; however, the quality of the image was poor. The best images were obtained with a matrix size of 256-256; the visualization of nodules with appropriate detection was possible with energy windows of 10 and 15%. It is not worthy that as the width of the energy window increased, the acquisition time decreased and wider spread Compton scattering was observed. By increasing the image acquisition time from 1 to 4 min, obviously the resolution improves, even with images acquired with 100 or 250 kcpm. However, it causes discomfort to patients because they need to stay longer immobilized. The results obtained for the phantom with nodules with a zoom of 1, 1.3, 1.5 and 2.0 used the same matrix of 256 × 256 in each image. The best resolution was obtained with the 1.3 zoom.

Frek J Beekman et al. (2005) developed gamma camera with Charge-Coupled Devices (CCD) to evaluate the performance of a new device. The EMCCD used in this work is the CCD65 from E2V Technologies. It is a front-illuminated device with 288 lines and 576 pixels per line, and has an active area of 11.52 mm × 8.64 mm (20 μm × 30 μm pixel size). To reduce the dark current, the EMCCD is cooled to -50 °C, using a Peltier element. The researcher used a 1000 μm thick microcolumnar scintillator module (CsI (Tl) FOS from Hamamatsu, type no. J6671), consisting of narrow CsI (Tl) needles (a few μm wide), grown on a 3 mm thick fibre-optic faceplate with fibres with a diameter of 6 μm, this scintillation module was coupled directly to the fibre-optic window of the CCD with optical grease; in the other set-up a fibre-optic taper with a taper ratio of 2.1:1 was inserted between the scintillation module and the EMCCD in order to increase the active area of the camera. The electronics board that drives and reads out the CCD is connected to a board containing a digital signal processor (DSP). An efficient photon-counting algorithm is executed on the DSP which detects and localizes scintillation events in real time by analyzing 50 entire CCD images per second. Spatial resolution measurements were performed for a Tc-99m source (140 keV, 37 MBq) and an I-125 source (about 30 keV, 37 MBq) using two tungsten blocks separated by a narrow slit (30 μm wide). Energy spectra of I-125, Tc-99m as well as a background noise spectrum were recorded. The influence of the number of scintillation events ('true counting rate') on the measured counting rate was determined by placing a Tc-99m point source at a distance of 28 mm from the CCD. A slab of lead with a hole of 2 mm at the centre was placed in front of the CCD. Different source strengths were obtained by natural decay. The maximum activity was 33 MBq, and the 'true counting rate' was estimated by fitting a line to the straight part of the curve that is measured at low counting rates (30–230 counts cm⁻² s⁻¹). The

result of this study determined that the Full Width at Half Maximum (FWHM) ^{99m}Tc $342\mu\text{m}$ and $270\mu\text{m}$ for ^{125}I while the Full Width at Ten Maximum was $1123\mu\text{m}$ for ^{99m}Tc and $778\mu\text{m}$ for ^{125}I . the energy resolution was estimated to be 24% FWHM (33 keV) for Tc-99m and 133% (36 keV) for I-125, the effects that an increasing event rate has on the fraction of scintillation flashes that can be detected, At event rates below a few hundred of counts $\text{cm}^{-2} \text{s}^{-1}$, the number of detected events increases almost linearly with the true even rate, for Single Photon Emission Computed Tomography (SPECT) in which the number of detected count not exceed 1000counts the researcher estimate count losses to be only 2.1% and 3.8% at counting rates of 500 counts $\text{cm}^{-2} \text{s}^{-1}$ and 600 counts $\text{cm}^{-2} \text{s}^{-1}$, respectively, the counting rate effects occurring at much higher event rates, count losses at high event rates can be explained by overlapping of light flashes that occur in the CCD images, The number of detected photon interactions for the 35% window ($140 \pm 25 \text{ keV}$) in curves I–IV are 216, 1023, 2090 and 2623 counts $\text{cm}^{-2} \text{s}^{-1}$, respectively.

Hosang et.al. (2008) determined the detective quantum efficiency (DQE) of small gamma camera with three pinhole (1,2, and 4mm in hole diameter) and one-coded aperture (uniformity redundant array (URA), 286 holes, hole diameter 2mm) collimator, using Modulation Transfer Function (MTF), normalized noise power spectrum (NNPS), and incoming signal to noise ratio (SNR). The researcher used small gamma camera that consists of CsI (Na) scintillation crystal (100mm in diameter, 3mm in thickness), a PSPMT (Hamamatsu R3292) with 28-X and 28-Y grid. The signal from PSPMT was amplified and digitized using ADC. Three pinhole 1, 2, and 4 mm diameter was used. Coded aperture used was uniformly redundant array (URA) designed by Fennimore and cannon. The MTF was measured using 1mm diameter line source of ^{99m}Tc . The NNPS was measured with plane source (1mm in thickness and 50mm in diameter), the activity in the plane source was 8mCi of ^{99m}Tc at the beginning of the study. The DQE was calculated with incoming SNR2 defined as the number of photon incident onto the collimator. The solid angle from the plane source to the collimator was used to calculate incoming SNR2 value given approximately $3.75\text{E}+6$ incident photon per cm^2 for all pinhole. In the case of URA the researcher reduced the collection time to escape saturation. Thus, $4.69\text{E}+5$ photon were incident onto the surface of URA collimator. The MTF value for 1mm pinhole is 0.93 at 0.6 lp/cm and 0.74 at 1.2 lp/cm for 2mm pinhole: 0.88 at 0.6 lp/cm and 0.58 at 1.2 lp/cm; for 4mm pinhole:

0.77 at 0.6 lp/cm and 0.31 at 1.2 lp/cm; for URA: 0.84 at 0.6 lp/cm and 0.48 at 1.2 lp/cm. The spatial resolution was inversely proportional to the diameter of the pinhole. Though each hole diameter of the URA is 2 mm, it was observed that the spatial resolution of the URA was equivalent to that of the pinhole, 3mm in diameter. The MTF decrease was caused by scatter effect at many holes, URA. The DQE values of URA were much higher than those of all pinholes. The DQE ratio of URA to 2mm pinhole was about 8.1 at zero spatial frequency. Although MTF values of URA were a little lower than those of theoretical URA, higher DQE values were given by very low noise levels. The determination of DQE with MTF and NNPS enables the researcher to verify the total quality of gamma camera system quantitatively and effectively. Moreover, the DQE can be a useful design parameter to develop gamma-imaging systems.

Hosang et.al. (2009) used the modulation transfer function (MTF) and normalized noise power spectrum (NNPS) instead of conventional NEMA standard to evaluate the performance of small gamma camera with changeable pinhole collimator using Monte Carlo simulation. For the acquisition of simulated gamma image, the small gamma camera used by the researcher was described by MCNP code. The energy of the gamma source was 140KeV which is the energy of ^{99m}Tc. The researcher used two kind of source geometry according to the NEMA standard, the one is a cylinder (30mm long; 1mm diameter), for the acquisition of line spread functions. The other is a disk (50mm diameter; 1mm thickness), for the acquisition of uniform flood images. Seven collimators with 1.0, 1.5, 2.0, 2.5, 3.0, 3.5 and 4.0mm diameter pinhole were simulated using lead material of 3mm thickness. The FWHM values were measured in seven line images according to NEMA standard using Line Spread Function (LSF) acquisition and MTF computation. Sensitivity and differential uniformity were measured in seven uniform flood image according to NEMA standard using Region of Interest (ROI) definition, normalization, 2D NNPS computation and 1 D NNPS computation. MTF was inversely proportional to FWHM with Pearson's correlation coefficient 0.995. the spatial resolution was described by the MTF of gamma camera system value for 1mm pinhole is 0.43 at 1 p/cm, 0.15 p/cm, 2mm is 0.40 at 1p/cm, 0.12 at 1.5 p/cm, 0.28 at p/cm and 0.02 at 1.5 p/cm. the average of MTF difference between 1 and 1.5 p/cm was 0.27 among seven pinhole collimator. NNPS was directly proportional to one of the sensitivities with Pearson's correlation coefficient 0.993. NNPS values For 1mm pinhole is 6.83E₋₄ at 1 p/cm and 2.22E₋₄ at 1.5 p/cm for 2mm pinhole is 8.47 E₋₅

at 1lp/cm and 4.44×10^{-5} at 1.5 lp/cm and 4mm pinhole is 1.14×10^{-5} at 1lp/cm and 4.64×10^{-6} at 1.5lp/cm. The spatial uniformity of gamma camera system is basically related with pixel-to-pixel data fluctuations of output image data. Because sensitivity and differential uniformity only reflect statistical fluctuation and difference of two pixel data, the entire evaluation of spatial uniformity was given by only NNPS. In this study, the researchers have verified that the spatial resolution of a gamma camera can be evaluated by the MTF as a function of spatial frequency. The NNPS of the gamma camera system enables the researcher to verify the total quality of the spatial uniformity.

Islamian et al. (2012) simulated a quality control Jaszczak phantom using SIMIND Monte Carlo and added the phantom as an accessory to the program. The researcher used the SIMIND Monte Carlo simulation program which is well established for SPECT with low energy photons for photonic physics and other applications; the program is freely downloadable from the related site: www.radfys.lu.se/simind, this program was originally designed for the calibration of Whole-body counters, but soon evolved to simulate scintillation cameras. It is now available in Fortran-90 and can be run on major computer platforms including PCs., SPECT Jaszczak phantom Deluxe which was specially design for high resolution camera, the phantom was constructed from Plexiglas material and consist of six spheres with different diameter (9.5, 12.7, 19.1, 15.9, 25.4, and 31.8) and 148 rods (4.8, 6.4, 7.9, 9.5, 11.1 and 12.7mm) used for measuring acceptance test and routine quality control of SPECT camera. The camera used in this study was E-Cam TM, Siemens Medical System. The phantom was filled with $370\text{MBq } ^{99\text{m}}\text{Tc}$ and image was acquired using 128 X 128 matrix, 128 views, 1.23 zoom factor, 3.9mm pixel size and images were reconstructed using Butterworth filter. The SIMIND Monte Carlo code simulated the SPECT reconstructed image of the Deluxe model of SPECT Jaszczak phantom. The qualities of the produced image were compared in term of image contrast and spatial resolution. Image contract was calculated according to the methods describe by Toossi et al. (2010). The image contract of cold experiment phantom is 0.77, 0.62, 0.57, 0.37, 0.19 and 0.13 for sphere diameter of 31.8, 25.4, 19.1, 15.9, 12.7 and 9.5 mm respectively while the image contract for cold simulated was 0.66, 0.52, 0.48, 0.40, 0.23 and 0.20 for 31.8, 25.4, 19.1, 15.9, 12.7 and 9.5 mm respectively. The reconstructed spatial resolution of both SPECTs was nearly equal to 9.5 mm. Implementation of the SIMIND Monte Carlo program with the executable Jaszczak phantom file and also the related input file may be considered as a benefit, from the point of view of time

saving and providing flexibility, for those who intend to plan a SPECT simulation study with the phantom. The researchers also suggest that the same phantom should be used for the simple assessment of X ray CT images and the assessment of image offset for SPECT/CT and PET/CT systems. Implementing such a phantom should provide a proper comparison of the assessment of SPECT image performance more extensively practicable by experiment and simulated systems. In this work the researcher used high count acquisitions which result in slight ring artifact in the sphere image but this artifact was not visible in the count statistics of the common clinical studies.

Staden et al (2007) designed and tested quality control phantom for gamma camera using standard inkjet printer. The ink used to print the phantoms was obtained by adding a well-mixed solution of black ink and ^{99m}Tc pertechnetate to the cartridge of a Hewlett-Packard inkjet printer (HP1220C), the cartridge was slightly modified by adding a tightly sealed plastic screw to accommodate easy filling of the cartridge, PowerPoint software was used to create an image that is representative of the radioactive distribution required, the distribution was then printed on paper (80 g m^{-2}) using the radioactive ink, all radioactive phantoms were placed into a plastic sheath to prevent them causing any possible contamination, imaging was performed with a GE 400AT Starcam camera (General Electric Medical Systems, Milwaukee) fitted with a low energy all purpose (LEAP) collimator and IM512P acquisition software (Alfanuclear SAIYC, Buenos Aires). The amount of ink deposited per unit area and the amount of activity added to phantom was measured. The uniformity of the camera was determined by measured the integral (IU) and differential uniformity (DU) for five printed radioactive flood source with $1200\text{MBq } ^{99m}\text{Tc}$ deposit in every sheet and using 64×64 matrix size. For comparison, the camera uniformity was also determined using National Electric Manufacture Association (NEMA2001) protocol with ^{57}Co flood source and (IU) and (DU) were measured. System spatial resolution was evaluated using two lines (1mm thick) printed 10 cm apart and two other printed perpendicular to the first, the paper was imaged at 10cm distance from detector with 512×512 matrix, also for comparison camera resolution was evaluated using NEMA2001 protocol using two capillaries tube, more, the four quadrant bar phantom was used to evaluate camera resolution. Result of this study showed that (IU) and (DU) obtained with NEMA method (^{57}Co) for Useful Field of View (UFOV) was 4.11 and 2.68% respectively, the IU of Central Field of View (CFOV) was 2.10%

while the IU of CFOV for printed source was $2.29 \pm 0.67\%$, the average DU of ^{57}Co source was 1.50% and for printed flood source $1.50 \pm 0.23\%$. The average Full Width at Half Maximum (FWHM) of printed phantom was 10.1 and for NEMA phantom was 10.5 while the average Full Width at Ten Maximum (FWTM) was 17.7 for printed source and 18.3 for NEMA source. The two images of bar phantom were visually very similar. Even though slightly different between the results of printed phantom and NEMA, the results were still acceptable when compared to accepted values of NEMA protocols.

Lees et al. (2011) developed small gamma cameras based on scintillator coated charge coupled device (CCD) technology that was originally developed for use in X-ray astronomy, this Communication describes the development of a prototype high resolution small field of view mini gamma camera that would be highly suited for intraoperative imaging. This new type of gamma camera has been designed to offer high spatial resolution imaging (1 mm, using a pinhole collimator), appropriate for medical and veterinary applications, which consists of a CCD, a CsI(Tl) scintillator and a pinhole collimator, the CCD to pinhole distance is fixed at 10 mm. The distance from the pinhole to the object being imaged determines the demagnification on the CCD. Lead shielding around the sides and back of the detector enclosure minimizes image degradation from scattered photons and background radiation. Single pin hole collimator was used, two collimators, with pinholes of 0.5 mm and 1.0 mm diameter, were manufactured (Ultimate Metals) from tungsten discs, 6mm thick and 45 mm in diameter, each having an acceptance angle of 60 degrees. As part of new camera development a CsI (Tl) columnar scintillator (600 mm thick on an amorphous carbon substrate) from Hamamatsu was coupled directly to the CCD with Dow Corning optical grease. The Mini Gamma Ray Camera (MGRC) has been designed to be sensitive over the energy range 20–140 keV. The CCD was cooled using a Melcor thermoelectric device with a finned forced-air heat sink, the camera housing being evacuated to prevent condensation on the CCD. The operating temperature of the device was approximately -10°C . The photons generated in the scintillator by the gamma rays are collected in the CCD and converted to charge in the image area during the integration time period. This charge is transferred to the store sections then into the readout register. Following transfer through the readout register, the charge is multiplied in the gain register before conversion to a voltage by a large signal output amplifier. The software used in this new camera were combined

from different algorithm which are multi-scale algorithms, automatic scale selection and Scale-Space Theory, and are used in a wide range of image analysis applications: detection of lung nodules, quantifying complex landscapes and blob analysis. The resulting spatial resolution of MGRC was less than 1mm after measured the Full Width at Half Maximum (FWHM). For real patient which was injected with 600MBq ^{99m}Tc -HDP, the indicated activity of the order of 200kBq within the imaged area, this would equate to about 0.03% of the amount of activity initially administered to the patient 3 hours previously, since this represents a relatively low count rate, some background activity can be seen around the uptake due to scattered photons arising from the body of the patient, this may be due to the sub-optimal shielding around the camera body. At the end the use of this small highly collimated probe systems for intraoperative and intensive care applications. These have been used for a wide range of applications with particular emphasis on identifying the uptake of radiopharmaceuticals in tumors during surgical operations. By injecting a radiopharmaceutical that selectively concentrates in tumor tissue, it is possible to identify sites of increased uptake of radioactivity. This allows the surgeon to identify the focal uptake of the tracer in lesions, thus aiding the identification of tissues requiring surgical removal.

John et.al (2011) Assessed gamma camera intrinsic uniformity in developing country with unstable power supply environment .the camera used in this study was the Siemens e.cam (signature series) SPET system with single head (Siemens Medical Solutions U.S.A, Inc.) which was installed at the center (Nigeria) in March, 2006. The camera set up for the flood uniformity test is as in Figure 1. A point source of technetium-99m pertechnetate ($^{99m}\text{TcO}_4$) of activity ranging from 0.74MBq to 3.7MBq was used each time the test was performed. A small piece of cotton wool was placed in the vial and drops of $^{99m}\text{TcO}_4$ were placed on the cotton wool while trying not to exceed the cotton's saturation capacity. The collimator was removed and the detector was fully retracted with the gantry rotated so that the detector was at 0°C . The integrated source holder was extended from its storage position on the rear bed and pulled until the source holder was approximately centered. The prepared point source in the vial was clamped, with the capped end of the vial, into the source holder making sure that the cotton tip with the activity was approximately centered above the detector. Thirty million counts were acquired using a matrix of 1024X1024 and a zoom factor of 1.0 (these parameters were automatically preset by

the camera) after the camera had been peaked for ^{99m}Tc i.e. its energy discrimination window adjusted to be centred on the photo peak of ^{99m}Tc . The researchers obtained 143 reading of camera intrinsic uniformity and the result showed that the integral uniformity for the CFOV lied between 3.43% and 1.49% against the acceptance test value of 3.29% while the integral uniformity for the UFOV lied between 4.51% and 1.9% as against 5.21% for the acceptance test. The differential uniformity for the CFOV had values between 1.99% and 1.04% against acceptance test value of 2.25% while that of the UFOV had values between 2.84% and 1.23% against 2.63% for the acceptance test. The shortest time the camera was on before the intrinsic flood uniformity test was performed was 15min and the test produced a flood uniformity of 2.27% and 2.32% for the integral uniformity for CFOV and UFOV, respectively. The differential uniformity for the same test was 1.34% and 1.34% respectively for the CFOV and the UFOV. These result showed that the uniformity of the gamma camera under this condition is within an acceptable range for both planar and SPET imaging.

Kazuki et.al. (2008) developed a balloon borne electron. Tracking Compton camera for sub-MeV to MeV gamma ray astronomy. The researcher used scintillation camera that consist of Hamamatsu 64-chanel multi anode sensitive photomultiplier tube (OSPMT-H8500), a pixilated scintillator array (PSA), and a GSO (Ce) ($\text{GD}_2\text{SiO}_5\text{.Ce}$) crystal that has advantage of a much smaller dead space and a larger effective area. In addition a read out system with low power consumption ($\leq 2\text{W}/64\text{chanel}$) was used because the researchers need 108 scintillation camera corresponding to 6912 channels. The read out system used was ASIC chips, VA32-HDR11 produced by IDEAS with $147\text{mW}/64\text{chanel}$ and a dynamic range of 35pC. The researcher irradiate the GSO(Ce)PSA with 662KeV gamma ray from a 1 MBq ^{137}Cs source at a distance of 30cm. for energy calibration different source of energy was also used including ^{54}Mn , ^{57}Co , ^{22}Na and ^{133}Ba . The researchers investigate the relation between the resistance and the attenuation factor. The result of the minimum to maximum gain ratio of the 662KeV peak value is $1:1.9 \pm 0.3$ (RMS), and the measured ratio with the attenuator board is $1:1.6 \pm 0.1$ while the energy resolution at 662 KeV is 10.6% FWHM These are fit to $\text{DE}/\text{E}(\text{FWHM})^{1/4} = 10.670.6(\text{E}/662 [\text{keV}])^{-0.4970.03}$, where fit parameters are given with RMS errors in the range from 31 to 835 keV. The measurable energy dynamic range of the system is about 30–900 keV at all 64 pixels. These results show that the system of the scintillation camera with the attenuator board performs

adequately with good energy resolution and a wide dynamic range with low power consumption. As a result, the researcher obtained good energy and position resolutions and a wide energy dynamic range of the scintillation camera with low power consumption. The performance of the system is sufficient for use as a Compton-scattered gamma-ray camera for balloon experiments. We have been constructing a Compton camera to be used with this system and testing its performance.

Koike et al. (2011) developed a prototype gaseous gamma camera with a Gas Electron Multiplier (GEM) for medical application in order to increase the spatial resolution of old anger camera. The system consists of three devices: a detector, an Ethernet hub, and a PC. The detector consists of a GEM-chamber and integrated readout electronics. The GEM chamber, which consists of three parts: a converter, an amplifier, and a read out component. The gamma-ray converter consists of four gold-plated GEM foils and a gold-plated cathode. Each converter converts incoming gamma rays into electrons. Both surfaces of the GEM foil are plated by gold, with which gamma rays interact easily because of its large atomic number. a liquid crystal polymer (LCP) was used. The readout electronics are integrated into the detector and linked to a PC with an Ethernet connection. All signals from the readout strips are processed and transferred to the PC as event data. The readout module consists of an ASIC and an FPGA. The ASICs processes analog signals and the FPGA processes digital signals. Researcher developed a simple application program for data acquisition; the program runs on Linux OS and has a number of Graphical User Interfaces (GUIs). In order to test the performance of new prototype camera, researcher conducted several measurements using a phantom filled with ^{99m}Tc (141 keV) as the radioactive source. The measurements with pinhole collimator, the distances between the radioactive source and the collimator and between the collimator and the detector were both 100 mm, respectively, and imaging was performed with a pinhole collimator of 2mm in diameter. The efficiency of gamma-ray-detection for a 141 keV gamma ray at a stable operating voltage (4900 V) was 2:57_0:05%. On the other hand, the efficiency calculated by the GEANT4 simulation was 2:78_0:02% for a similar detector setup. This indicates that we achieved a detector setup with sufficient effective gas gain. The relationship between radioactivity and acquisition count was linear. The Full Width at Half Maximum (FWHM) was measured and

within the acceptable limits. Gamma camera with GEM provides spatial resolution of 2-3mm compared to 6-10mm for old anger gamma camera.

Lees et al. (2010) investigated the use of high resolution mini-phantoms for the evaluation of planar imaging devices with spatial resolution of the order of 1 mm. the researcher have developed a new type of gamma camera that offers high spatial resolution imaging (1 mm, using a parallel hole collimator), highly appropriate for medical and veterinary applications Lees et al. (2010). The simplest form of the mini phantom was a three- hole design in a piece of Perspex 5 mm thick with one large hole, 3 mm in diameter and two other holes of 2 mm in diameter on 5 mm perpendicular spacing. The researchers used the concept of the “Williams Phantom”, they designed two high resolution (HR) phantom s giving the option of having “hot” spots or a uniform source with “cold” spots”. The first HR mini-phantom has four holes, 4, 3, 2 and 1 mm diameter drilled in a piece of Perspex 12 mm thick. The second phantom had four pins with diameters 4,3,2 and 1 mm with the same spacing as the “hole” version. All imaging was undertaken in the Medical Physics Department at Queen’s Medical Centre using the high resolution gamma camera. All images were recorded in frame mode and stored on a dedicated personal computer. A fine bore hypodermic needle, 0.5 mm diameter and 25mm long (25G_100) commonly found in nuclear medicine departments , was used to fill the HR four hole phantom with liquid ^{99m}Tc pertechnetate obtained from the radiopharmacy unit in Medical Physics. Visualization of such small volumes of clear radioactive solution presented potential problems with spillage of small drops resulting in contamination. Addition of a small amount of dye (food coloring) made the process of filling the phantom and visualization of any accidental spillage easier to observe. Subsequent use of a 200 ml air displacement micro pipette pipe tmans enabled accurate filling of the hole sin the mini- phantom with calibrated amounts of radioactive solution. The three-hole phantom was filled from a 1 ml stock solution containing 388 MBq of ^{99m}Tc (the small total volume of the holes resulted in an overall phantom activity of 3.4 MBq. The phantom was placed 13 mm above the camera and was imaged for 18 min (200 counts per second). Initial attempts at phantom imaging showed irregular distribution of activity within the holes. Although the 3mm diameter hole was completely filled, on closer inspection the two smaller 2mm diameter holes contained air bubbles and an uneven distribution was seen in early gamma camera images. After modification of the filling procedure consistent uniform filling of the smaller holes

was achieved. The three holes can be clearly visualized. The slice through the two small holes (on 5mm pitch) shows clear separation. The spatial resolution at FWHM was calculated to be 0.9 mm, slightly less than the theoretical on-axis spatial resolution of 1.2 mm expected from the detector geometry and single pinhole collimator (Mettivier et al., 2003).

Holstensson et al (2010) experimentally measured the effect of energy and source location on gamma camera intrinsic and extrinsic spatial resolution. The two main factors that determine the spatial resolution of a system are (i) the collimator design and (ii) the accuracy with which scintillation events can be localized, which is limited by statistical variation in the number of scintillation photons produced. Although a value for $R_{intrinsic}$ is typically measured as part of the clinical acceptance testing of a gamma camera for the radionuclide ^{99m}Tc , $R_{intrinsic}$ varies with photon energy. A different value of $R_{intrinsic}$ is therefore required for accurate simulation of each different radioisotope and photon emission energy. Experimental images were acquired on a dual-head 9.5 mm NaI (Tl) crystal Philips FORTE and a dual-head 15.9 mm NaI(Tl) crystal Philips SKY Light gamma camera (Royal Philips Electronics, The Netherlands). Both cameras were equipped with 55 PM tubes arranged in a hexagonal array and with a rectangular FOV measuring 38.1 cm in the x -direction and 50.8 cm in the y -direction. For anterior–posterior images, the x -direction corresponds to the cranio-caudal axis and the y -direction corresponds to the mediolateral axis in the patient frame. The result demonstrates the improvement in R_{exp} intrinsic as a function of energy of the photons being imaged for the thin crystal camera. The improvement in R_{exp} intrinsic from ^{99m}Tc (140.5 keV) to ^{131}I (364.5 keV) is 21% for the thin crystal and 17% for the thick crystal. The measured R_{exp} intrinsic values for both the thin and the thick crystal cameras are 2.66 \pm 0.07, 2.54 \pm 0.07, 2.23 and 2.1 \pm 0.1 mm for 140.5, 171.3, 245.4 and 364.5 KeV simultaneously for thin crystal and 3.1 \pm 0.1, 3.0 \pm 0.2, 2.9 \pm 0.2 and 2.6 \pm 0.2 for 140.5, 171.3, 245.4 and 364.5 Kev simultaneously for thick crystal. The result also shows The calculated profile widths of the line and maximum pixel count rates in the images of the sphere created using energy-dependent R electronics 0.00mm values for FWHM are 7.18 \pm 0.06, 10.6 \pm 0.1 and 15 \pm 0.3 mm for 1cm, 5cm and 10cm depth of source simultaneously and R electronics 1.55mm values for FWHM are 7.45 \pm 0.03, 10.8 \pm 0.1 and 15.2 \pm 0.3 mm for 1cm, 5cm and 10cm depth of source simultaneously and R electronics 2,49 mm values for FWHM are 7.84 \pm 0.07, 11.1 \pm 0.1 and 15.4 \pm 0.3 mm for 1cm, 5cm and 10cm depth of source simultaneously

Maro A. Coca Perez et.al. (2008) established a national program for the quality control of nuclear medicine instrument in Cuba and was certified and approved by the regulatory authorities. The program was developed the national Cuba guidelines for a set of standardized and uniform quality control procedure taking into account the technical features of the local instrumentation and the availability of local resources such as phantom. These protocols were based on international publication such as IAEA and NEMA. The documents include the quality control of dose calibrator, directional detectors and well counter, planner gamma camera, SPECT system, whole body system and interface system. The program establishes official regulations and audit service, set-up educational activities, distributes technical documentations, and maintains a national phantom bank, constitutes valuable and useful tools to guarantee the quality of nuclear medicine instrumentation. A national course on the quality control of nuclear medicine instrumentation was organized and established, its main objective was to educate and train the persons responsible for carrying out these tasks in each nuclear medicine department in Cuba, the course was registered at the National College of Health, including forty hours of theory and practical. A data base was created of phantoms and accessories available within the Cuba for quality control of nuclear medicine instrumentation, the data was organized at the web site www.sld.cu/phbank/nmphincu.htm, and the program organized the share of quality control phantom between the Cuba nuclear medicine centers and hospitals by delivered the required phantom to the center according to their need. An audit service licensed and registered by the Centro Nacional de Seguridad Nuclear (National Center of Nuclear Security) was organized and created. The role of the audit service is to annually assess the state of the instrumentation in all nuclear medicine departments within the country and to evaluate compliance with the quality control programs. More than 10 inspections have been performed by the CCEEM to date and have been useful in improving the quality control programs for nuclear medicine instrumentation. Finally, measurements were performed in situ in all the national nuclear medicine services to evaluate the current state of gamma-cameras and SPECT systems. The selected tests and procedures were based on the nuclear medicine instrumentation quality control program previously established. The 5 gamma-cameras and 5 SPECT systems in the country were evaluated for uniformity, spatial resolution, sensitivity, energy resolution, linearity, and tomographic uniformity, center of rotation, tomographic resolution, and total performance.

Jeong et. al.(2004) improvement the performance of small gamma camera using NaI(Tl) plate and position sensitive photomultiplier tube (PSPMTs) and check the camera performance before and after correction methods applied. The camera used in this study was small gamma camera consisted of a general purpose parallel hole collimator (24 mm in length, with a hole diameter of 1.5 mm and a septum thickness of 0.2 mm), a scintillation crystal (NaI(Tl) plate, 120 mm in diameter and 6 mm in thickness), a 5 inch PSPMT (Fifty-six signals from the R3292 PSPMT were reduced to four signals, the four signals were amplified and digitized using ADC with 40 M samples s^{-1} sampling rate then used to localize an event employing the Anger logic), the data acquisition programs were based on Kmax. Position mapping correction developed in order to correct the distorted hole position on the image obtained by scintillation crystal using A lead hole mask (150 mm \times 150 mm \times 4 mm, 1 mm hole diameter, 5 mm pitch) placed in contact with the NaI(Tl) plate crystal without a collimator, and acquired images at different distance (0, 0), (2.5 mm, 0), (0, 2.5 mm) and (2.5 mm, 2.5 mm). Energy calibration was performed using the pulse height spectra obtained from each hole position, obtained for 10 hours using a point source (2 mCi ^{99m}Tc) located 40 cm above the detector. Flood correction was performed using uniformity correction table. Spatial resolution was measured using two capillary tubes having 50 μCi ^{99m}Tc each with inner diameter measurements of 0.4 mm, Full width at half-maximums (FWHMs) of the profiles of the two-line images were measured. Linearity was measured with a parallel-line bar phantom, and was expressed as a standard deviation of the line spread function peak separation, and then the linearity was calculated using the line image. The uniformity was measured using a uniformity phantom that was filled with radioactive solution (500 μCi ^{99m}Tc), and integral uniformity and differential uniformity were also measured. In order to comparative NaI (Tl) crystal result, CsI (Tl) plate was applied to the camera and checked the performance at the same parameter as NaI(Tl) images acquired. The result of this study showed that the resolution of the NaI (Tl) plate system was improved by about 16% using the correction method, and was similar to that of the CsI(Tl) array system after correction, FWHM improved 6.7mm to 3.2 after correction at 30mm distance. The sensitivity of the NaI(Tl) plate system at the centre of the FOV remained similar both before and after correction , however, the sensitivity of the NaI(Tl) plate system at 30mm off-centre considerably increased after correction, from 0.7 cps μCi^{-1} to 2.0 cps μCi^{-1} , the sensitivity of the NaI(Tl) plate system was considerably better than that of the CsI(Tl) array system over the entire FOV after correction (NaI(Tl) plate: 3.4 cps

$\mu\text{Ci-1}$, CsI(Tl) array: 1.4 cps $\mu\text{Ci-1}$ at the centre. The linearity of the NaI (Tl) plate system improved after correction, from 0.5 mm to 0 mm at the centre of the FOV, and from 1.5 mm to 0 mm, at 35 mm off-centre. Before correction, the linearity of the NaI (Tl) plate system was slightly worse than that of the CsI(Tl) array system, but after correction the linearity of both systems was about the same. The integral and differential uniformity of the NaI (Tl) plate system both improved after correction, from 9.7% to 5.2% and from 3.6% to 2.1%, respectively. The uniformity of the NaI (Tl) plate system was better than that of the CsI(Tl) array system after correction.

Holen et.al. (2008) assessed the quality of an image obtained with a rotating slat (RS) collimator in comparison to classical projection image obtained using parallel hole (PH) collimator. The methods used in this study was Monte Carlo Detector Model, the researcher used also Geant4 application for tomographic Emission (GATE), it was used to model both the RS and the PH collimated camera. The detector was the same for both systems and was modeled as a pixilated solid state detector consisting of 192X192 individual CdZnTe crystals. The surface of one pixel is 1.8 mm \times 1.8 mm while its height was set to 5 mm. To make the efficiency of the detector independent of the collimator type, the active area of one pixel is set to be only 1.5 mm \times 1.5 mm, allowing the collimator to have septa of 0.3 mm thickness. The active area will thus be independent of the collimator type since the area covered by the collimator coincides with the inactive detector area. The RS collimator was simulated as 193 parallel lead slats of height 40 mm, placed in between two detector pixels rows. The thickness of a slat was set to 0.3 mm while the length was equal to the length of the detector; being 345.6 mm. The PH collimator had the same height and thickness as the RS collimator (40 mm) and was matched to the pixilated detector. This resulted in a parallel hole collimator with square holes of 1.5 mm \times 1.5 mm. The RS collimator/detector pair was rotated around its own axis in 128 discrete steps at a speed of 20 s per rotation. The PH collimator/detector pair did not move during simulation. The reconstruction of the plane integral data to projection images was performed using a MLEM algorithm the PH projection images were deconvolved using the Richardson–Lucy method in order to make a fair comparison, also Contrast to Noise Ratio (CNR) was obtained using classical methods of gamma camera .the object size was measured as Point Spread Function (PSF).and also image of MCAT phantom was taken in which MCAT simulate the bone scan

which is very wide spread nuclear medicine scintigraphy. The result of this study showed that cold spot contrast recovery is worse for the RS collimator and the differences becoming larger as the cold lesion become smaller an increased contrast recovery can however be obtained for the hot spot this improvement is larger as the hot lesion become larger. The CNR for 9, 12 mm hot spot is six, ten times larger respectively, the PH collimator has a better resolution ,the RS collimator in a very small low contrast and this situation however different when considering more realistic with larger lesion or high contrast . The RS collimator appeared relative improvement when the lesion become larger the improvement is 34% for 6mm lesion and 54% for 10mm lesion.

S. Baechler et.al (2008) measured the feasibility of gamma camera acceptance test for different manufacture but all these cameras are introduced by the SWISS Federal Office of Public Health found on Switzerland. Three types of cameras used in this study which are a single head system (Millennium – General Electric - USA), a two head system (E.Cam - Siemens - Germany) and a three head system (Triad - Trionix – USA) with NEMA (National Electrical Manufacturers Association) - NU-1, 2001 and/or IEC (International Electrotechnical Commission) 61675-2, 1998. Intrinsic homogeneity was done with appoint source without collimator placed in lead box with copper filtration of at least 2mm at distance higher than 5 times useful field of view (UFOV) of the camera, the count rate should not exceed 20 Kcps with pixel size 6.4mm +/-30% and contain at least 10,000 events these measurements applied for both UFOV and central field of view (CFOV). Intrinsic spatial resolution and geometrical linearity also measured with 3 mm thick lead plate with 1 mm slits spaced by 30 mm, covering the whole surface of the camera, the Line Spread Function (LSF), Full Width at Half Maximum (FWHM) and Full Width at Ten Maximum (FWTM) were measured. Spatial resolution and system sensitivity also detected by use two capillaries <1mm filled with Tc-99m and placed on a Styro foam at 10 cm of the collimator and FWHM and FWTM were measured. Intrinsic energy resolution done using 2 point source Co-57 and Tc-99m placed successively in front of head of camera with counting rate not exceed 20Kcps, and the photopeak spectrum were measured with FWHM for two different energy. Behaviour of the counting rate according to the activity with scattered radiation for every camera was done using PMMA cylinder phantom filled by 10GBq of Tc-99m, and recorded activity when the count rate decreased by 20% of the expected value. The result of this

study showed that the integral uniformity% of UFOV is 3.00, 7.15 and 10 and the CFOV is 2.37, 5.75 and 2.03 for E.cam, Millennium and Triad respectively. Also the result showed that the FWHM (mm) for linearity was 3.9, 4.2, and 4.2 and FWTM is 7.4, 8.3, and 8.0 for E.cam, Millennium and Triad respectively. The sensitivity ($\text{count}\cdot\text{s}^{-1}\cdot\text{MBq}^{-1}$) of the cameras is 33.0, 30.9, and 54.7 for E.Cam LEHR, Millennium LEHR and Triad LEGP respectively. The count rate (Kcps) of E.Cam camera is 84.3, for Millennium camera is 110 and 48.1 for Triad camera while the dead time (μs) for Millennium camera is <3.3 , 4.4 for E.Cam camera and 7.6 for Triad camera.

Seiichi Yamamoto (2010) developed and tested a small field of view (FOV) gamma camera using a new LaBr_3 (Ce) scintillator. The gamma camera developed consists of a 2mm thick LaBr_3 (Ce) scintillator (Saint Gobain, BrillanCe 380, USA) and a 25.4mm (2in) square multi-anode PSPMT (Hamamatsu H8500, Photonix, Japan). The LaBr_3 (Ce) scintillator was directly coupled to the PSPMT by its manufacture and was contained in a hermetically and light sealed aluminum case. The detection efficiency of 2mm thick LaBr_3 (Ce) for $^{99\text{m}}\text{Tc}$ gamma photon (141KeV) was around 40%. The size of LaBr_3 (Ce) is 50.8mm X 2mm and the upper side was covered by a white reflector while the other side was painted black to reduce the stray light in the scintillator. The thickness of the aluminum case was 0.5mm. The size of the detector is 58mm X 58mm X 32.5mm. The signal from PSPMT was read out by 64 coaxial cable and fed to the gain control amplifier, the output from amplifier were fed to weighted summing amplifier and digitized by 100MHz free running AD convertor. Energy resolution were measured without collimator using ^{57}Co and ^{241}Am which result was 8.9 % Full Width at Half Maximum (FWHM) for Co and 13.4% FWHM for Am. The intrinsic spatial resolution was measured using a 2mm thick tungsten slit phantom with 1mm slit positioned on the detector, the result showed for ^{57}Co was 0.75 mm FWHM and 1.4 mm FWHM for ^{241}Am after correction applied. Sensitivity was measured for the camera using 50 μCi point source with less than 1 mm size, the source was positioned in front of the pinhole collimator and the count rate was measured by changing the distance between collimator surface and the point source in 5 mm step from 0 to 30mm, the result of sensitivity was 0.0047% at 10 mm and 0.0017% at 20 mm from the collimator surface. The image quality in the corrected mode was measured using several phantoms but the result was assessed visually showed. The flood image shows good uniformity and has no observable system non-uniformity.

Flood images of Co-57 measured at approximately two month and two years after the fabrication , The flood image showed significant distortion due to the change in LaBr3(Ce) of its hygroscopic characteristic . Almost half area of the FOV produced no signal.

Sokole et al. (2010) recommended some procedure for quality control of nuclear medicine instruments. After installation, and before it is put into clinical use, a nuclear medicine instrument must undergo thorough and careful acceptance testing, the aim being to verify that the instrument performs according to its specifications and its clinical purpose. Once the instrument has been accepted for clinical use, its performance needs to be tested routinely with simple QC procedures that are sensitive to changes in performance. Records of test results should be kept in a log-book or digital record. The routine test for planer gamma camera includes 1- Physical inspection, the purpose of the test is To check collimator and detector head mountings, and to check for any damage to the collimator and must be carried daily (Inspect for mechanical and other defects that may compromise safety of patient or staff; if collimator damage is detected or suspected, immediately perform a high-count extrinsic uniformity test). 2- Collimator touch pad and gantry emergency stop To test that the touch pads and emergency stops are functioning, the frequency of the test is Daily (Both the collimator touch pads and gantry emergency stop must function if there is an unexpected collision with the patient or an obstacle during motion; the touch pads must be checked each time the collimators are changed). 3- Energy window setting for ^{99m}Tc to check and centre the preset energy window on the ^{99m}Tc photopeak, should be done daily (The test is intended to check the correct ^{99m}Tc energy window). 4- Background count rate to detect radioactive contamination/excess electronic noise and performed daily (The background count rate should be stable under constant measuring conditions). 5- Intrinsic/extrinsic uniformity and sensitivity for ^{99m}Tc (or ^{57}Co) – visual To test the response to a spatially uniform flux of ^{99m}Tc (or ^{57}Co) photons, for uniformity and overall sensitivity and must be carried daily (Visually inspect either an intrinsic or extrinsic (whichever is most convenient) low count uniformity acquisition; if intrinsic method is selected, each collimator must be checked periodically by an extrinsic uniformity test (preferably with high-count acquisition); record the cps/MBq to check and monitor sensitivity). 6- Intrinsic/extrinsic uniformity and sensitivity for ^{99m}Tc (or ^{57}Co) – quantitative- To monitor the trend in uniformity with quantitative uniformity indices, and to check the sensitivity, may be carried weekly or monthly. 7- Spatial resolution and

linearity – visual- To detect distortion of spatial resolution and linearity carried monthly or each Six-monthly (Visual-quadrant bar or orthogonal hole pattern; intrinsic or extrinsic, depending on convenience; if an orthogonal hole pattern is used, the results can be quantified if special software is available).

Starck et al. (2005) evaluated the performance of gamma camera using detective quantum efficiency (DQE). The use of DQE related to measure of Point Spread Function (PSF), Line Spread Function (LSF), Full Width at Half Maximum (FWHM), Modulation Transfer Function (MTF), Signal to Noise Ratio (SNR) and Normalized Noise Power Spectrum (NNPS). This study was made on a Siemens ECAM gamma camera with a 3/8inc crystal and an ECAM+ gamma camera with a 5/8inc crystal, both with rectangular detectors. All purpose and high resolution parallel hole collimators were used. The intrinsic spatial resolution was 3.9 mm for the ECAM camera and 4.6 mm FWHM for the ECAM+ camera. The system planar sensitivity was about 10% higher for the ECAM+ camera. The MTF of a gamma camera was measured with a 1 mm diameter line source. Uniform images were acquired with the same collecting time per activity unit with a NEMA (National Electrical Manufacture Association) sensitivity plane source (NEMA 1994). The plane source, 1 mm thick and with a diameter of 100 mm, was filled with ^{99m}Tc . The measurements were made in a water tank at 2 cm and 12 cm depth. Measurements were made with ^{99m}Tc , using three different pulse height windows 103–154 keV (40%), and 126–154 keV (20%) and 132–154 keV (15%). The activity in the plane source was at the beginning of the measurement series 123.7 MBq and at the end 87.2 MBq with a collection time between 90s and 128s. From the line source images the tails of the LSF were extrapolated exponentially (Extrapolation levels between 1% and 0.1% of the maximum of the LSF were used) then the MTFs were calculated by Fourier transformation of the LSF, from calculated MTF and normalized noise power spectrum calculated from uniformity Images the noise-equivalent quanta were calculated, lastly DQE was calculated with SNR. Measurements showed that the 40% energy window had a high DQE compared to the other energy windows for frequencies up to about 0.03 cm^{-1} at 12 cm depth and for frequencies up to about 0.07 cm^{-1} at 2 cm depth, At 12 cm depth, 15% window was preferable for frequencies over approximately $0.05\text{--}0.07\text{ cm}^{-1}$ for both the HR and AP collimators, The AP collimator was found to be superior for frequencies below $0.4\text{--}0.5\text{ cm}^{-1}$, while the HR collimator was superior for frequencies over 0.5 cm^{-1} ,

Measurements at 2 cm showed that the AP collimator and a 20% window was best for all frequencies of clinical interest ($<1.2 \text{ cm}^{-1}$), for frequencies exceeding 0.6 cm^{-1} , window widths of 20% and 15% gave almost identical results. A difference was found in DQE between the two crystal thicknesses, with a slightly better result for the thick crystal for measurements at 12 cm depth, At 2 cm depth, the thinner crystal was slightly better for frequencies over 0.5 cm^{-1} . The thicker crystal gave higher values for DQE, whereas when the organ was near the collimator surface the thinner crystal was slightly better especially for the AP collimator at frequencies over 0.5 cm^{-1} . The system spatial resolution for the HR and AP collimators was 7.4 mm and 9.4 mm FWHM at 10 cm and about 0.4 mm higher, respectively, with the thick crystal. The difference in spatial resolution between the crystals was smaller and about 0.2 mm when measured with scatter. The difference in sensitivity between the collimators is about 65%. In nuclear medicine examinations using $^{99\text{m}}\text{Tc}$ and when the organ of interest is at greater depths in the body, a 15% window, compared to a 20% window, results in a better contrast and improved MTF curve due to rejection of scattered radiation.

Valentin et al. (2001) upgraded analog gamma camera with digital acquisition system with PC based system from International Atomic Energy Agency (IAEA) and ministry of science and technology of Slovenia, several national research groups were involved in the IAEA development project for the acquisition card with software and the standard set of clinical protocols from China, India, Cuba, and Slovenia, upgrading involved development of acquisition card by using ISA format acquisition card, solution for adjusting amplitude and timings for input signals from a variety of gamma Cameras, acquisition driver incorporated in PIP (Portable Image Processing), on-line energy and count correction of image data, stable function of the system for all kind of possible clinical studies (fast and slow dynamic, static, gated and combined studies), continuous upgrading. Also the software was developed using MSDOS operating system in WINDOWS (3.1, 95, 98), PIP system for patient database and general data processing, tools for end-user development of clinical protocols (C++ library, macro functions) , algorithms for automatic analysis of clinical data with possible manual intervention, tools for image, dynamic curves and ROI processing, images from study analysis in standard picture formats (i.e. PCX, BMP), set of gamma camera quality control functions (NEMA tests), converter to and from “Interfile” format, SVGA color scale for display, results of analysis on one page, printing of

documents in high spatial resolution (1200x1200 dots/inch) and on low cost high quality media (paper, transparencies), archiving the original image data and reporting documents on low cost CD as “soft” copy, network support. The acquisition system developed mainly depending on three universities project, first Acquisition card from Bombay Nuclear Research Institute with signal's gain and offset control, AD conversion, energy correction, creating images and gate control, second Acquisition card from Havana University Institute with signal's gain and offset control, AD conversion with saving the position, energy and other control data (i.e. gate signal, signal for gantry control) are transferred to the computer's memory using PORT transfer, the third one is Acquisition card from Ljubljana University Medical Centre with signal's gain and Offset control, time control, AD conversion, saving of position, energy and all other control data for each detected gamma event by computer's PORT transfer to the computer memory. The project applied for 300 gamma cameras spread over 52 developing countries. The Slovenian system GAMMA-PF is the most adequate, due to better technical performance, stability of functioning, facility of installation, technical support, lower price, accomplishing in delivery time schedules and professionalism of the involved team.

Zanzonico (2009) reviewed the quality control procedures for nuclear medicine instruments. Nuclear medicine is critically dependent on the accurate, reproducible performance of clinical radionuclide counting and imaging instrumentation. Gamma camera is the most widely used imaging device in nuclear medicine. The performance parameters most commonly evaluated as a part of routine gamma camera quality control program include uniformity, spatial resolution, spatial linearity, and energy resolution and peaking. Gamma camera uniformity may be evaluated either intrinsically (without collimation) or extrinsically (with collimation). Intrinsically, a point source (<1mL in volume and containing about 18.5 MBq) of ^{99m}Tc placed 5 crystal dimensions from and centered over the uncollimated detector. Extrinsically, a uniform flood, or sheet source (typically 185- 555MBq) of ^{57}Co or ^{99m}Tc placed directly on the collimated detector. In both intrinsic and extrinsic type of uniformity a total of 10-15 million count is acquired and uniformity quantities for integral uniformity (maximum count per pixel – minimum count per pixel / maximum count per pixel + minimum count per pixel X100%) and differential uniformity (same equation of integral put applied for every 5 pixels segment in every row and column of the flood image). Integral uniformity of 3% or better and differential

uniformity >5% are routinely obtained for modern gamma camera. For radionuclides other than ^{99m}Tc used clinically on a particular gamma camera (i.e., ^{201}Tl , ^{123}I , ^{111}In , ^{67}Ga , or ^{131}I), intrinsic uniformity should be checked at least quarterly. Spatial resolution and spatial linearity, in practice, are generally assessed semi quantitatively using some sort of resolution phantom (or mask) such as the 4-quadrant bar phantom. Such a semi quantitative (i.e., visual) assessment is faster and more convenient than actual measurement of spatial resolution of the FWHM of the line-spread function. A 4-quadrant bar phantom consists of 4 sectors of radio opaque lead bars and intervening radio-lucent plastic strips 2, 2.5, 3, and 4 mm in width. A point source of ^{99m}Tc is placed 5 crystal dimensions from and centered over the uncollimated detector, with the phantom placed directly over the detector. A 5- to 10-million-count transmission image is then acquired and visually inspected. The lead bars in at least the 2 coarsest quadrants (i.e., with the 3- and 4-mm-wide bars) should be visually resolvable. Nowadays, at least a portion of the lead bars in the third coarsest quadrant (i.e., with the 2.5-mm-wide bars) should be visible as well. All bars should appear straight. Spatial resolution and spatial linearity should be checked with such a phantom at least weekly.

Zeinali et al. (2007) introduced and tested a newly developed computer controlled device called Adaptive Quality Control Phantom (AQCP) that designed to perform the Quality Control test of the gamma camera. AQCP is an electro mechanic device that designed to perform a uniform set of procedure that can be used for routine quality control of a gamma camera by moving a radioactive source with the Field of View (FOV) of the camera (uniformity, COR, and CHA). The cylindrical coordinates is chosen for the motion and simulation of AQCP, combination of ball screw and reel system are used to position the point source in any desired point in space with a precision of 0.06mm, two motor was used with accuracy of 10% (0.18 degree/step). The Haematocrit-capillaries with external diameter of 1.5 – 1.6mm and ^{99m}Tc with high specific activity (>50mCi/cc) were used to make line and point source. The AQCP was operated and controlled using specific software. SMV double head gamma camera model DSX-XL SPECT was used. System uniformity was assessed using 10mCi ^{99m}Tc -Flood source placed on the parallel hole LEHR collimator and system uniformity with AQCP was measured using line source (1mCi activity, 20% window, 10cm distance to collimator source) moved over FOV, the technologist dose was measured using electronic personal dose meter model Dose GUARD. The

mean (+/- S.D) of integral Uniformity I.U parameter using IAEA-TECDOC-602 method is 9.56 (+/-0.959) while for AQCP is 9.55 (+/- 0.92) and the absorbed dose of technologist is 6.18 (+/- 0.19) μSv for IAEA method and 0.82 (+/- 0.10) μSv for AQCP method. Collimator Hole Angulations (CHA) was measured with AQCP using point source (≤ 1.6 mm diameter, 200 μCi of $^{99\text{m}}\text{Tc}$, 20% E.W) for three collimator types LEHR, LEHS and LEUHR with 256 X 256 matrix and two image was taken for any collimator at vertical distance of 10cm and 13cm, the point source was imaged for a total of 50K counts. The approximate X and Y coordinate of each point source image is determined by calculation of the centroid of each point source image. The maximum of CHA for LEHR, LEHS and LEUHR collimator were 0.78° , 0.67° and 0.66° respectively. Center of Rotation (COR) was calculated as IAEA-TECDOC-602 using 200 μCi $^{99\text{m}}\text{Tc}$ point source, 64 X 64 matrix, 20% energy window, each projection requires 50K count for 360° . Also COR was measured as AQCP by holding the camera position and AQCP moves the point source on the circle. The offset error was measured which was 0.28 deviation of X offset and 0.31 deviation of Y offset for IAEA method and 0.94 and 0.293 for X and Y offset respectively for AQCP method. The advantages of AQCP in comparison with classic methods are: reduction of radioactive material consumption, reduction of radiation exposure to the staff, reduction of QC test cost, implementation of QC program with one phantom, perform a uniform set of procedures, increase the accuracy and precision of some QC tests, automation of the measurements and evaluation process make by AQCP suitable for both acceptance tests and routine quality control checks.

Chapter three

Materials and methods

3-1 Model one:

The phantom system was designed according to the parameters researched, measured and recommended by International Atomic Energy Agency (IAEA-DOC-602), National Electronic Manufacturing Association (NEMA 2001), Connor et.al. (2000), Staden et.al. (2007), A.H.Ng et.al. (2008), Baechler et.al. (2008), Seret (2010), Lees et.al. (2010), Holstensson et.al. (2010), Ejed et.al. (2011), and Islamian et.al. (2012).

Model one consist of two parts, the flood phantom and the bar phantom. The flood phantom manufactured from two pieces of white color Perspex material, each piece has dimension of 40cm X 40cm with 1mm thickness, the dimension of 40cm X 40cm is occupying the field of view (FOV) of the most of the gamma camera installed in Sudan- nuclear medicine centers (Fig 3-1), the two pieces of Perspex were linked together using four pieces of Perspex each have dimension of 40cm X 1cm with 1 mm thickness using silicon material. At one side of the flood phantom two opening apparatus were made, one of the apparatus act as entering passage of the water and radioactive materials and the other apparatus used for decrease the chance of air bubble formation (fig 3-2). The flood phantom of this study was designed to measure the extrinsic integral uniformity and extrinsic differential uniformity as well as the activity emitted from the flood source will be the source of bar phantom to measure the resolution and linearity of the gamma camera. The design of the flood phantom was manufactured and introduced by Khartoum Engineering Company as researcher request.



Figure 3-1: a camera shoot image represent the Perspex sheet with dimension of 42 X 42cm



Figure 3-2: image showed a sheet of Perspex used for flood phantom fabrication



Figure 3-3: image shows the whole liquid flood phantom, the holes for passage the water and radioactive material at the left side

Part two which simulate the bar quadrature phantom. The researcher used a quadrature shape of the bar phantom as recommended by Zanzorico (2009). The bar phantom was designed and manufactured from five different division. Division one was 1 mm thickness Perspex material with dimension of 42cm X 42 cm, division two was piece of Perspex with dimension of 42cm X 42cm and thickness of 1 mm, division three was sheet of rubber material with dimension of 40cm X 40cm and thickness of 5 mm and in this rubber sheet a grooves with different width was made to hold the lead within these grooves, division four was 1mm thickness lead with different width to be compatible in the size with the width made in the rubber sheet, and division five was four different Nails, The two pieces of Perspex was manufactured and introduced by AZHARE ABDALHALEM FOR ALUMINUM Co..Ltd and the main function of it are to hold the rubber sheet in one piece while the other piece is using to cover the rubber sheet containing the lead. The rubber sheet was designed, manufactured and introduced as researcher request from Khartoum packing company, the rubber sheet used have dimension of 40 cm X 40 cm similar to that size of the liquid flood phantom, the whole size of the rubber sheet was divided into main four zones each has dimension of 20cm X 20cm, the segment one which is located at the right upper corner of the sheet composed of 23 grooves with dimension of 16cm length and 3.5mm width and 3.5mm distance between each adjacent two grooves, the second part was located at the right lower corner of the rubber sheet and consist of 29 grooves each have dimension of 16 cm

length and 3mm width with 3mm far between each grooves, the third quadrate was located at the left upper corner of the sheet and consist of 35 grooves with dimension of 16cm length and 2.5mm width and 2.5mm space between each nearest grooves, and the last corner of the sheet is the left lower part of the sheet that containing 43 grooves with 2mm width and 16cm length and 2mm space between each two closing grooves. The rubber sheet was fixed to one piece of Perspex using silicone gel material.

The lead used was 1mm thickness lead, introduced from Hassan Hamada Company for Lead, the sheet of lead was cuts into small parts as, 23 lead pieces with dimension of 16cm length and 3.5mm width, 29 lead pieces with 16cm length and 3mm width, 35 lead pieces with dimension of 16cm length and 2.5mm width, and 43 Lead pieces with 2mm width and 16cm length. The lead sheet was divided into small pieces with that size to be compatible with the size of grooves made on the rubber sheet. The cuts of the lead sheet was done manually and the researcher using analog vernia as measuring tools to insure the correct width of the lead pieces and also used ruler to detect the length of each segments of lead.

After the rubber sheet was cleaned from any type of dusts, the segments of the lead was embedded inside the grooves of the rubber sheet and then cover using the second piece of Perspex (fig 3-4).



Figure 3-4: image show the lead within rubber sheet grooves of the bar quadrate phantom

The first piece of Perspex, the rubber sheet in which the lead was embedded on it and the second piece of Perspex was linked together using four Nails putted at each corner of the phantom.

The quadrate bar phantom was designed to perform intrinsic linearity, intrinsic resolution, extrinsic linearity and extrinsic resolution quality control test for planer and Single Photon Emission Computed Tomography (SPECT) gamma camera.

The resolution as general, the normalize edge of the lead within grooves of the phantom and the linearity of the pieces of the lead was determined and assessed before the phantom was used on the gamma camera. The general assessment of the bar quadrate phantom was made at Royal Care International Hospital, diagnostic radiology department, under supervision of radiology technologist Ahd Elsir Hassen, the phantom was placed on the table of the X-ray machine and the X-ray tube was centered to cover all the size of the bar phantom and An image was made using 140KeV (similar to gamma photon energy of ^{99m}Tc) and 100mAs without collimation (fig 3-5). The X-Ray machine used was TOSHEBA Rot anode CTM, DXR-1824B manufactured AUG 2009 in Japan. The researcher used 140KeV energy of the X-ray to simulate the gamma emission from ^{99m}Tc which will be using as the radioactive source in the real experiments on the gamma camera. The image was printed using printer from Care Stream Health Company model F3517 made in United State of America. The image of the bar phantom was assessed visually and the line of the lead appeared linear with smooth edge of the lead segments.

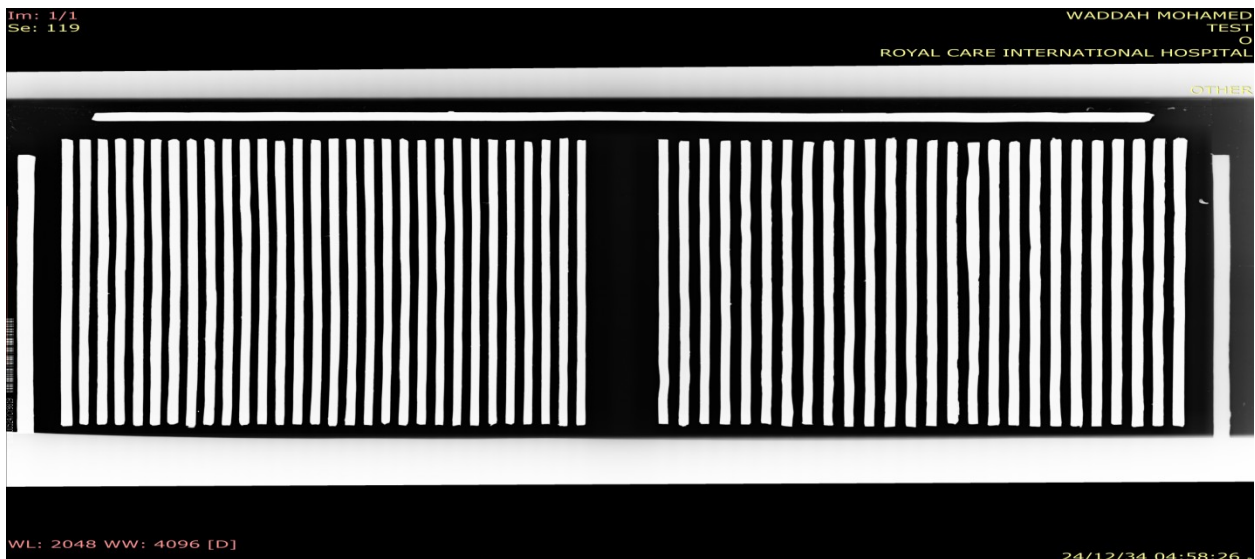


Figure3- 5: an X-ray image showed the lead line after exposed to 140KeV

The manufactured liquid flood source and bar quadrate phantom was introduced to Shandi university Hospital, nuclear medicine department and the experiments of the phantom were made on the gamma camera under supervision of the staff of the department. The gamma camera used for experiments was Mediso SPECT single head, Nucline Sprit Model, hangar, installed 2009 (fig 3-6 and fig 3-7). The method of images taken and data collection was performed according to the parameters recommended by Zanzonico (2009), Sokole et.al. (2010) and specific parameter from camera manual. The liquid flood phantom was prepared by adding 1600ml of water within the phantom using open apparatus, then 1mCi of $\text{Na}^{99\text{m}}\text{TcO}_4$ in 0.1 mL volume was injected into the phantom (fig 3-10) and gentle shacking was made to insure the homogeneity distribution of the radiotracer within the flood phantom (fig 3-8 and fig 3-9).



Figure 3-6: image of the gamma camera used for expermint

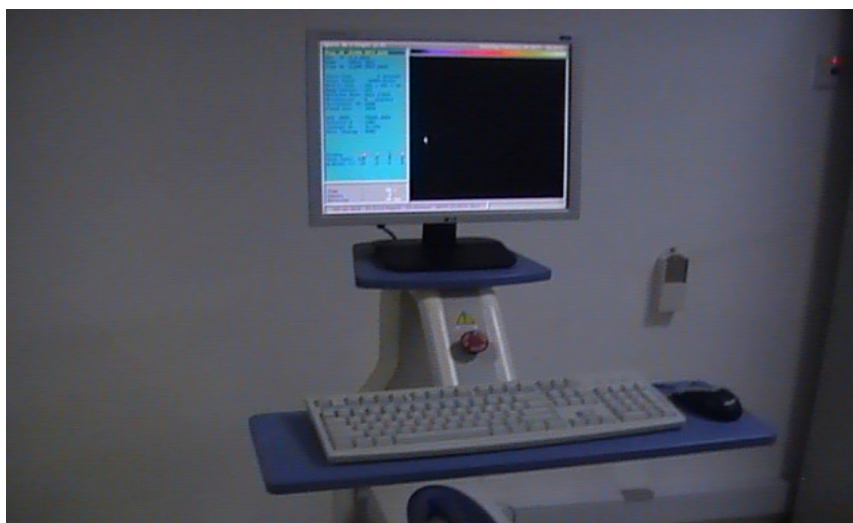


Figure 3-7: image of the workstation of the gamma camera used for expermint



Figure 3- 8: image show the flood phantom during filling with water (side view)



Figure 3-9: image show the flood phantom during filling with water (front view)



Figure 3-10: image show the flood phantom during filling with ^{99m}Tc (side view)

The flood phantom was placed on the gamma camera table and centered over the field of view of the camera, an images was taken using different matrix size of 256 X 256, 512 X 512 and 1024 X 1024 with energy window set at 20%, the total count contained in each image was approximately one million count and an each image was acquired in approximately 200 seconds (fig 3-11 and fig 3-12).



Figure 3-11: image show the flood phantom center during uniformity quality control test (side view)



Figure 3-12: image show the flood phantom center during uniformity quality control test (front view)



Figure 3-13: image show the workstation during uniformity quality control test acquisition

The quadrant bar phantom was placed over the liquid flood phantom which was already centered on the table of the gamma camera and a number of images were taken using different matrix size

of 256 X 256, 512 X 512 and 1024 X 1024 with 20% energy window center (fig 3-14 and fig 3-15).

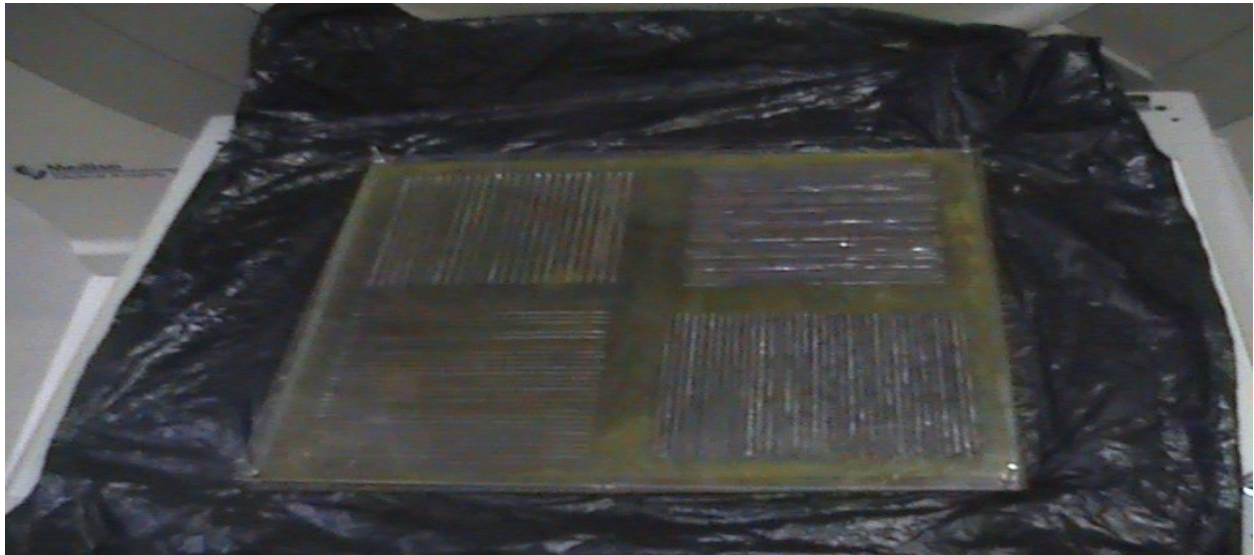


Figure 3-14: image show the bar quadrate phantom center during intrinsic linearity and resolution quality control test acquisition



Figure 3-15: image show the bar quadrate phantom center during intrinsic linearity and resolution quality control test acquisition

The third sets of images was taken using point source of 1mCi of ^{99m}Tc , the source was placed five times distance of the Field of View (FOV) size as recommended by NEMA 2001 to insure a uniform irradiation of the bar phantom, and the bar phantom was centred over the camera head and an images were taken using 20% energy window with different matrix size of 256 X 256, 512 X 512 and 1024 X 1024 (fig 3-16).



Figure 3-16: image showed the point source centered at floor during intrinsic linearity and resolution quality control acquisition

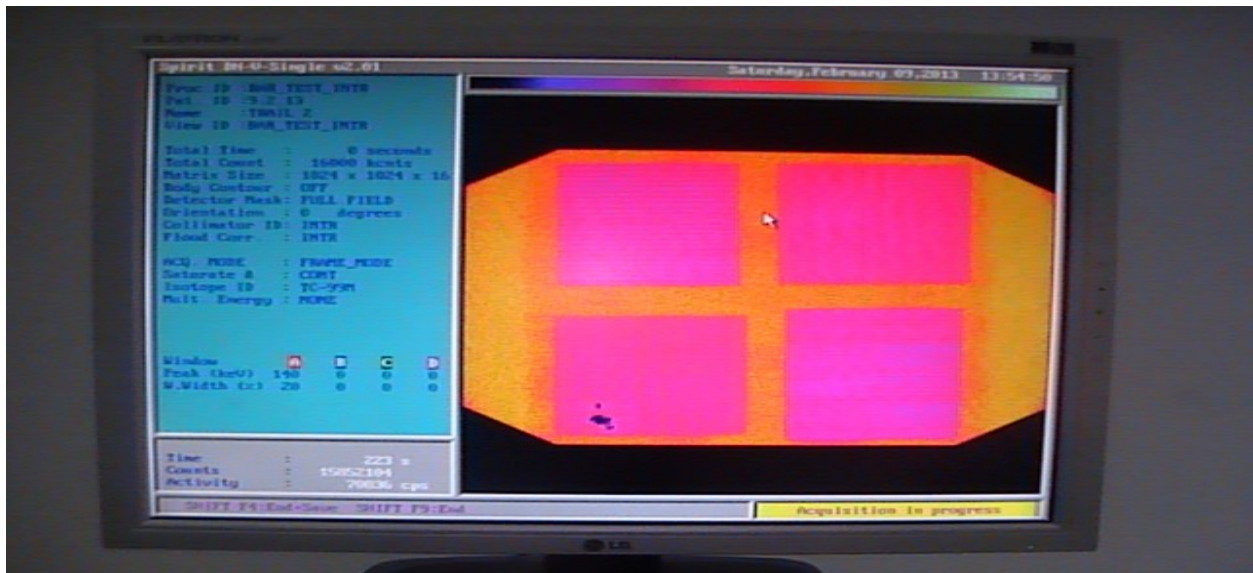


Figure 3-17: image show the workstation during linearity and resolution quality control test acquisition

The resolution of the gamma camera was measured according to the camera software as Full Width at Half Maximum (FWHM) and Full Width at Ten Maximum (FWTM) for Center Field of View (CFOV) and Useful field of View (UFOV). For extrinsic resolution the FWHM for CFOV was 4.55 and 4.63 for FWTM, for CFOV the FWHM was 4.49 and 4.55 for FWTM. For intrinsic resolution the FWHM for CFOV was 4.38 and 4.46 for FWTM, for UFOV the FWHM was 4.44 and 4.50 for FWTM. The differential uniformity was also measured and was equal 25% for UFOV and 12.2% for CFOV compared to the acceptance values of 21.9 % and 1.6% for UFOV and CFOV respectively. The integral uniformity was 44.2% for UFOV and 29.3% for CFOV compare to acceptable values of 22.9% for UFOV and 2.1% for CFOV.

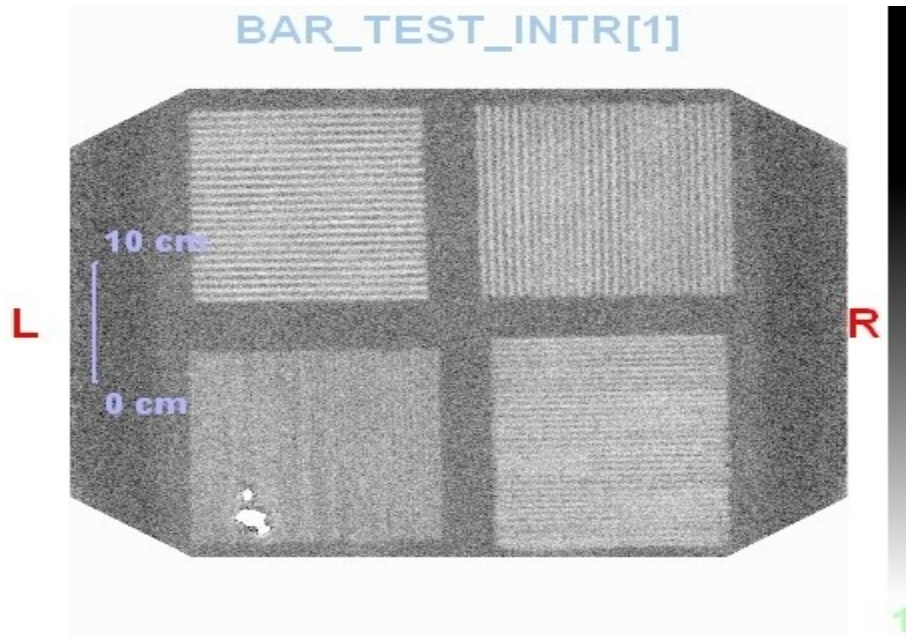


Figure 3-18: image of the bar phantom

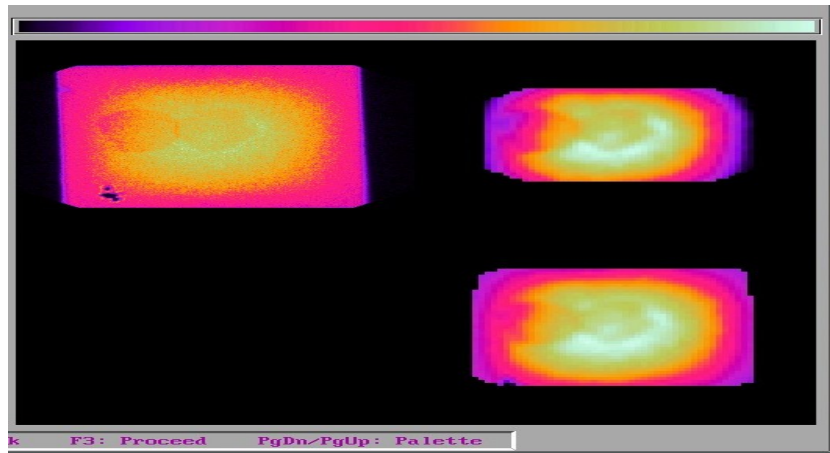


Figure 3-19: image of the liquid flood phantom

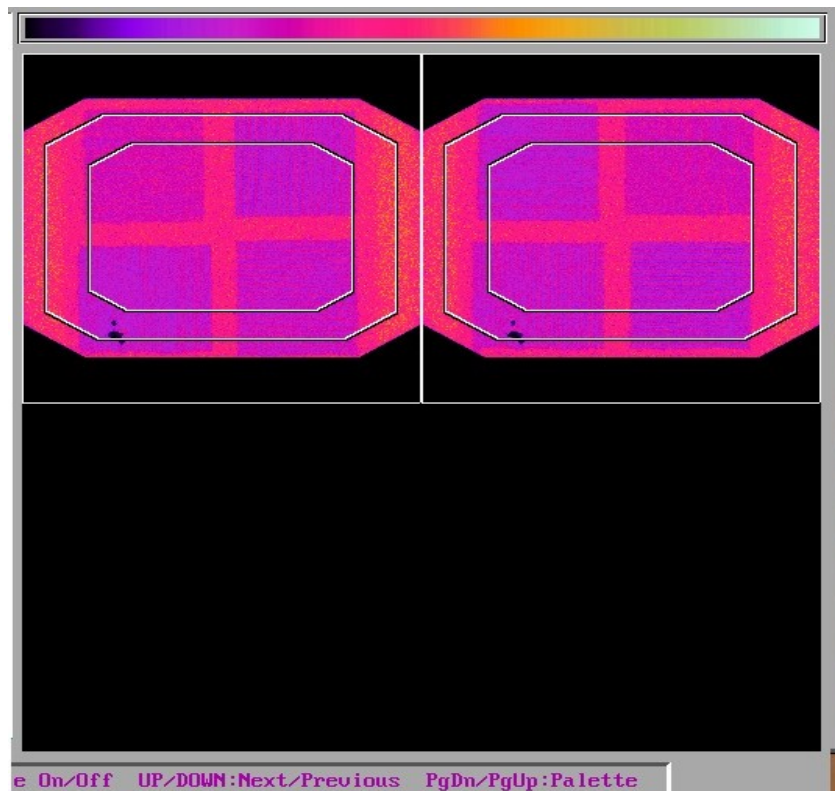


Figure 3-20: image of the bar quadrate phantom with CFOV and UFOV presented

There was some limitation appeared in the first model includes the non homogeneity of the radioactive source in the liquid flood phantom result from the weak thickness of the Perspex material used in manufacturing the phantom and from smallest open apparatus which result in

the presence of some air bubble within the phantom, the presence of the bubble affect the measure of integral and differential uniformity directly because the air acts as artifact in source homogeneity and result in bad uniformity image because of the bad distribution of the activity in the phantom i.e. presence of hot and cold spot in the image. The 1 mm thickness of lead appeared to be not enough thickness to absorbed abundance of the gamma photon especially the high flux photon from liquid phantom, however the 1 mm lead thickness showed good result in the low photon flux of the point source i.e. the 1 mm thickness was good for intrinsic resolution and linearity while it result in poor image quality of extrinsic resolution and extrinsic linearity measurements. The researcher takes into account the disadvantages and the limitations of the first model to design a new model that overcomes the limitation of the first model.

3-2 Model two:

When fabricate the second phantom, the researcher designed it to overcome the problems facing the first phantom by use 10mm lead thickness with computerized cutter machine instead of 1 mm lead thickness with manual cutter, and the use of Perspex instated of rubber in which the Perspex allow the grooves to be in deep of in 10mm instead of 1mm in the rubber, and lastly using 10 mm thickness Perspex instead of 1mm Perspex in fabrication of liquid flood phantom. The model number two also composed of two parts, part one which simulate the liquid flood phantom for measure all types of uniformity, and part two which simulate the quadrant bar phantom for measure the resolution and linearity of the planer and Single Photon Emission Computed Tomography SPECT gamma camera.

Part one is a combination of six different pieces of Perspex material, piece number one was a Perspex of 42 X 42cm in diameter and 10mm thickness, piece number two was a Perspex of 42 X 42cm with thickness of 1cm and open apparatus with 0.5cm diameter was made on it at the top of the Perspex sheet to be acts as entrance pathway of the water and radioactive materials and also acts as controlling the presence of the air bubble in the phantom and also to insure the homogeneity of the radiotracer inside the flood phantom, the other remaining four pieces were dimension of 42 X 1 cm and using to link Perspex pieces number one and two, the linking done using silicon materials. The open apparatus made on the phantom have a diameter of 0.5cm and closed and reopened using a pyramidal shape made from wood.

The researcher used a 10mm thickness of Perspex instead of 1mm thickness used in the first model to overcome the limitation showed in the first model by insuring a well homogeneity of the radioactive material and decrease the chance of the air bubble formation which lead to presence of hot and cold spots that affect the result of the test directly i.e. the researcher used 1cm thickness to overcome the limitation of the flood phantom of the first model and to overcome the disadvantage of the result of the liquid phantom. The liquid flood phantom of the second model was manufactured and introduced by Khartoum engineering company as researcher request.

Part two which simulate the bar quadrant phantom and used to measure some gamma camera quality control tests includes extrinsic linearity and resolution, and intrinsic linearity and resolution. The quadrate bar phantom was composed of five main subjects include:

- A 46 X 46 cm with 5mm thickness Perspex sheet with four small holes (0.2mm in diameter) at each corner of the sheet, these holes play a role in fixing the whole component of the phantom together. The function of the sheet was to hold all other subjects of the phantom on it.
- The second subjects containing the phantom was a Perspex sheet with dimension of 46 X 46 cm diameter and 5mm thickness, also with holes made at each corner of the sheet to play a role in fixing all the component of the phantom together. The main function of this sheet was to cover other subjects of the phantom which was already fixed at the sheet on the first point.
- The third parts of the bar quadrate phantom was a Perspex sheet with dimension of 42 X 42 cm and 5mm thickness, the sheet of Perspex was divided into main four areas each have dimension of 20 X 20cm, a grooves within this areas of sheet with defined dimension was made using laser cutter machine the first area located at the right upper corner of the sheet which contain 26 grooves with dimensions of 18cm X 0.35cm and separated from each other by distance of 3.5mm, the area located at the right lower corner was the second area and in this area a 30 grooves was made with 18cm length and 3mm width and each adjacent grooves was separated by distance of 3mm, the third area located at the left lower area containing 32 grooves with dimension of 18cm X 0.25 cm with 2.5mm distance separate the every nearest grooves from each other, and the last quadrate which located at the left upper corner of the sheet containing 32 Grooves with 18 cm length and 2mm width and separated from each other

by factor of 2mm. at the edge of the phantom i.e. the remaining 2 cm a big grooves was made with dimension of 36cm length and 5mm width and the main objective of this grooves was to measure the linearity of the gamma camera by measuring Modulation transfer function (MTF) of the Line Spread Function (LSF).

The part number four of the phantom was lead materials. Lead was manufactured with dimension similar to that dimension of the grooves which discuss in the previous point by factors that the lead will embedding inside that grooves. First a big sheet of steel materials (lower affecting by temperature than lead) was introduced and grooves within the steel sheet was made using cutter milling machine (knee type. England 1957) machine. The dimension of the grooves was 18cm X 0.35cm, 18cm X 0.3cm, 18cm X 0.25cm, 18cm X 0.2cm, and 36cm X 0.5cm. the second step was putted the lead material in heating machine (Gas stove) for 10 min at more than 327.5° C (melting point of lead) so the lead was converted to the liquid phase instead of sold phase, then the liquid lead was distributed over the grooves of the steel sheet (fig 3-21), after short interval time the liquid lead was reconverted to solid status and Hit the steel mold by hummers to separate the lead from the steel mold then lead pieces was collected after Insure that there was no any cracks filling defect in the lead bar.

- . The researcher repeat this process until collected whom numbers that compatible with the number of grooves that made at the Perspex sheet. Then the pieces of lead collected were smoothed using special cutter.



Figure 3-21: image shows the Steel mold

- The last subjects of the phantom was four Nails which act as fixer to the whole component of the phantom.

The Perspex with grooves (point 3) was fixed to the sheet of Perspex (point 1) using silicon material, after that a pieces of lead (point 4) was introduced and embedded inside the grooves of Perspex (point 3), the second sheet of Perspex (point 2) was putted at the top of the phantom and all the component of the phantom was fixed together using the four Nails (Point 5).

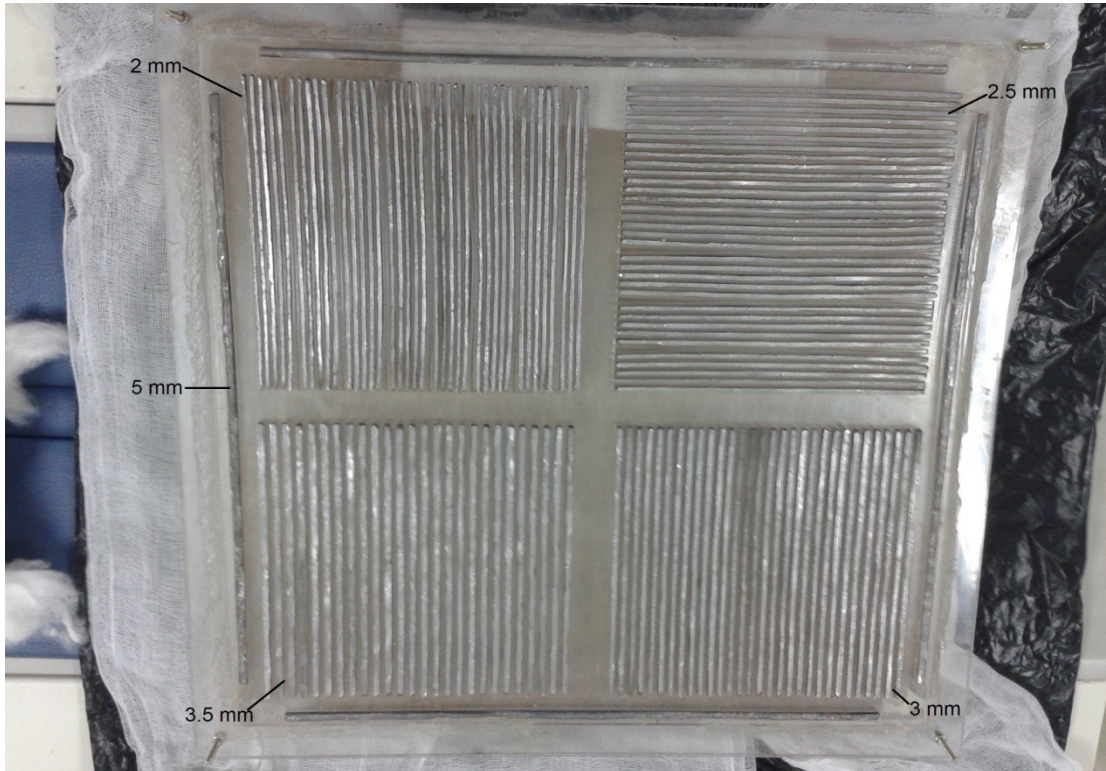


Figure 3-22 : image shows the par phantom with lead thickness presented

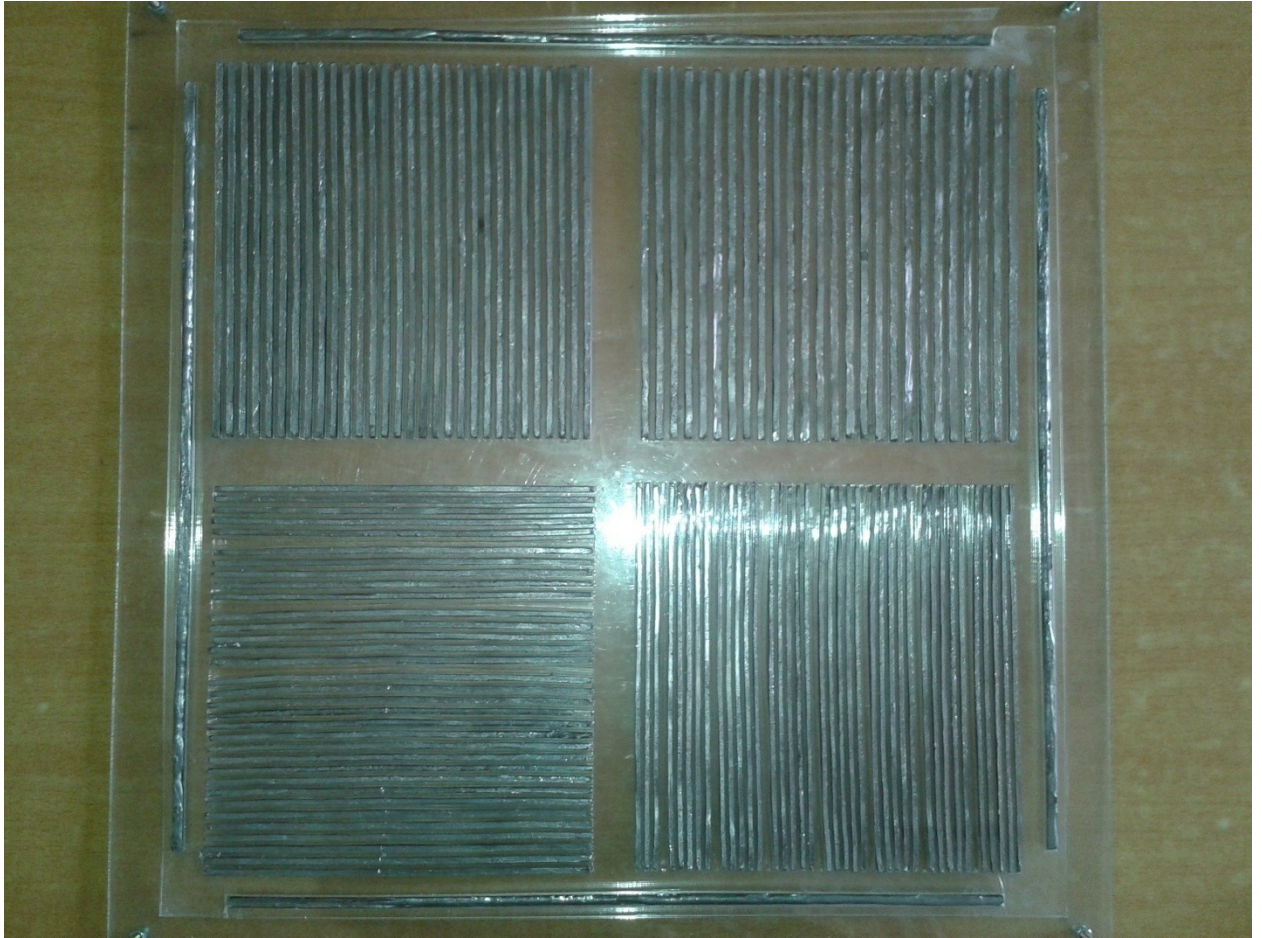


Figure 3-23: image shows the whole par phantom

3-2-1 Methods of data collection:

The whole phantom was tested and experimented in Mak Nimr University Hospital, Nuclear medicine department, Nucline Sprit model, single head SPECT gamma camera made at hunger and installed 2009 in Sudan. The method of experiment, image acquisition and data collection was performed according to the parameters recommended by NEMA, IAEA, Zenzonico (2009), Sokolo et.al. (2010) and specific parameters from the camera manual.

The first step was the preparation of the liquid flood phantom by added mixture of water (1500ml) and $\text{Na}^{99\text{m}}\text{TcO}_4$ (1.3 mCi) into the phantom by using the open apparatus of the phantom, after insured there was no any presence of the air bubble on the phantom a gentle shaking was made to insure the homogeneity of the radioactive material within the phantom. the $\text{Na}^{99\text{m}}\text{TcO}_4$ was collected from 15GBq ^{99}Mo - $^{99\text{m}}\text{Tc}$ generator, Monrol, Turkey by elution process

using 10ml NaCl and specific activity was measured to determine the amount of volume adding to the phantom.



Figure 3-24: image shows the nuclear medicine technologist during preparation of ^{99m}Tc for Flood phantom



Figure 3-25: image shows the flood phantom after preparation



Figure 3-26: image shows ^{99}Mo - $^{99\text{m}}\text{Tc}$ generator used

The second step was centering the liquid phantom on the camera table facing the central Field of View (CFOV) and image was acquired using count mode of 16 million counts take 2014seconds

at rate of 7749 cps using the parameter of 256 X 256 X 16 matrix size, body contour off, full field detector mask, 0 degree orientation, Low Energy High Resolution collimator, Intrinsic flood correction, 140KeV energy peak and 20% energy window width. The researcher used plastic bags and absorbable materials, placed between the liquid phantom and gamma camera table and head, as preventing step to avoid any chance of contamination may occur during the experiment.



Figure 3-27: image shows the plastic bags and absorbable material on gamma camera head



Figure 3-28: image shows the flood phantom center on the camera table with collimator inferior

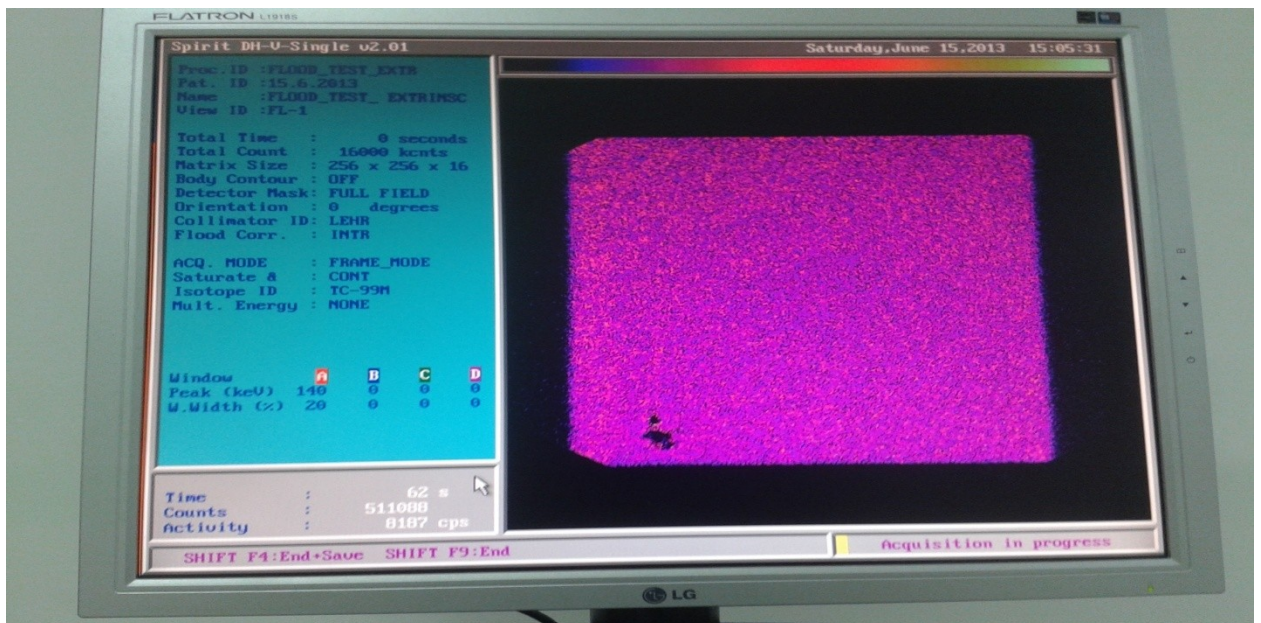


Figure 3-29: image shows the work station computer during flood source image

The third step was collected and centering the bar quadrant phantom over the centred flood phantom on gamma camera table, while the detector superior to the phantom and centred to be perpendicular to each other. Also plastic bags and absorbable materials was used to avoid any contamination may occur during load of heavy bar phantom on the liquid flood source. Serial sets of images was acquired using one variable parameter of matrix size of the image which include 64 X 64 X 16, 128 X 128 X 16, 256 X 256 X 16, 512 X 512 X 16, 1024 X 1024 X 16, 64 X 64 X 32, 128 X 128 X 32, 256 X 256 X 32, 512 X 512 X 32 and 1024 X 1024 X 32 matrix size while the fixed parameters includes frame mode acquisition mode, 140KeV energy peak window, 20% energy window, 0 degree orientation, Low Energy General Purpose collimator, full field detector mask and intrinsic system Flood correction. Energy image contain at least 16000Kcounts and the mean acquisition time for every image about 200 seconds.

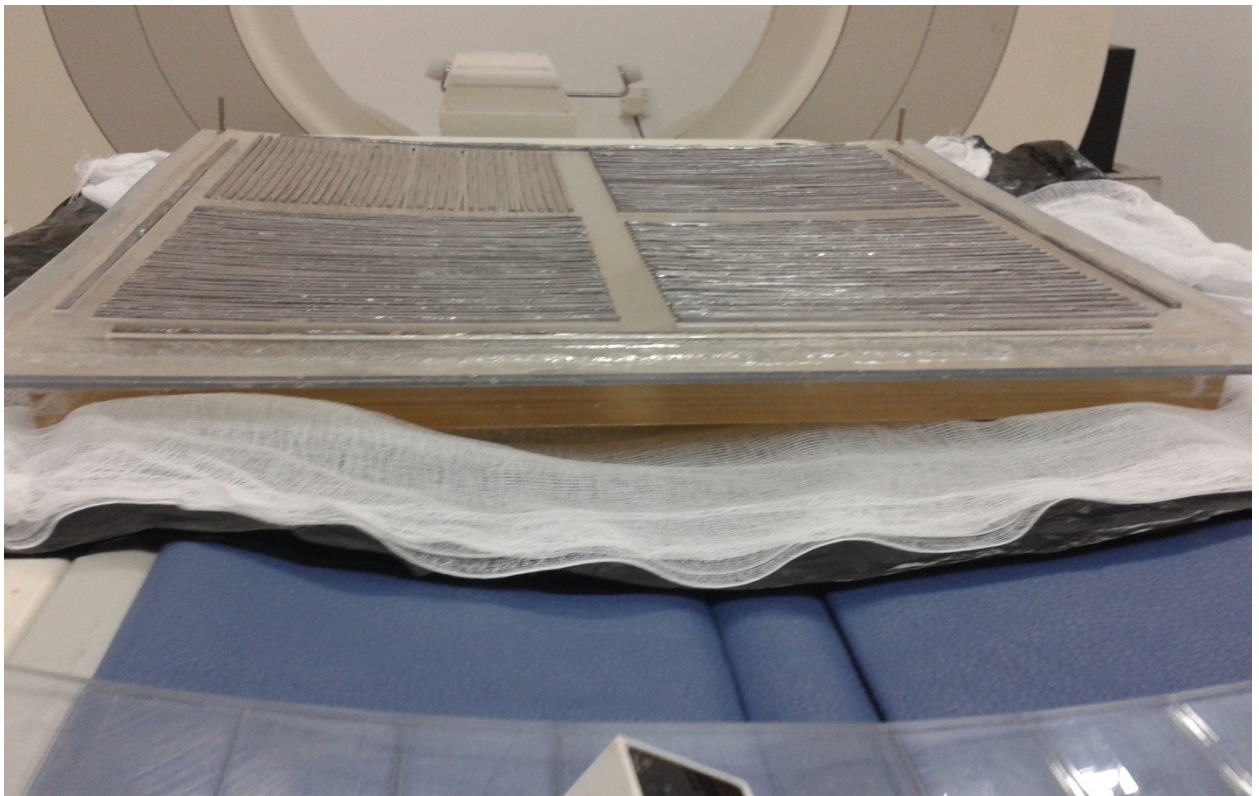


Figure 3-30: image shows the par phantom centering over the flood phantom (front view)



Figure 3-31: image shows the par phantom centering over the flood phantom (side view)

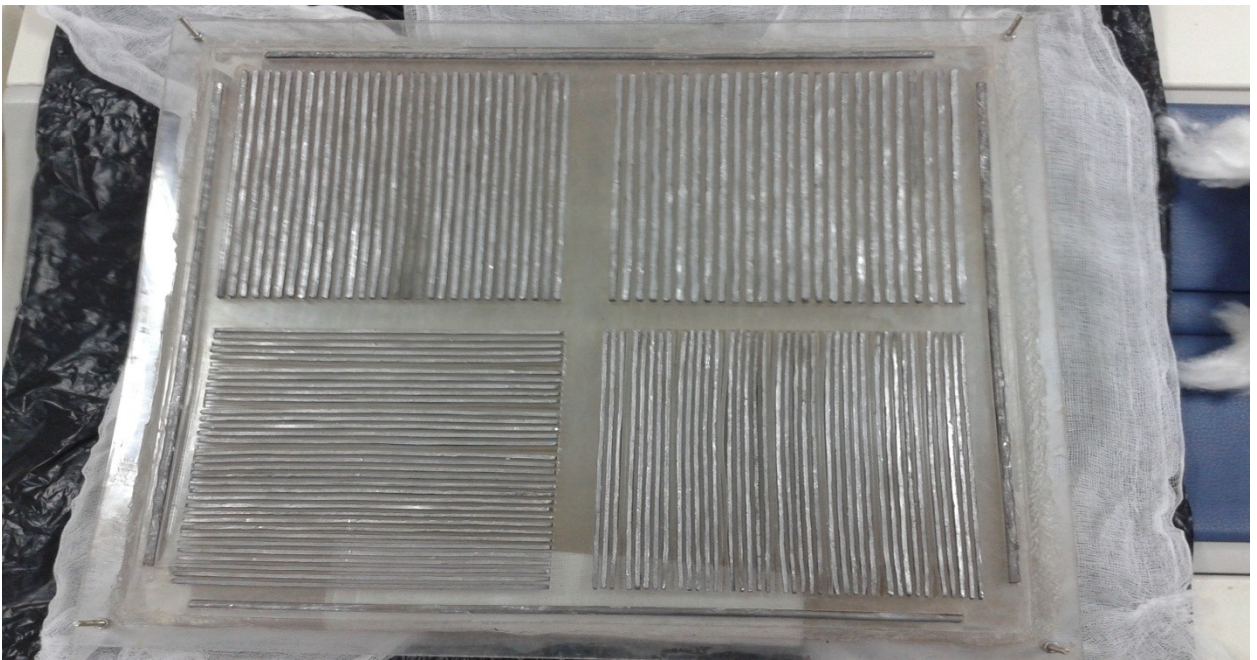


Figure 3-32: image shows the par phantom centering over the flood phantom (superior view)

The fourth steps was remove of collimator from gamma camera detector with point source of $1\text{mCi } ^{99\text{m}}\text{Tc}$ fixed at the ceiling perpendicular to camera head, the researcher used the same positioning center in the third step, a sets of serial images were acquired using full field detector mask, 0 degree orientation, intrinsic detector without collimator, intrinsic flood correction, frame mode acquisition mode, 140 KeV energy peak and 20% energy window width with sets of variable matrix size of 64×64 , 128×128 , 256×256 , 512×512 and 1024×1024 with 16 or 32 word. Every image contains 16 million counts acquired at interval mean time of 200 seconds.

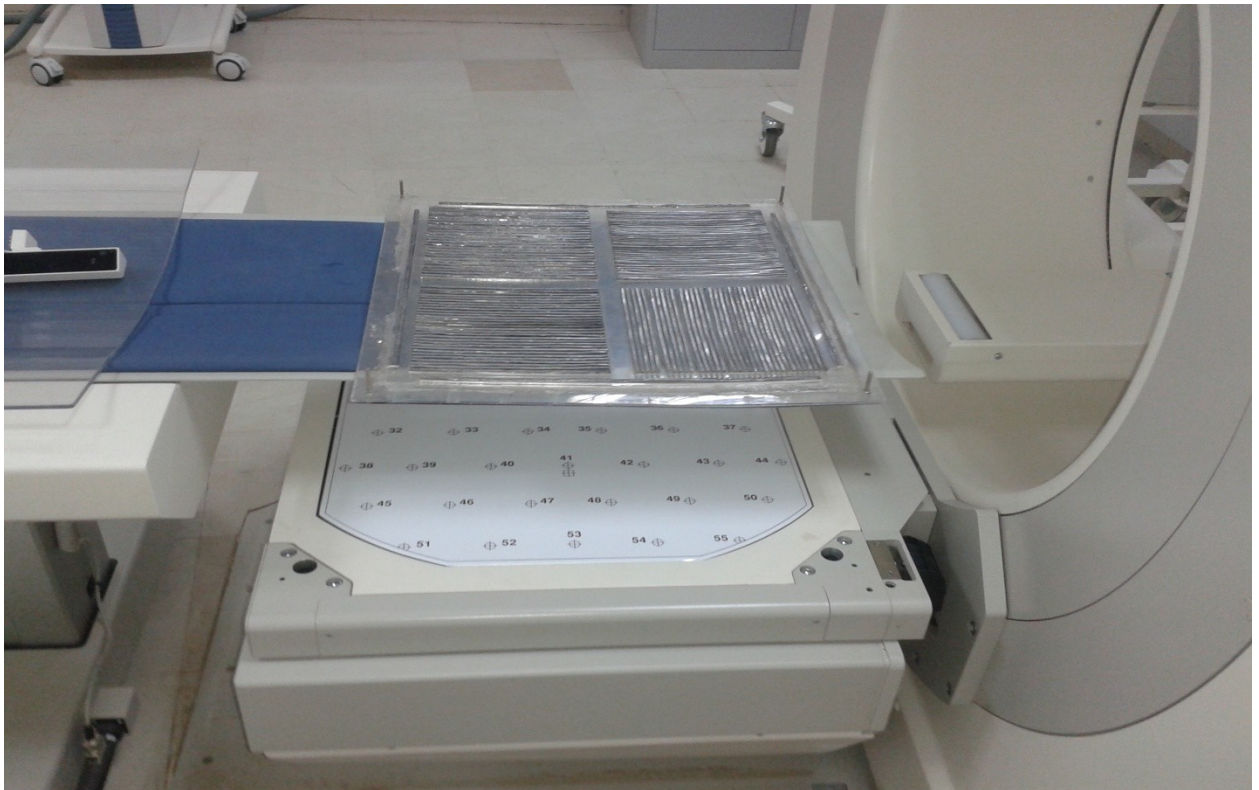


Figure 3-33: image shows the par phantom centering over the camera table and head below the phantom without collimator (front view)



Figure 3-34: image shows the point source centering over the camera head at ceiling

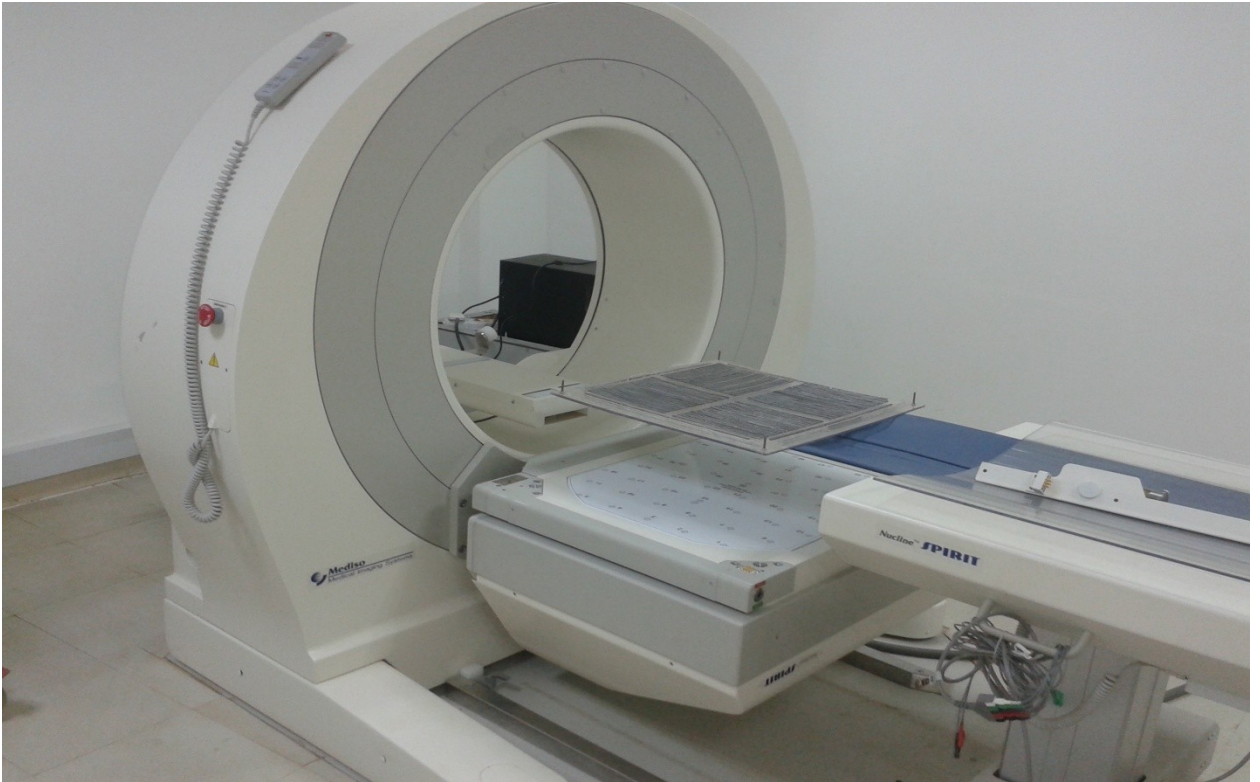


Figure 3-35: image shows the par phantom centering between the camera head and point source on camera table

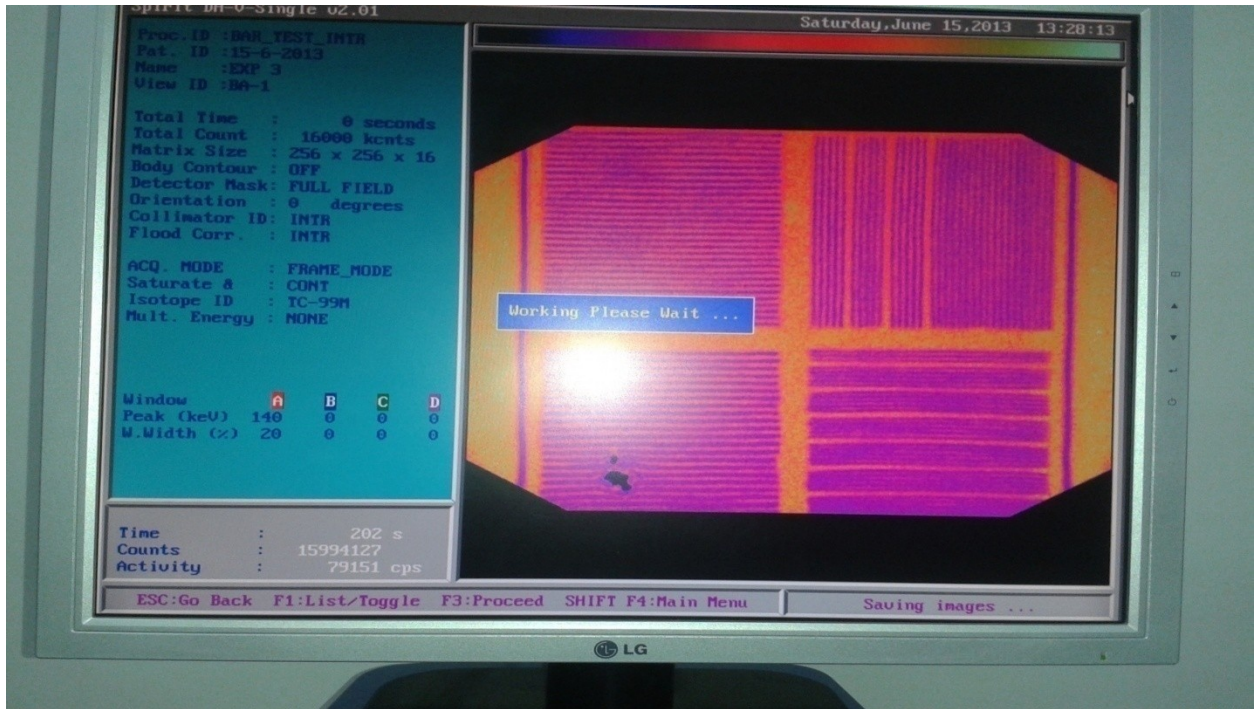


Figure 3-36: image shows the work station during intrinsic bar phantom image with 256 X 256 matrix size

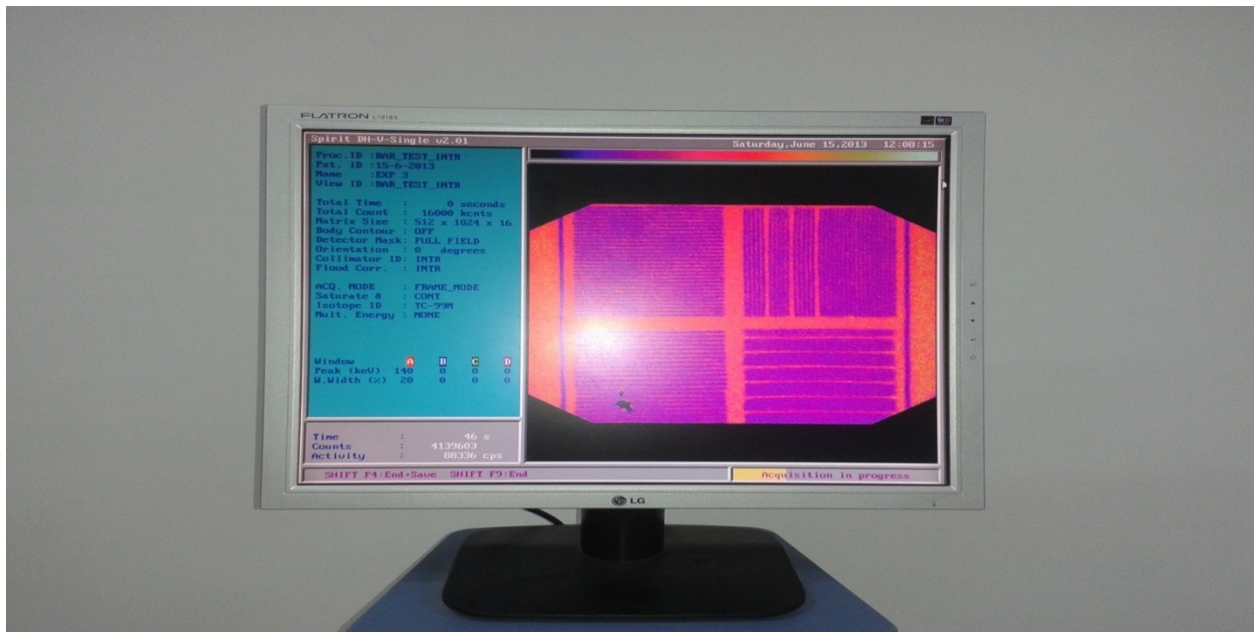


Figure 3-37: image shows the work station during intrinsic bar phantom image with 512 X 512 matrix size

The fifth step was the remove of collimator and remove of radioactive material from flood phantom using simple decontamination precautions to insure there was any type of contamination, also contamination detector and survey meter was used by the researcher to scan all areas of work during experiment including the hot lab, gamma camera room and waste storage, the researcher insured that there was no any type of contaminations generated as a result of the experiment.

Even with the development in the result from the first phantom, the researcher follows the recommendation of the Michael K et.al. That: While the 4-quadrant bar phantom is the most commonly used phantom for measurements of system resolution, it is not ideally suited to the assessment of system linearity. Hence, test pattern such as the orthogonal hole pattern or the parallel line equal spacing phantom are preferable to the four-quadrant phantom as they allow assessment of both linearity and resolution. The researcher used a modified slit phantom for measuring both linearity and resolution instead of four quadrant phantom, this s the basic idea for the fabrication the last version of the phantom.

3-3 Phantom No Three:

Slit phantom and four quadrate bar phantom are two types of phantoms that used to measure the resolution and linearity of the gamma camera. The researcher fabricated the slit phantom to compare the results of these two phantoms.

3-3-1 Part one: slit phantom, when made from pure lead materials, a piece of 20cm X 20cm lead was made after converted the lead materials into liquid from using 400C⁰ oven for 10min and then the liquid lead was shaping as required by the researcher and let to be reconverted into the sold format of that shape, the piece of lead was then introduced to CNC machine at KHARTOUM CENTER FOR TAINNG THR TRAINEE and grooves within the piece of lead was made with different length and thickness, the length of grooves was range from 5 cm to 18cm while the thickness is range from 10mm to 4 mm .

3-3-2 Part two: the liquid flood phantom. one is a combination of six different pieces of Perspex material, piece number one was a Perspex of 42 X 42cm in diameter and 10mm thickness, piece number two was a Perspex of 42 X 42cm with thickness of 1cm and open apparatus with 0.5cm diameter was made on it at the top of the Perspex sheet to be acts as entrance pathway of the

water and radioactive materials and also acts as controlling the presence of the air bubble in the phantom and also to insure the homogeneity of the radiotracer inside the flood phantom, the other remaining four pieces were dimension of 42 X 1 cm and using to link Perspex pieces number one and two, the linking done using silicon materials.

The open apparatus made on the phantom have a diameter of 0.5cm and closed and reopened using a pyramidal shape made from wood.



Figure 3-38: image of Flood phantom

The researcher used a 10mm thickness of Perspex instead of 1mm thickness used in the first model to overcome the limitation showed in the first model by insuring a well homogeneity of the radioactive material and decrease the chance of the air bubble formation which lead to presence of hot and cold spots that affect the result of the test directly i.e. the researcher used 1cm thickness to overcome the limitation of the flood phantom of the first model and to overcome the disadvantage of the result of the liquid phantom. The liquid flood phantom of the

second model was manufactured and introduced by Khartoum engineering company as researcher request.

3-3-3 Method of data collection:

The two phantoms was introduced to Royal Care International Hospital (RCIH), Nuclear Medicine Department, Nucline Spirt dual head gamma camera made in Hungary and installed 2011 and to Radiations and Isotopes Center of Khartoum (RICK), Nuclear Medicine Department, Nucline Spirt dual head gamma camera made in Hungary and installed 2007. A flood phantom was prepared by addition of 1.3 mCi, $\text{Na}^{99\text{m}}\text{TcO}_4$ to a volume of one liter, the $^{99\text{m}}\text{Tc}$ isotope was obtained from $^{99}\text{Mo}/^{99\text{m}}\text{Tc}$ generator, Monrol company, made in Turkish (fig 3-29). The flood phantom was checked that it free from any air bubble and gently shake was done to insure the homogeneity of the radiotracer in the phantom, then the phantom was lied in the gamma camera table facing the Central Field of View (CFOV) and image was acquired using 512 X 512 matrix size, the image contain on million counts and this image demonstrate the extrinsic uniformity of the camera.



Figure 3-39: Image showed the $^{99}\text{Mo}/^{99\text{m}}\text{Tc}$ generator



Figure 3-40: Image showed the liquid flood phantom during acquisition

The slit phantom was then placed in the center of the liquid flood phantom perpendicular to the camera head and facing the CFOV of the camera, a set of image was then acquired using 512 X 512 matrix size, and the slit phantom was oriented each image for 90°, this sets of images demonstrate the extrinsic resolution and linearity of the camera.



Figure 3-41: Image show the slit phantom and flood phantom during acquisition

Then the two phantoms was removed from the camera and also camera collimator was removed, and point source of 1 mCi ^{99m}Tc was placed in the roof of the imaging room with distance that equal to the five times the camera FOV and image was acquired using 512 X 512 matrix size, this image was demonstrated the intrinsic uniformity of the camera. Then the slit phantom was centered between the point source and the camera head and images wad acquired using the same matrix size and this mage was demonstrated the intrinsic linearity and resolution of the camera.



Figure 3-42: Image show the slit phantom centred during intrinsic image

The researcher used the slit phantom instead of 4-bar quadrant phantom as recommended by Michael K. et al. which demonstrate that the four bar quadrant phantom was not ideal in the measuring of camera linearity on the one hand the slit phantom was recorded to be the ideal for measuring both camera linearity and resolution.

3-4 Description of the independent programme:

The developed Q.C software complements camera specific manufacture software by providing an independent processing platform regardless the type of camera. The software must be based on NEMA recommendation regarding processing and analysis of the data (9), Our independent software for analysis of the gamma camera quality control image was basically designed according to the equations and parameter recommended by The NEMA Standards Publication NU 1-2007 which described how to perform process and report QC tests for gamma and SPECT cameras and run in IDL (Interactive Data Language for windows integrated development environment version 6.1) it is capable of calculating intrinsic spatial resolution and linearity (ISR

and ISL), intrinsic spatial resolution and linearity (ESR and ESL), intrinsic and extrinsic integral and differential uniformity. The program is aimed to make the processing of Q.C data simple, easy and independent on manufacture. Making our program independent of IDL environment and development of an automatic-report generation using e.g. LaTeX are our vision that the software will be open access.

LSF acquisition: the line profile containing maximum pixel data was acquired and linear extrapolation was performed to condition the data for spectral estimation (8).

MTF computation: the MTF was obtained from the Fast Fourier Transformation (FFT) of the line spread function LSF and normalization to unity of zero spatial frequency.

Chapter four

Result

The fabricated phantom has been compared with the standard SPECT phantom to determine to what extent it mimics the standard one in view of QC test.

4-1 Resolution:

The designed phantom has been excerpted from the phantom parameters stated by International Atomic Energy Agency DOC-602 , NEMA-2001, Ng et al, Holstensson et al, and Islamian et al, , which consists of four quadrat bars as recommended by Zanzorico et al. The frontal part of the phantom made of Perspex (42×42×10 cm) shown in Figure 4-1 that simulates the four quadrant bars phantom each one was 20×20 cm, which have been grooved by laser cutting bed (BCL-B series model BCL1318B china 1991). The first quadrant implies 26 grooves with dimensions of 18×0.35 cm and separated from each other by distance of 3.5mm. The second quadrant contains 30 grooves as 18 cm×3mm and each adjacent grooves was separated by distance of 3 mm, the third quadrant contains 32 grooves with dimension of 18cm × 0.25 cm separated by 2.5 mm distance, and the forth quadrant contains 32 Grooves with 18 cm× 2 mm and separated from each other by factor of 2 mm. The edge of the phantom i.e. the remaining 2 cm; a big grooves was made with dimension of 36 cm length and 5 mm width, which is used to measure the linearity of the gamma camera by measuring Modulation transfer function (MTF) of the Line Spread Function (LSF). The back part simulates the liquid flood phantom made of Perspex (42×42×1 cm) Figure 4-2 and has orifice 0.5 cm to be fill with a liquid radioactive material, controlling the air bubbles and insuring the homogeneity. Then some lead wires have been fabricated in smooth and fine shapes according the dimension of the grooves (18 × 0.35cm, 18×0.3 cm, 18×0.25 cm, 18× 0.2 cm and 36×0.5 cm) which then have been mounted in the relevant grooves in the front quadrants. Then a mixture of water (1500ml) and Na^{99m}TcO₄ (1.3 mCi) has been flushed into the phantom via the orifice, shacked to maintain the homogeneity and air bubbles free. Then, the phantom has been put on the couch and centered to the gamma camera (Nucline Sprit model, single head SPECT-Hungarian) facing the central Field of View (CFOV) and image was acquired using count mode of 16 million counts last for 2014 seconds at rate of 7749 count/second (cps) using the parameter of 256 × 256 × 16 matrix size, body contour and full

field. The method of imaging acquisition, phantom parameters and data collection was performed according to the parameters recommended by NEMA, IAEA, and Ellinor et al.



Figure 4-1: shows the frontal part of the phantom made of Perspex (42×42×10 cm) that simulates the four quadrant bars phantom each one was 20×20 cm.



Figure 4-2: shows the back part simulates the liquid flood phantom made of Perspex (42×42×1 cm) and has orifice 0.5 cm to be fill with a liquid radioactive material

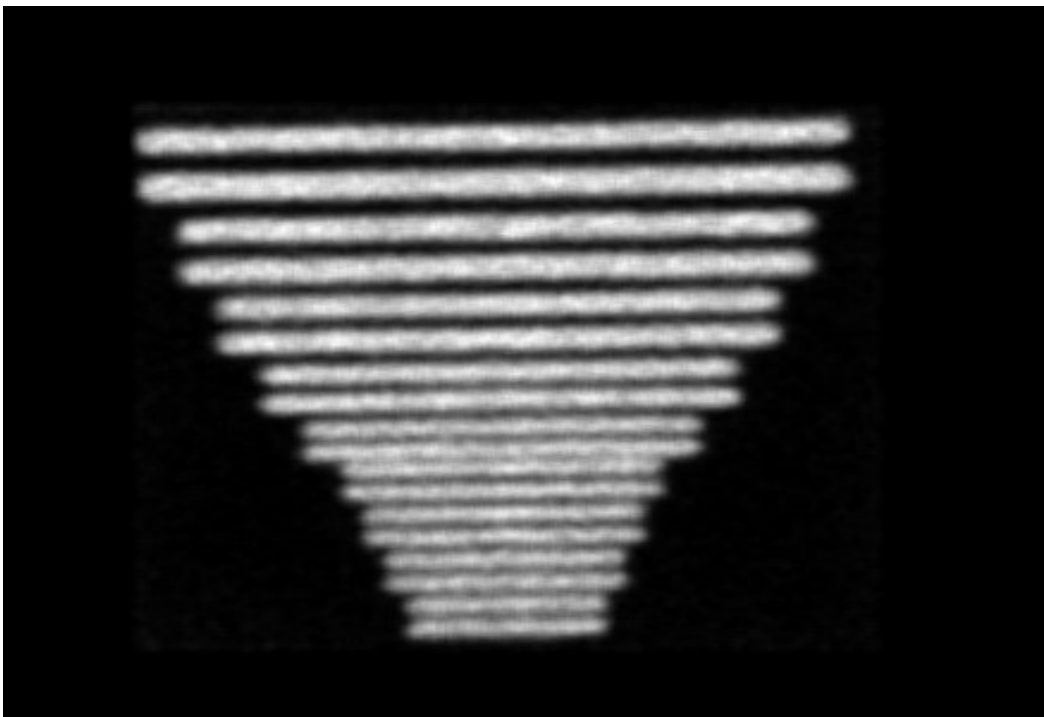
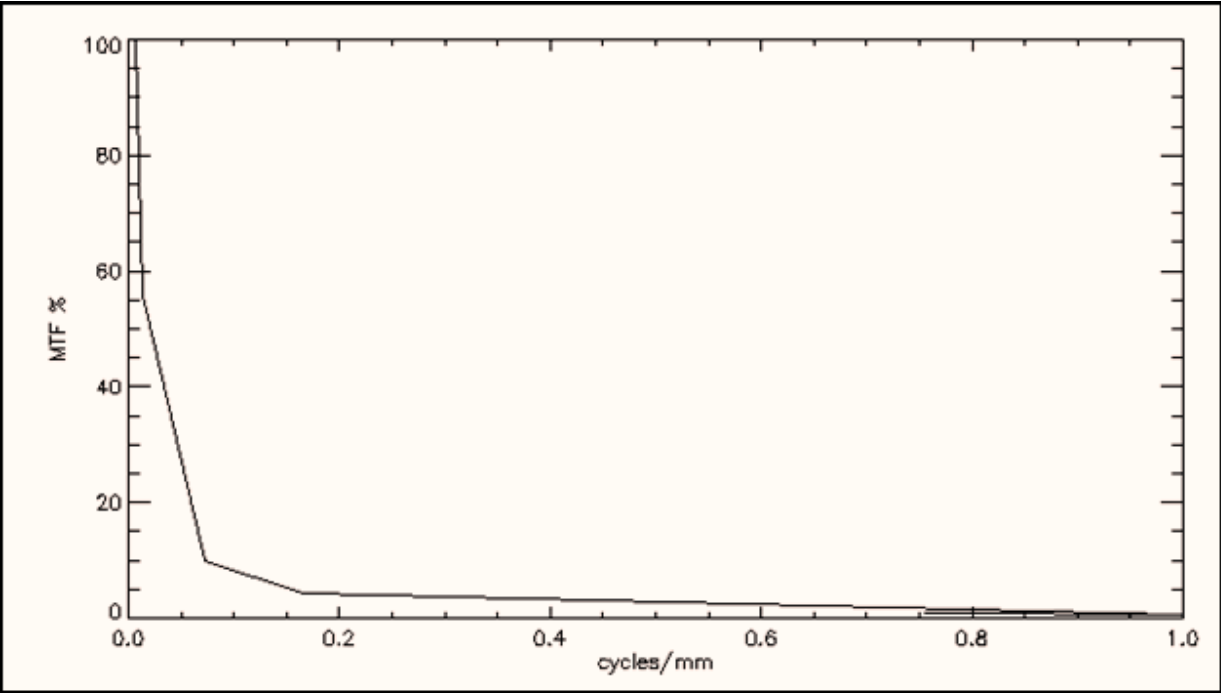


Figure 4-3: Showed example image of our fabricated phantom

Fig3: is the result of our program for measuring MTF at 10%, the MTF% plotted in the (Y) axis, while the frequencies (cycle/mm), where plotted on the × axis. As a result the MTF at 10% is corresponding to 0.07 cycle/mm.

Figure 4-4: showed our program result for measuring the resolution



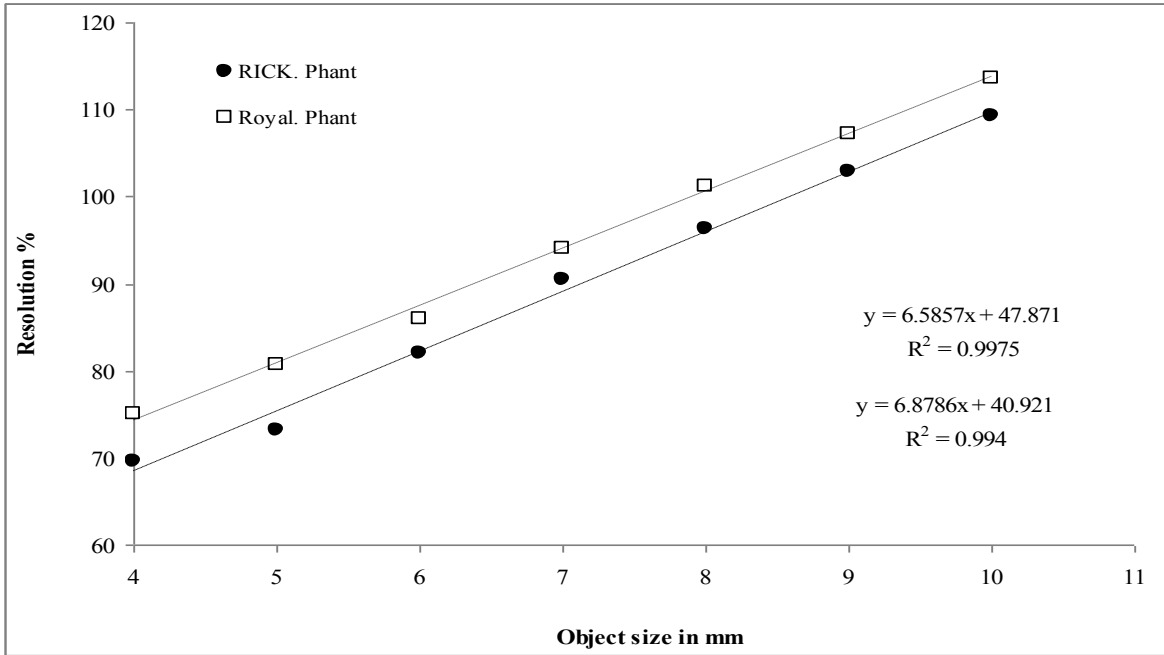


Figure 4-5: shows the resolution % vs. objects size for SPECT in RICK and Royal care hospitals-Khartoum Sudan using developed phantom.

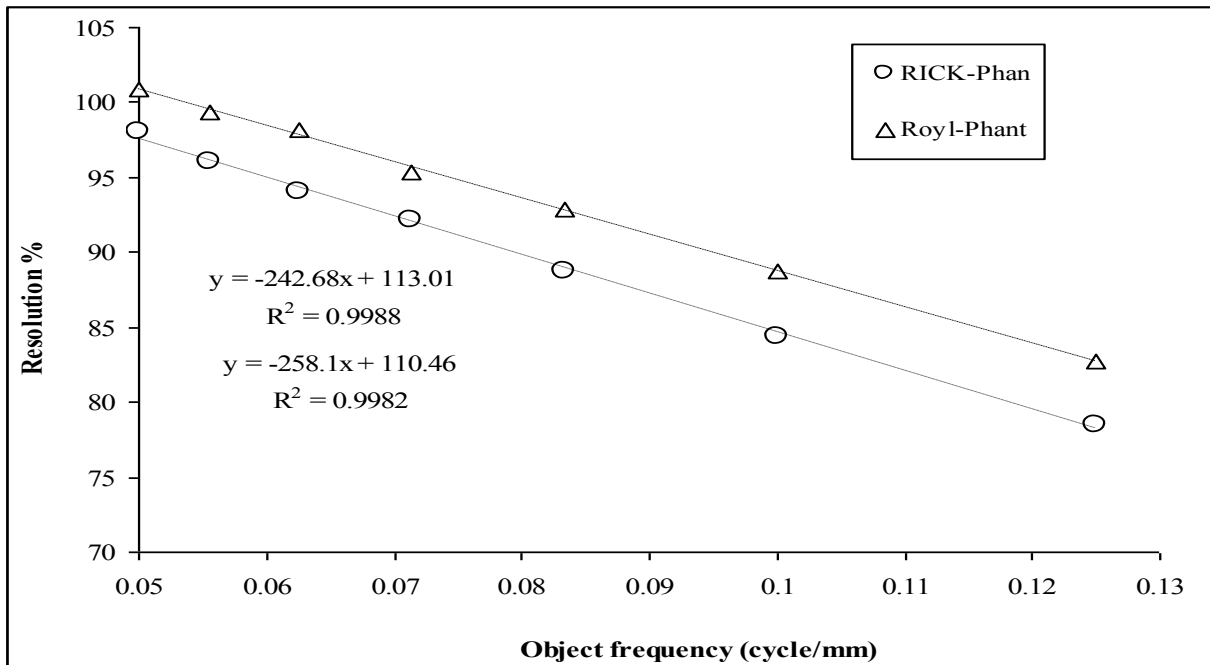


Figure 4-6: shows the resolution % vs. objects frequency for SPECT in RICK and Royal care hospitals-Khartoum Sudan using developed phantom.

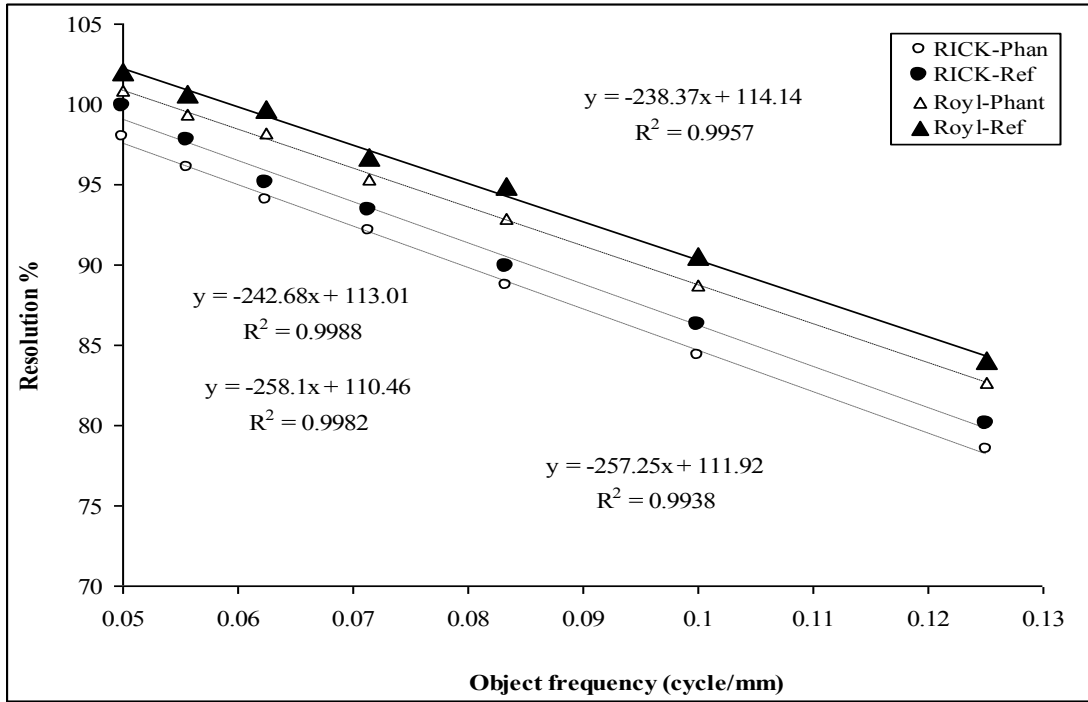


Figure 4-7: shows the comparison resolution% measured by phantom and the QA base line for Royal Care and RICK hospitals.

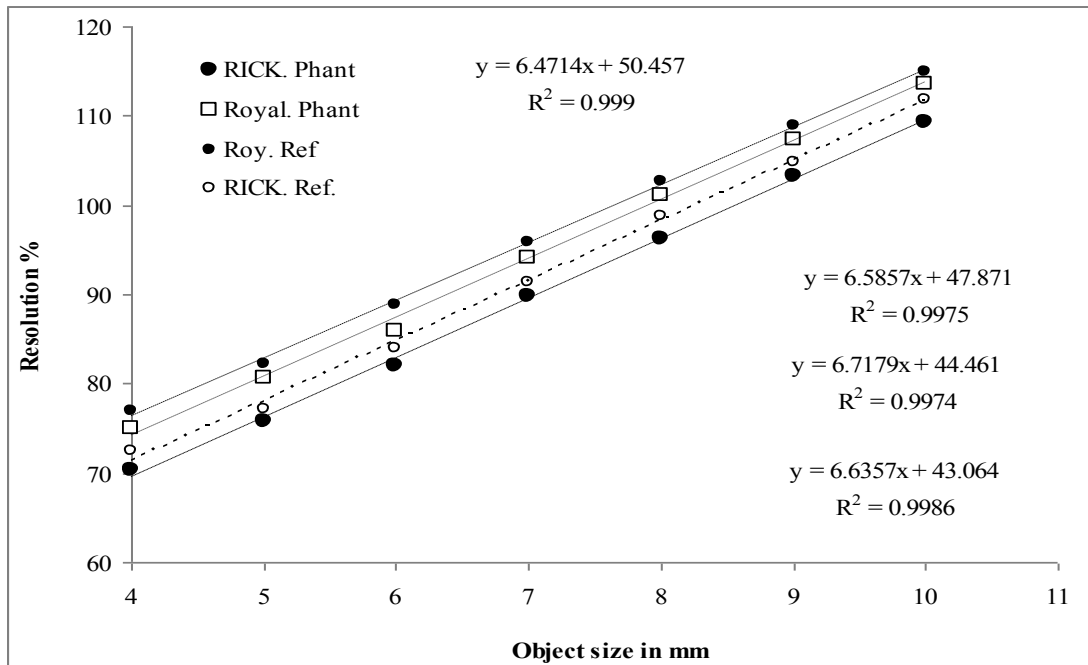


Figure 4-8: shows the comparison resolution% measured by phantom and the QA base line for Royal Care and RICK.

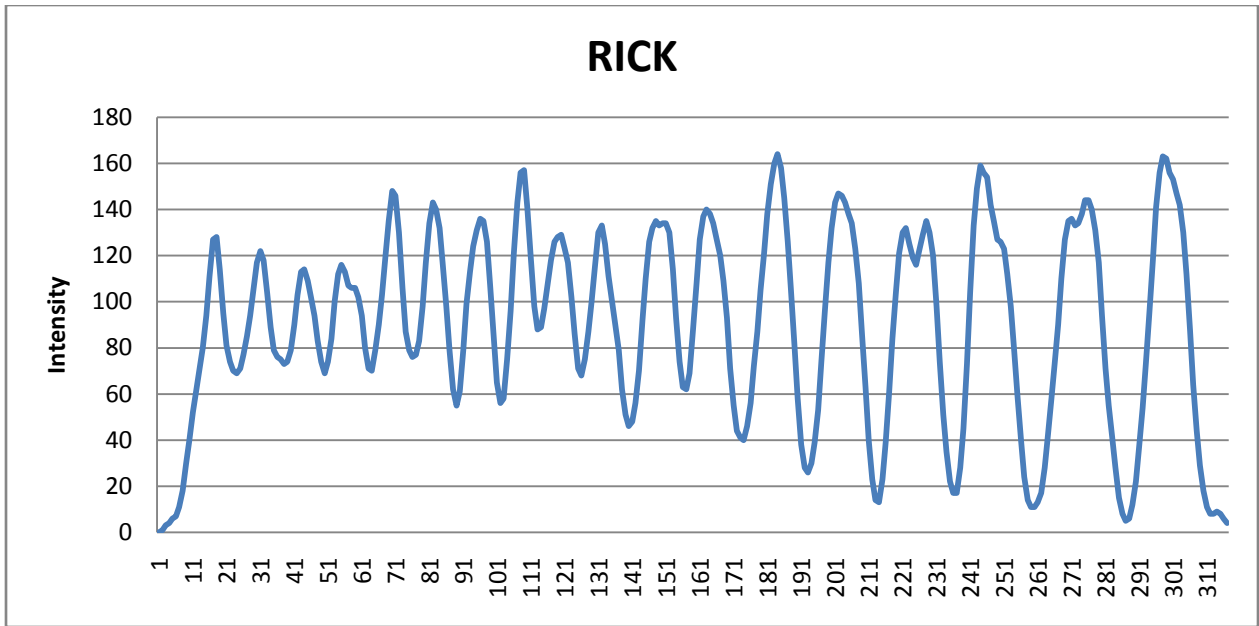


Figure 4-9: showed the intensity of all lines of slit phantom at RICK

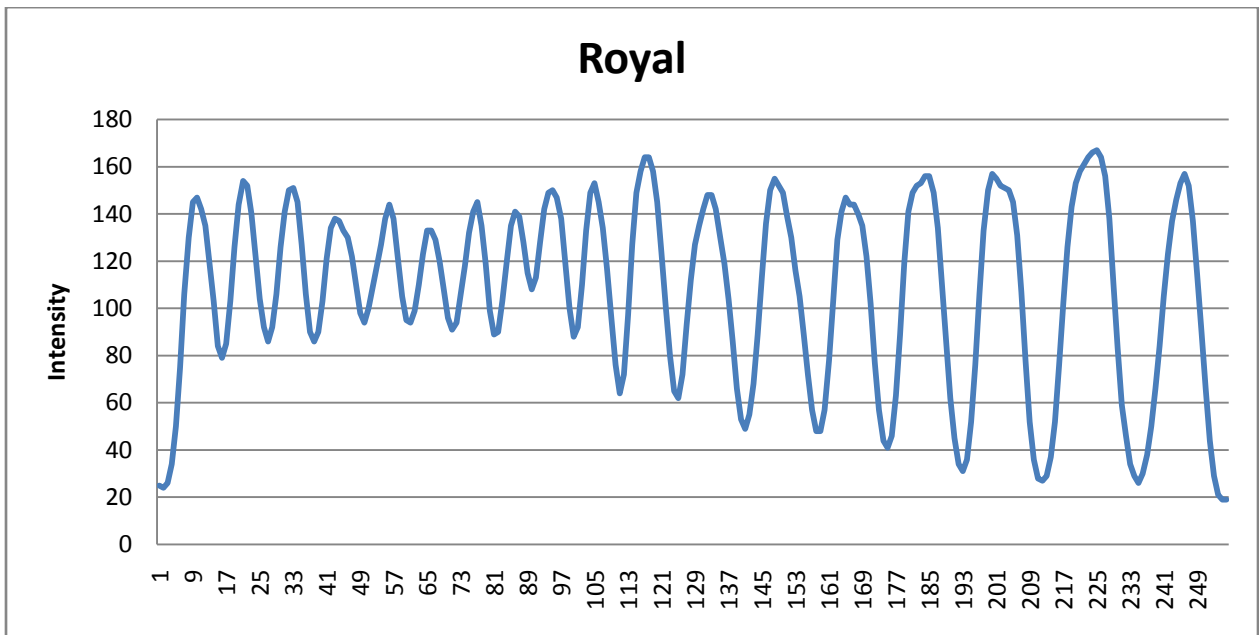


Figure 4-10: showed the intensity of all lines of slit phantom at RCIH

4-2 Uniformity and linearity:

The following results shows the data of Gama Camera SPECT as counts obtained by the developed phantom in X-axis and Y-axis direction for assessing the linearity as well as the flood field uniformity obtain from the gamma camera and the analyzed one using IDL program which is constructed as phantom specific program to convert the flood field uniformity of the gamma camera into point spread function image.

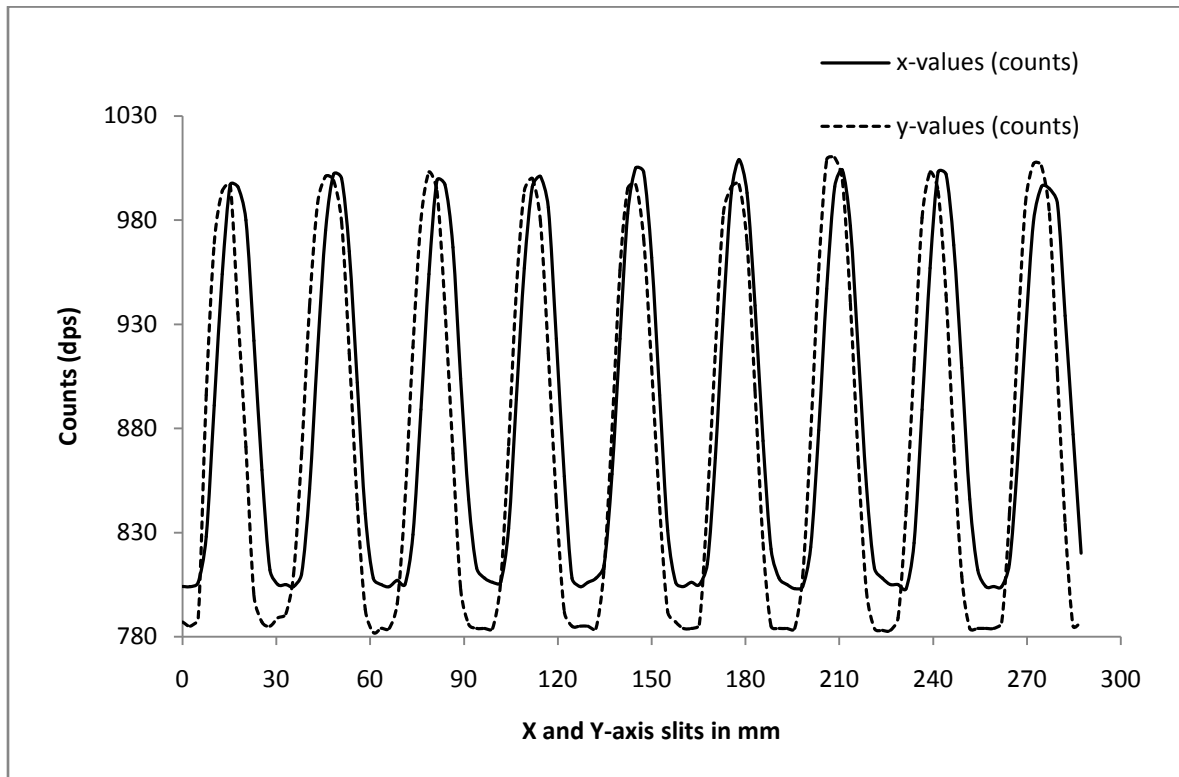


Figure 4-11: shows the counts distributions in X and Y-axis direction via phantom lead slits

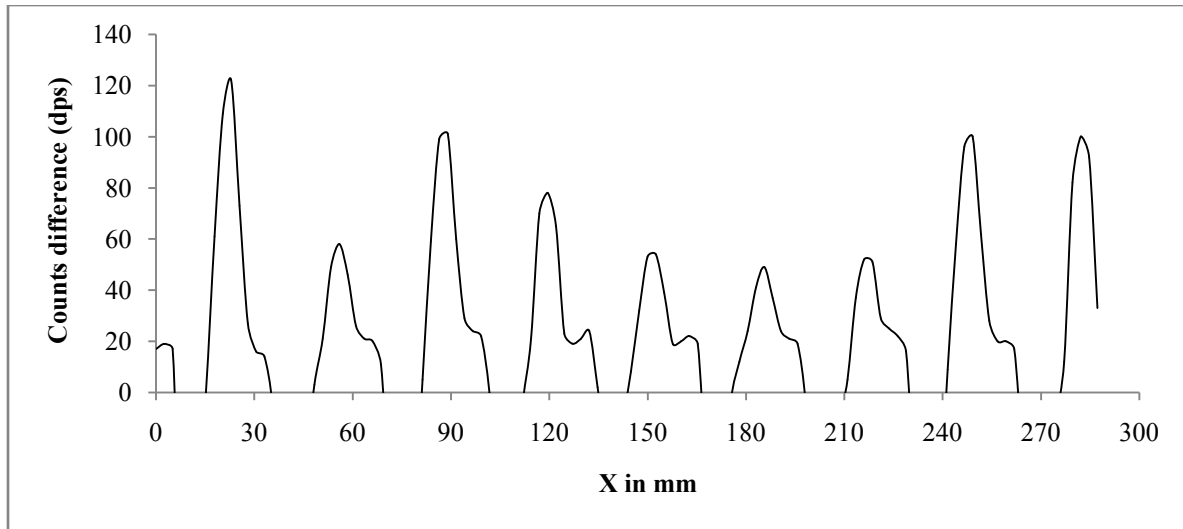


Figure 4-12: shows the counts difference in X and Y-axis direction via phantom lead slits

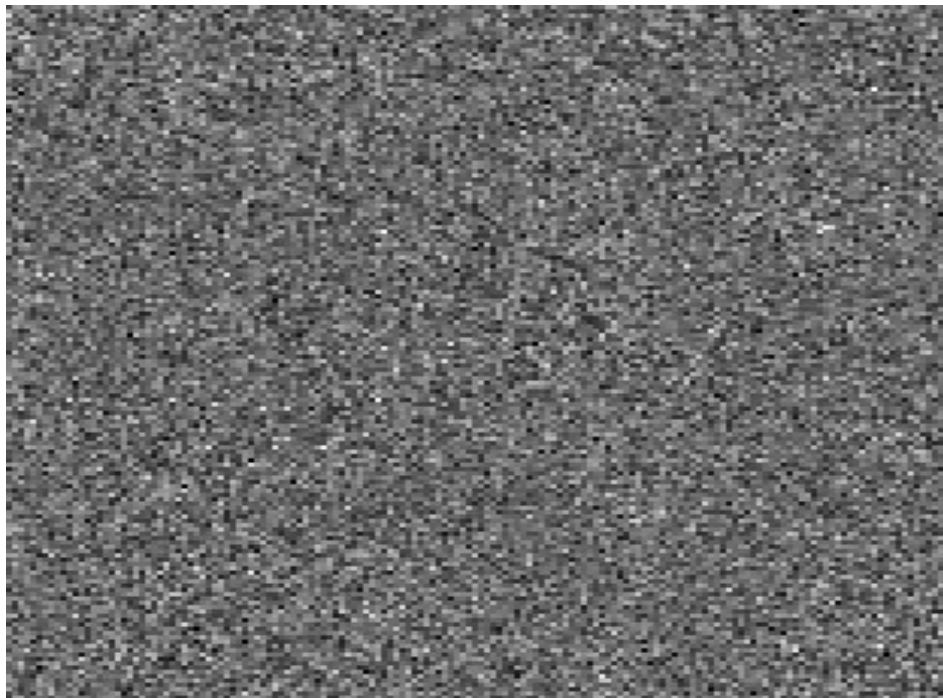


Figure 4-13: shows the image uniformity of the developed flood phantom obtained from gamma camera SPECT

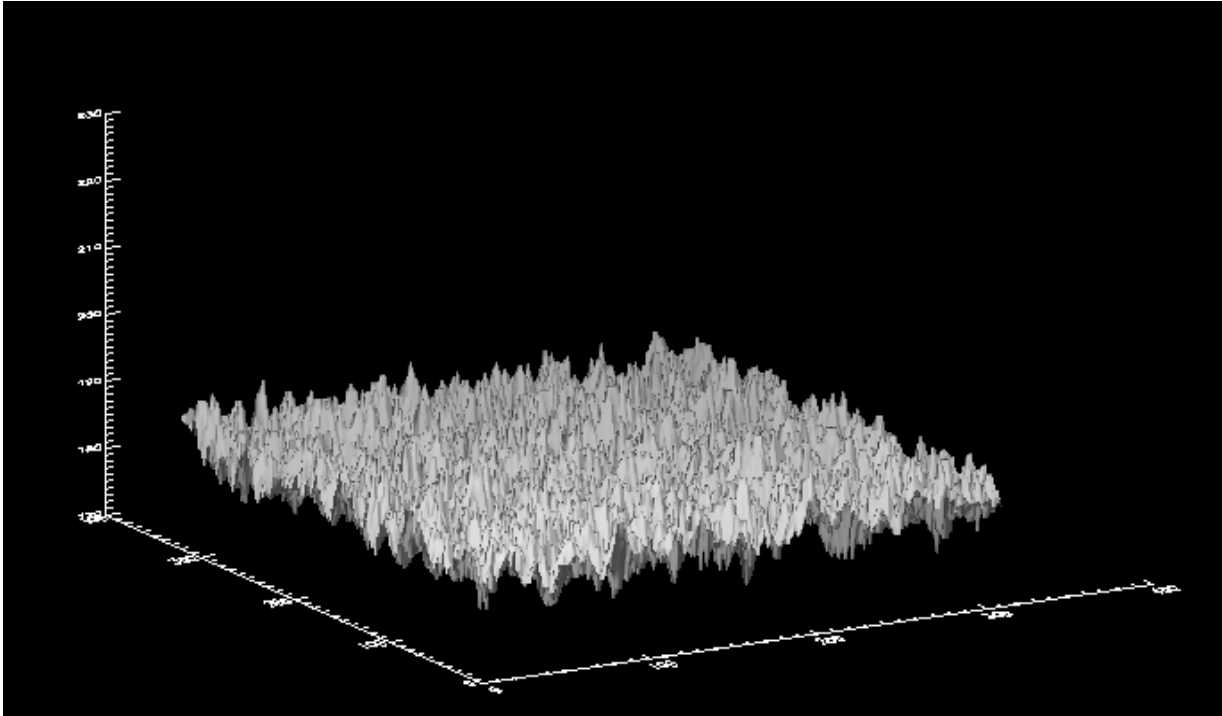


Fig 4-14 A

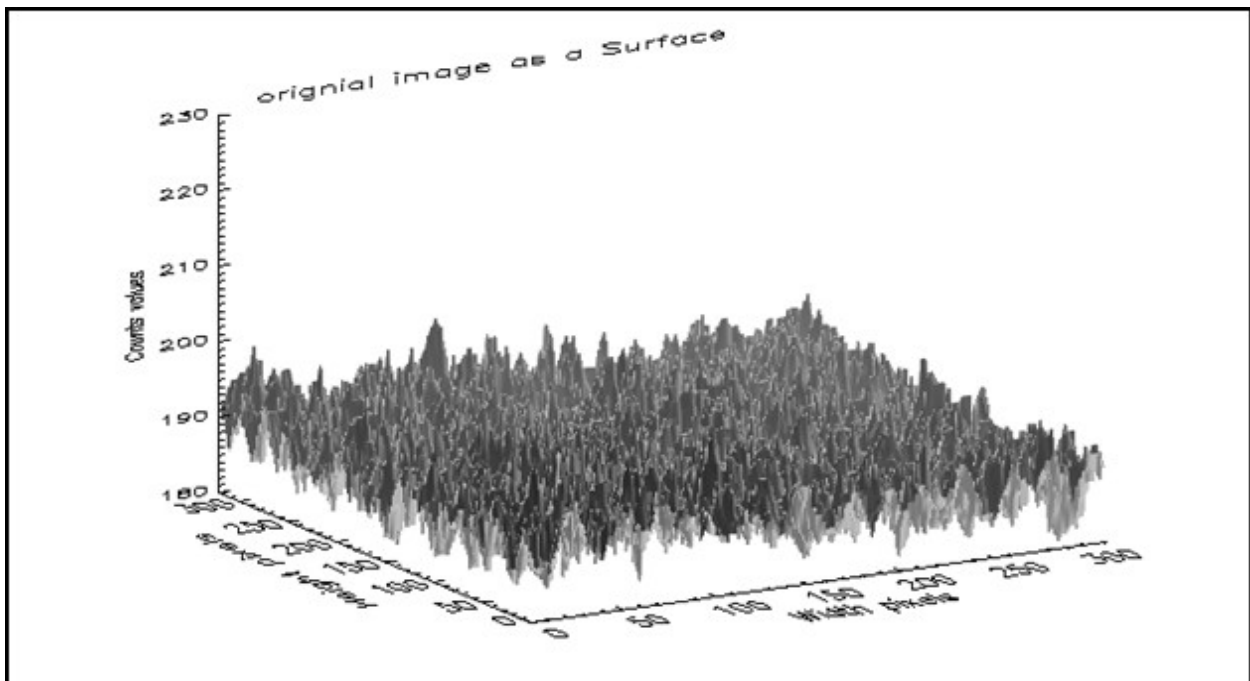


Figure 4-14 A and B: shows the point spread function of flood field uniformity obtained by developed phantom and analyzed by IDL program.

Uniformity: Two uniformity parameters as integral and differential (I.U. & D. U.) were measured and evaluated using interactive data language (IDL) program. The I.U. focused on the whole numbers of the pixels that contain the image while the D.U. measured for every 5x5 rows and column of the pixels. Serial of images were taken using the low-cost locally manufactured phantom according to the NEMA standard publication in acquisitions of the image and analysis. Figure 4-13 shows the image uniformity of the developed flood phantom obtained from gamma camera SPECT which is processed by using IDL program and shown in Figure 4-14 A, B which is a point spread function spectrum with homogeneous surface. The analysis revealed that: the I.U. and D.U. were 3.18% and 2.27% for UFOV respectively. And in comparison with the standard acceptance tests I. U. and D. U. for the UFOV which are 2.0 and 1.5% respectively, the analysis deduced that: there is no significant difference; hence the phantom could be applicable for flood field uniformity measurement.

Development of Uniformity correction map:

Correction map develop to uniform the original image, where each pixel is divided by the corresponding pixel value.

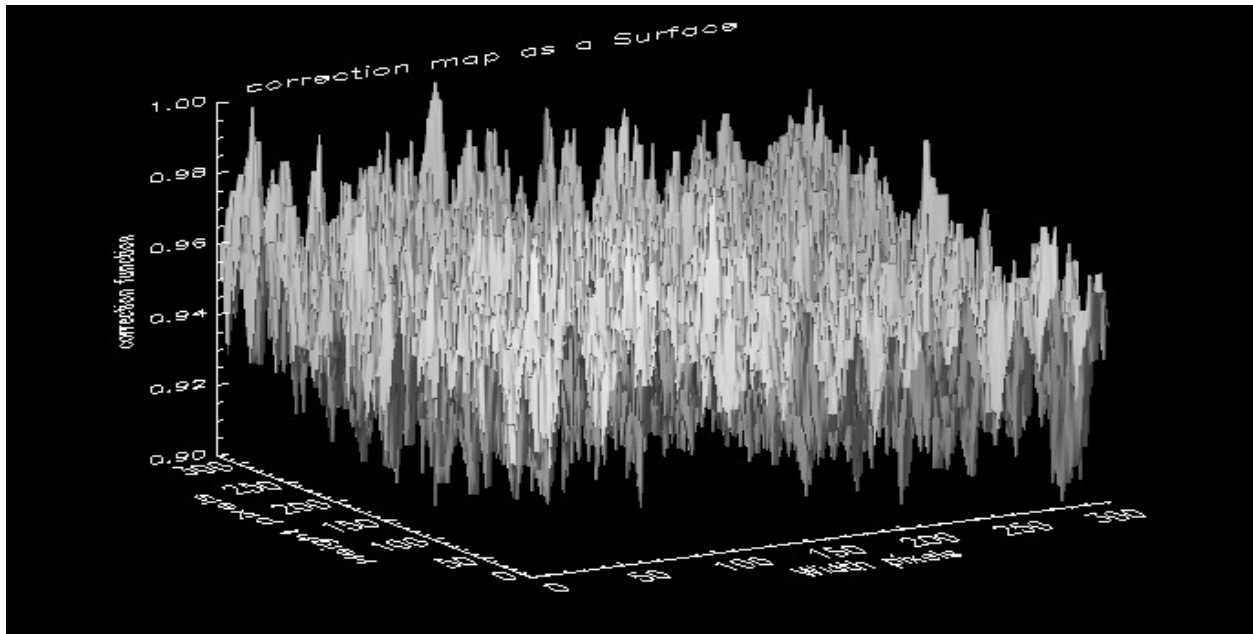


Fig 4-15 A

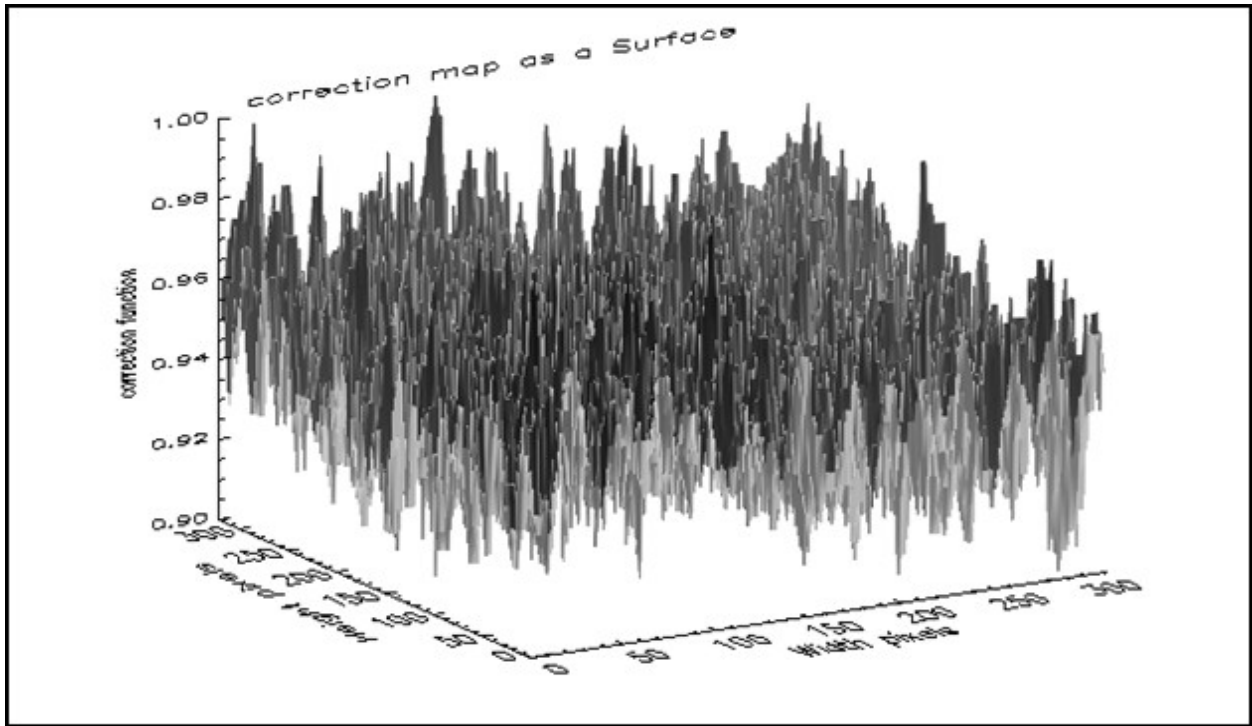


Fig 4-15 B

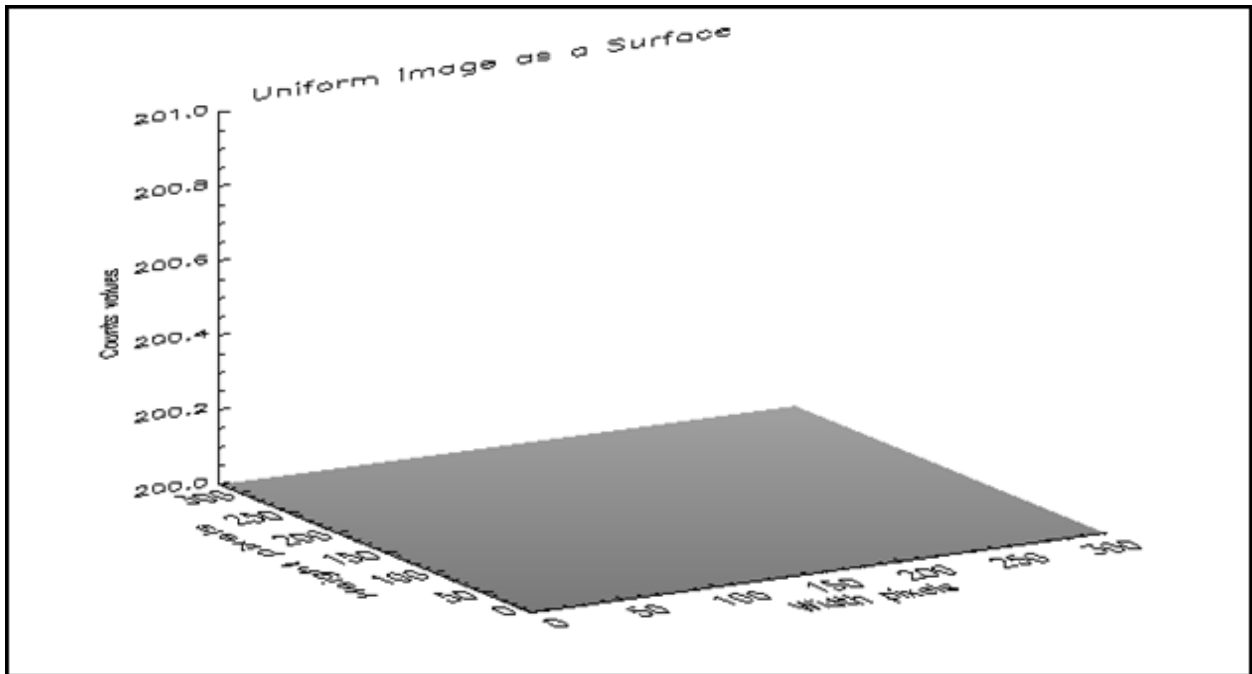


Fig 4-15 A, B and C: image of Uniformity after applied of correction map

Chapter five

Discussion, conclusion and recommendation

5-1 Discussion:

Q.C is now mandatory practice for any diagnostic imaging department and may be the subject of review and audit procedures to ensure the appropriate standard of service. Such procedures would also be requirements for any department wishing to achieve a level of formal accreditation (10). We have describe the design, construction and tests of a low-cost multipurpose phantom with a program as an accessories to the phantom to provide a basic Q.C of SPECT system in the fast time manner and assess the result of the Q.C data simply and accurately. Fig 4-3: Represent an image of our phantom. The frequency of the LTF was calculated depend on the formula that $F=1/2 \Delta$, while (F) is the frequency (Δ) is referred to the amplitude of the frequency. In the MTF at 10% resolution (10% resolution was recommended for nuclear medicine equipment) was calculated using that: MTF at 10% resolution = frequency of MTF at 10% / frequency of an object.

From the images of the resolution % vs. objects size for SPECT at RICK and RCH-Khartoum Sudan. The analysis reveals that: the resolution percent increases following the objects size increment for both hospitals i.e. RCH and RICK, however RCH and RICK showed the average resolution of 94.0% and 89.5% respectively as measured by the designed phantom relative to the standard resolution measured by the NEMA phantom which was 95.5% and 90.8%, while the correlation between the resolution% and the objects size in mm could be fitted to the following equation $y = 6.59x + 47.87$ and $y = 6.64x + 43.1$ for Royal Care and RICK respectively with significant correlation as $R^2 = 0.98$. The system resolution at RCH has been within the tolerance level i.e. 3-5% from the optimum resolution (100%), however the system at RICK showed an action level which is $> 5\%$ relative to the optimum resolution (100%) as has been mention by IAEA, and Ellinor et al.,. Therefore the system installed at RICK should be subjected to serious QC process to reassure the optimum or at least tolerance level of resolution. Figure 4-2 shows the comparative resolution % vs. objects frequency for SPECT at RICK and RCH. The analysis showed that: there is inverse linear relationship between the resolution% and the objects frequency (number of wires/cm) i.e. as the frequency increases the resolution% decreases for

both hospitals and the average resolution% was 94% and 90.3% respectively as measured by the designed phantom and in comparison with that obtained by NEMA phantom which was 95.5% and 91.8% respectively, the average deviation factor of the designed phantom from the standard was -1.5%. in contrast with the standard ranged of resolution stated by Ellinor et al, both systems installed at RCH and RICK have been shifted from the standard range but the system at RICK was at action level. The correlation between resolution % and the objects frequency could be fitted in equations: $y = -242.68x + 113.01$ for RCH and $y = -258.1x + 110.46$ for RICK, where x refers to objects frequency and y refers to resolution%, such correlation was significant as $R^2 = 1$. The average resolution% measured by the phantom was 94% and 90.3% respectively. Figure 3 shows the comparison resolution% versus object frequency measured by developed phantom and the QA base line for RCH and RICK. The general trend of the analyzed data showed that: there were inversely linear relationships between object frequency and resolution with significant point at $R^2 = 0.9$ % i.e. as the object frequency increases the resolution% decreases. The average resolution measured by the developed phantom was 94.0% and 90.3% for RCH and RICK respectively, these results relative to the standard NEMA QA phantom which was 95.5% and 91.8% respectively. Same resolution as 94.0% and 89.5% have been obtained for RCH and RICK respectively depending on the resolved object size as shown in Figure 4-4 which is compared with standard results obtained by NEMA phantom as 95.8% and 91.5% to deduce that: the average shift of the designed phantom relative to standard one was also 1.9%. Hence the developed designed phantom could be use successfully to carry out the QC tests for SPECT in Sudan with an average deviation factor of -1.3% from the optimum resolution measured by NEMA phantom.

In Figure 4: shows the counts (dps) distributions spectrum in X-axis and Y-axis direction via phantom lead slits. In which there is semi symmetrical and superimposition between the spectrums obtained in X-axis and that in Y-axis. The average count has been compared with that obtained by standard phantom which gives an acceptable variation of 0.7% indicating there is acceptable linearity between the developed phantom and the standard one. The difference in counts between X-axis and Y-axis direction has been plotted versus phantom slits Figure 4-5, which in turn reveals that: there is about 4% difference per each slit of phantom relative to standard one as shown in Figure 4-5. Also the absolute linearity has been measured for the central field of view (CFOV) of the gamma camera depending on NEMA specifications with

respect to the real position coordinate x and y which shows the counts (dps) versus phantom slits. And the calculation has been carried out using line spread function (LSF) which in turn determined as the average of the interpolated half maximum locations on both sides of each peak. The value of spatial linearity is calculated as the standard deviation of the location of the peaks in each slit and was 0.631 mm in X-axis direction and 0.636 mm in Y-axis direction for the useful field of view (UFOV) with no significant deviations between the X-axis and Y-axis direction. The comparison this result relative the acceptance test of the gamma camera and the recommendation values from manufacture, the researchers found that there is no significant difference as the acceptance values for absolute linearity for UFOV is 0.70mm while the manufacture recommended a value of 0.28 mm.

From Fig 4-5 we find that the resolution of the Gamma camera increase with an object size (mm) increase. For RICK Gamma camera the resolution for minimum object used (4mm) is 40% and increase as object size increased to reach 1% at size object of 9mm and above, with resolution % = $4.797 \times \text{object size} + 95.19$. in comparison with the RCIH Gamma camera we find that the resolution is much higher at smallest object (4mm) to be 70% and increased with object size increased to reach 1% resolution for 7,8,8 and 10mm object size with resolution % = $11.45 \times \text{object size} + 5.854$. our phantom and program showed the ability to detect the change in the camera resolution and found that the resolution% of a Gamma camera installed in RCIH has a greater resolution with the same type of camera installed in RICK.

Form Fig 4-6 which when plotted the resolution % (Y axis) various the object frequency in cycle/mm (X axis) we found that there in an inverse proportionality between the resolution and object frequency i.e. the smallest object frequency have higher resolution. The result of RICK camera represent 10% resolution at object frequency 0.05 and 0.06 while the result of RICH camera showed 10% resolution at object size of 0.05, 0.06 and 0.07. Also at the largest object frequency (0.13 cycle/mm the RICK camera provides resolution of 40% compare with 70% resolution of the same object for RCIH. Fig4 and 5 showed that there is an direct proportionality between camera resolution and object size and inverse proportionality between resolution and frequency. And also showed that when the object size is increase the frequency (cycle/mm) was decreased and vice versa. Fig6 and 7 represent the intensity of the all lines acquired from our fabricated phantom. The researcher can shows easily the intensity of lines of RCIH have smooth

peak opposite to the lines of RICK camera which indicate that the resolution of the camera used in RCIH have a good resolution than that used in RICK even in the same type and version of the camera, but the camera of RICK installed 4 years earlier than the camera of RCIH.

5-2 Conclusion:

The developed designed phantom with locally manufacturing with low cost materials could be use successfully to carry out the Resolution QC tests for SPECT in Sudan with an average deviation factor of -1.5% from the optimum resolution measured by NEMA phantom and 0.07mm deviation factors from NEMA phantom for linearity and 1.6% and 0.27% average deviation from standard NEMA phantom for measuring Integral uniformity and differential uniformity respectively. So the developed phantom could be used with acceptable accuracy in the field of nuclear medicine to carry out the quality control tests of gamma camera SPECT, which is consider as general multi functional phantom as it could measures the resolution, linearity and flood field uniformity independency on type or manufactures of camera.

4-5 Recommendation:

- Future development of locally manufactured low-cost phantoms is recommended in order to cover all the Q.C parameters of gamma camera and SPECT regardless the types or manufactures of camera.
- Resolution and linearity Q.C parameter can be evaluate using simple designed phantom that contain single line of radioactivity.(further study recommended).
- The researcher recommends the simulation of a quality control Jaszczak phantom using SIMIND Monte Carlo.
- Assessment of the gamma camera Q.C parameters using MATLAB and compare the result to the IDL.
- Fabrication of phantoms for Tomographic image resolution and linearity assessment.(Jaszczak phantom)
- Study the efficiency of phantom result using inkjet printer.
- Establishing a national program for the quality control of nuclear medicine instrument in Sudan.

References:

A Marco. Coca, Leonel. Torres, Gladys, Roberto, Consuelo, and Adlin (2008). Establishment of a National Program for Quality Control of Nuclear Medicine Instrumentation. *J Nucl Med Technol* 36:203–206.

baechler S., corminboeuf, linder, malterre, bischof, bochud and Verdun (2008). Feasibility of the gamma camera acceptance Testing procedure introduced by the swiss federal Office of public health.

Beekman Freek J and Vree Gerralt A de (2005). Photon-counting versus an integrating CCD-based gamma camera: important consequences for spatial Resolution. *Phys. Med. Biol.* 50 , N109–N119.

Burrell Steven, and Anita. (2006). Artifacts and Pitfalls in Myocardial Perfusion Imaging. *Journal of Nucl. Med. Technol.* Vol. 34, P: 193–211.

Chandra, and Ramesh (2004). Essential nuclear medicine physics. *Nuclear Medicine Physics: The Basics, 6th Edition.*

E John (2011). Gamma camera intrinsic uniformity in an unstable power supply environment. *Hell J Nucl Med* 2011; 14(2).

E. Porrassa, B. Escata, J.M. Benllocha, D. Kadi-Hanifia, S. L!opezb, N. Pav!ona, J.A. Ruiza, F. S!ancheza, A. Sebasti" a (2002). Portable mini gamma camera for medical applications. *Nuclear Instruments and Methods in Physics Research A* 486 , 186–190.

Ejeh John E., Kayode, Bidemi, Bola. (2011). Gamma camera intrinsic uniformity in an unstable power supply environment. *Hellenic Journal of Nuclear Medicine*, vol. 14 (2), P: 1790-5427.

Elkamdawy Abdelhamid A, Joseph. Rothenbach, Srikanth Damaraju, and Badruddin. (2000). Intrinsic Uniformity and Relative Sensitivity Quality Control Tests for Single-Head Gamma Cameras, *J. Nucl. Med. Technol.* Vol. 28, P: 252–256.

Ellinor Busemann Sokole, Anna Plachcinska, Alan Britten, M. Lyra Georgosopoulou, W. Tindale and R. Klett. (2010). Routine quality control recommendations for nuclear medicine instrumentation. *Eur J. Nucl. Med. Mol Imaging*, vol. 37, P: 662–671.

Elshemey Wael M., Mohamed, M.H.Khader (2013). Scattered radiation effects on the extrinsic sensitivity and counting efficiency of a gamma camera. *Applied Radiation and Isotopes* 77 , 18–22.

EM Smith. (1998). Scintillation camera quality control, part 1: establishing the quality control program. *J Nucl Med Technol.* Vol. 26, P: 9-13.

Ferreira Fernanda Carla Lima, Souza Divanizado Nascimento (2010). Liver phantom for quality control and training in nuclear medicine. *Nuclear Instruments and Methods in Physics Research A* 652 ,791–793.

Fidler Valentin, Prepadnik Milan and Xie Yanfen (2001). Upgrading of gamma cameras for developing countries. *Radiol Oncol* 35(1); 53-61.

FJ Bone, Graham, and Dowdey. (1971). Image Aberration Produced By Multi-Channel Collimators for a Scintillation Camera. *Radiology*, Vol. 98, P: 329 – 334.

H. Ng A., K.H.Ng, H. Dharmendra, A. C. Perkins. (2009). A low-cost phantom for simple routine testing of single photon emission computed tomography (SPECT) cameras. *Applied Radiation and Isotopes*, vol. 67, P: 1864–1868.

Holstensson Maria, Mike, Susan and Glenn (2010). The effect of energy and source location on gamma camera intrinsic and extrinsic spatial resolution: an experimental and Monte Carlo study. *Phys. Med. Biol.* 55 , 1735–1751.

IAEA (1991)-TECDOC-602 –page 11-*Quality control of nuclear medicine instruments.*

IAEA. (2009). Quality Assurance for SPECT system (Human Health Series No. 6), Vienna, Austria.

International Atomic Energy Agency, “Quality control of nuclear medicine instrumentations, IAEA-TECDOC602”, 1991.

International Atomic Energy Agency, “Quality control of nuclear medicine instrumentations, IAEA-TECDOC602”, 1991.

Islamian Jalil Pirayesh, Mohammad, Mehdi, Shahrokh, Michael (2012). Simulation of a Quality Control Jaszczak Phantom with SIMIND Monte Carlo and Adding the Phantom as an Accessory to the Program. *Iranian Journal of Medical Physics* Vol. 9, No. 2, 135-140.

Jalil Islamian Pirayesh, Mohammad Toossi, Mehdi, Shahrokh and Michael (2012). Simulation of a Quality Control Jaszczak Phantom with SIMIND Monte Carlo and Adding the Phantom as an Accessory to the Program. *Iranian Journal of Medical Physics*, Vol. 9, No. 2, P: 135-140.

Jeon Hosang, Kim Hyunduk, Cha Bo Kyung, Kim Jong Yul, Gyuseong Cho, Chung Yong Hyun, Jong Yun (2009). Performance evaluation for pinhole collimators of small gamma camera by MTF and NNPS analysis: Monte Carlo simulation study. *Nuclear Instruments and Methods in Physics Research A* 604 , 93–96.

Jeon Hosang, Cho Gyuseong (2008). The detective quantum efficiency (DQE) for evaluating the performance of a small gamma camera system with a uniformly redundant array (URA) collimator. *Nuclear Instruments and Methods in Physics Research A* 591 , 279–281.

Jeong Myung Hwan, Yong, Yong, Tae, Jin, Key, Byung, Yearn, Kyung and Byung (2004). Performance improvement of small gamma camera using NaI(Tl) plate and position sensitive photo-multiplier tubes. *Phys. Med. Biol.* 49 , 4961–4970.

K .O'Connor M., Vermeersch. (1991). Critical Examination of the Uniformity Requirements for Single Photon Emission Computed Tomography. *Med Phys* vol. 18, P: 190-197.

KC Young, K Kouris, M Awdeh, HM Abdel-Dayem. (1990). Reproducibility and Action Level for Gamma Camera Uniformity. *Nucl Med Commun*, Vol. 11, P: 95-101.

Lees J.E., Bassford, Blake, Blackshaw and Perkins (2011). A high resolution Small Field Of View (SFOV) gamma camera: a columnar scintillator coated CCD imager for medical applications. The 9th international conference on position sensitive detectors, 12–16 september, ABERYSTWYTH, U.K.

Lees J.E., Bassford , Blackshaw , Perkins (2010) . Design and use of mini-phantoms for high resolution planar gamma cameras. *Applied Radiation and Isotopes* 68 ,2448–2451.

Lin, PJP, TU.; Borrás, C., et al. (1993). Specification and acceptance testing of computed tomography scanner, American association of physics in medicine; New York.

LS Graham, FH Fahey, MT Madsen, Aswegen A, Yester MV. (1995). Quantitation of SPECT performance: report of task group 4, Nuclear Medicine Committee. *Med Phys* Vol. 22, P: 401 – 409.

M Holstenson, C Hindrof, Ljungberg, Partridge, Flux GD. (2007). Optimization of energy-window setting for scatter correction in quantitative ¹¹¹In imaging: Comparison of measurements and Monte Carlo simulations. *Cancer Biother. Radiopharm.* Vol. 22(1), P: 136-142.

Maria Holstensson, Partridge Mike, Buckley Susan E and Flux Glenn D. (2010). The effect of energy and source location on gamma camera intrinsic and extrinsic spatial resolution: an experimental and Monte Carlo study. *Phys. Med. Biol.* Vol.55, P: 1735–1751.

Minarik D, Gleisner and Ljungberg (2008). Evaluation of quantitative ^{90}Y SPECT based on experimental phantom studies. *Phys. Med. Biol.* 53 5689–5703.

National Electrical Manufacture Association (2007). performance measurements of Gamma cameras NEMA standard publication NU 1 – 2007.

National Electrical Manufacturers Association (NEMA), (2001). Performance Measurements of Scintillation Cameras; NEMA Standards Publication NU 1-2001, Washington, D.C.-USA: Global Engineering Documents.

Ng A.H. , Ng K.H. , Dharmendra , Perkins (2008) . A low-cost phantom for simple routine testing of single photon emission computed tomography (SPECT) cameras. *Applied Radiation and Isotopes* 67 1864–1868.

O .H Anger (1958) “Scintillation camera,” *Rev. Sci. Instrum.* 29, 27–33.

O’Connor Michael K., Mayo, Rochester, MN (2000). Quality Control of Scintillation Cameras (Planar and SPECT).

On behalf of the EANM Physics Committee: Sokole Ellinor Busemann & Płachcńska Anna & Britten Alan With contribution from the EANM Working Group on Nuclear Medicine Instrumentation Quality Control: Georgosopoulou Maria Lyra & Tindale Wendy & Klett Rigobert (2010). Routine quality control recommendations for nuclear medicine instrumentation. *Eur J Nucl Med Mol Imaging* 37:662–671.

Pat Zanzonico. (2008). Routine Quality Control of Clinical Nuclear Medicine Instrumentation: A Brief Review. *J. Nucl. Med.* Vol. 49(7), P: 1114–1131.

RJ Jaszczak, Coleman, Lim. (1980) SPECT: Single photon emission computed tomography. *IEEE Tran Nucl Sci.* ;NS-27:1137–1153.

Rova Andrew, Anna, and Hamarneh (2007). Development of NEMA-based Software for Gamma Camera Quality Control. *Journal of Digital Imaging*, Vol 21, No 2: pp 243-255.

S .T. Koike, Uno, Uchid, Sekimoto. Murakami, Shoji, Nagashima, Yamamoto and Nakano (2011). A new gamma camera with a Gas Electron Multiplier. 2nd International Conference on Micro Pattern Gaseous Detectors, 29 August – 1 September 2011, KOBE, JAPAN.

SB Doed. (1994). Practical radiation protection and applied radiobiology. W.B. Saunders Co: Philadelphia.

Seo Youngho , Carina , and Bruce . (2008). Technological Development and Advances in SPECT/CT. *Semin Nucl Med.* Vol. 38(3), P: 177–198.

Seret Alain (2010). NEMA NU1-2001 performance tests of four Philips Brightview cameras. *Nuclear Instruments and Methods in Physics Research A* 648 S89–S92.

SR Cherry, Sorenson , and Phelps . *Physics in Nuclear Medicine*. Philadelphia: Saunders; 2003.

Staden J A van, Raan, L`otter, Aswegen and Herbst (2007). Production of radioactive quality assurance phantoms using a standard inkjet printer. *Phys. Med. Biol.* 52 N329–N337.

Starck Sven-A° ke, Magnus, and Sten (2005). The use of detective quantum efficiency (DQE) in evaluating the performance of gamma camera systems. *Phys. Med. Biol.* 50 1601–1609.

Ueno Kazuki, Kaori, Chihiro, Satoru, Shigeto, Hidetoshi, Shunsuke, Kentaro, Tsutomu, Hironobu, Reiko, Atsushi and Toru (2008). Performance of the gamma-ray camera based on

GSO(Ce) scintillator array and PSPMT with the ASIC readout system. *Nuclear Instruments and Methods in Physics Research A* 591 268–271.

Van Hoken Roel, Stefaan, Staelens and Lemahieu (2008). Comparing planar image quality of rotating slit and parallel hole collimation: influence of system modeling. *Phys. Med. Biol.* 53 1989–2002.

Van Staden JA, H Dv, MG, A Van and CP. (2007). Production of Radioactive Quality Assurance Phantoms Using Standard Inkjet Printer. *Phys Med. Biol.* Vol. 52, N 329 – N 337.

Vickery A, Jørgensen and Nijs (2011). NEMA NU-1 2007 based and independent quality control software for gamma cameras and SPECT. *Journal of Physics: Conference Series* 317 012023 . doi:10.1088/1742-6596/317/1/012023.

Yamamoto Seiichi, MasaoImaizumi, Eku, Jun (2010). Development of a compact and high spatial resolution gamma camera system using LaBr₃(Ce). *Nuclear Instruments and Methods in Physics Research A* 622 261–269.

Zanzonico Pat (2009). Routine Quality Control of Clinical Nuclear Medicine Instrumentation. *J Nucl Med.* July; 49(7): 1114–1131. doi: 10.2967 /jnumed. 107.050203.

Zeinali Hossein Zamani, Nejad Mehdi Ghiassi- and Mirzaii Aliakbar (2007). Design an Adaptive Quality Control Phantom to Optimize QC Test Methods. *The Open Medical Imaging Journal*, 1, 1-6.